

ENCLOSURE 8

**TENNESSEE VALLEY AUTHORITY
BROWNS FERRY NUCLEAR PLANT (BFN)
UNITS 1, 2, AND 3**

**TECHNICAL SPECIFICATIONS (TS) CHANGES TS-431 AND TS-418
EXTENDED POWER UPRATE (EPU)**

**CDI REPORT NO. 08-15NP, "STRESS ASSESSMENT OF BROWNS FERRY NUCLEAR UNIT
1 STEAM DRYER WITH TIE-BAR MODIFICATIONS"**

(NON-PROPRIETARY VERSION)

Attached is the **Non-Proprietary Version** of CDI Report No. 08-15, "Stress Assessment of Browns Ferry Nuclear Unit 1 Steam Dryer with Tie-Bar Modifications."

Stress Assessment of Browns Ferry Nuclear
Unit 1 Steam Dryer with Tie-Bar Modifications

Revision 1

Prepared by

Continuum Dynamics, Inc.
34 Lexington Avenue
Ewing, NJ 08618

Prepared under Purchase Order No. 00053157 for

TVA / Browns Ferry Nuclear Plant
Nuclear Plant Road, P. O. Box 2000 PAB-2M
Decatur, AL 35609

Approved by



Alan J. Bilanin

Reviewed by



Milton E. Teske

June 2008

This report complies with Continuum Dynamics, Inc. Nuclear Quality Assurance Program currently in effect.

Executive Summary

The finite element model and analysis methodology, used to assess stresses induced by the flow of steam through the steam dryer at Brown Ferry Nuclear Unit 1 (BFN1), are described and applied to obtain stresses at CLTP conditions. The resulting stresses are assessed for compliance with the ASME B&PV Code, Section III, subsection NG, for the load combination corresponding to normal operation (the Level A Service Condition). The results presented herein account for proposed modifications to the BFN1 steam dryer designed to improve stress margins under EPU operation. In particular, changes to the tie-bars and steam dam gussets have been incorporated to promote alternating stress ratios above 2.0 at EPU conditions.

The analysis is carried out in the frequency domain, which confers a number of useful computational advantages over a time-accurate transient analysis including the ability to assess the effects of frequency scalings in the loads without the need for additional finite element calculations. [[

⁽³⁾] The analysis develops a series of unit stress solutions corresponding to the application of a unit pressure at a MSL at specified frequency, f . Each unit solution is obtained by first calculating the associated acoustic pressure field using a separate analysis that solves the damped Helmholtz equation within the steam dryer [1]. This pressure field is then applied to a finite element structural model of the steam dryer and the harmonic stress response at frequency, f , is calculated using the commercial ANSYS 10.0 finite element analysis software. This stress response constitutes the unit solution and is stored as a file for subsequent processing. Once all unit solutions have been computed, the stress response for any combination of MSL pressure spectrums (obtained by Fast Fourier Transform of the pressure histories in the MSLs) is determined by a simple matrix multiplication of these spectrums with the unit solutions.

Results obtained from application of the methodology to the BFN1 steam dryer show that at nominal CLTP operation the minimum alternating stress ratio (SR-a) anywhere on the steam dryer is $SR-a=3.23$. The loads used to obtain this value account for all the end-to-end biases and uncertainties in the loads model [2] and finite element analysis. In order to account for uncertainties in the modal frequency predictions of the finite element model, the stresses are also computed for loads that are shifted in the frequency domain by $\pm 2.5\%$, $\pm 5\%$, $\pm 7.5\%$ and $\pm 10\%$. The minimum alternating stress ratio encountered at any frequency shift is found to be $SR-a=2.91$ occurring at the $+7.5\%$ shift. The stress ratio due to maximum stresses (SR-P) is $SR-P=1.75$ without frequency shifts and $SR-P=1.67$ when frequency shifts are considered. Given the high alternating stress ratio SR-a and the comparatively small dependence of SR-P upon acoustic loads, these values are expected to qualify the Unit 1 dryer at EPU conditions.

Table of Contents

Section	Page
Executive Summary	i
Table of Contents	ii
1. Introduction and Purpose	1
2. Methodology	3
2.1 Overview	3
2.2 [[..... ⁽³⁾]]	5
2.3 Computational Considerations	6
3. Finite Element Model Description	9
3.1 Steam Dryer Geometry	9
3.2 Material Properties	13
3.3 Model Simplifications	13
3.4 Perforated Plate Model	14
3.5 Vane Bank Model	15
3.6 Water Inertia Effect on Submerged Panels	16
3.7 Structural Damping	16
3.8 Mesh Details and Element Types	16
3.9 Connections Between Structural Components	17
3.10 Pressure Loading	26
4. Structural Analysis	29
4.1 Static Analysis	29
4.2 Harmonic Analysis	29
4.3 Post-Processing	34
4.4 Computation of Stress Ratios for Structural Assessment	34
4.5 Substructure Modeling	37
5. Results	39
5.1 General Stress Distribution and High Stress Locations	40
5.2 Load Combinations and Allowable Stress Intensities	58
5.3 Frequency Content	77
6. Conclusions	83
7. References	84

1. Introduction and Purpose

Plans to qualify the Browns Ferry nuclear plant for operation at Extended Power Uprate (EPU) operating condition require an assessment of the steam dryer stresses experienced under the increased loads. The steam dryer loads due to pressure fluctuations in the main steam lines (MSLs) are potentially damaging and the cyclic stresses from these loads can produce fatigue cracking if loads are sufficiently high. The industry has addressed this problem with physical modifications to the dryers, as well as a program to define steam dryer loads and their resulting stresses. The purpose of the stress analysis discussed here is to calculate the maximum and alternating stresses generated during Current Licensed Thermal Power (CLTP) and determine the margins that exist when compared to stresses that comply with the ASME Code (ASME B&PV Code, Section III, subsection NG).

The stress analysis considered here incorporates proposed design changes to the Browns Ferry Unit 1 (BFN1) steam dryer. In a previous stress analysis of the BFN1 steam dryer [3] using the same methodology, it was determined that the limiting alternating stress was $SR-a=1.56$ at CLTP which, when extrapolated to EPU conditions, arrives significantly below the desired $SR-a=2.0$ EPU target. Virtually all of the high stress regions occurred where the tie bars connect to the top cover plates of the vane banks. This prompted a redesign of the tie bars to alleviate these stresses. Using the frequency-based stress analysis described herein it was possible to rapidly analyze proposed modifications and thus arrive at a successful tie bar design with tapered and widened ends that brings the alternating stress ratios at the tie bar/top cover plate connections to well above 3.0 at CLTP operation. Since the outermost tie bars on the existing configuration also help support the steam dam, it was found necessary to add additional steam dam gussets. The final design of the modified steam dam and associated gussets is also included in the present analysis.

The stress analysis of the modified BFN1 steam dryer establishes whether the existing and proposed modifications are adequate for sustaining structural integrity and preventing future weld cracking under planned EPU operating conditions. The load combination considered here corresponds to normal operation (the Level A Service Condition) and includes fluctuating pressure loads developed from BFN1 main steam line data, and weight. The fluctuating pressure loads, induced by the flowing steam, are predicted using a separate acoustic circuit analysis of the steam dome and main steam lines [4]. Level B service conditions, which include seismic loads, are not included in this evaluation.

[[

(3)]]

[[⁽³⁾]] This approach also affords a number of additional computational advantages over transient simulations including: [[

⁽³⁾]] This last advantage is realized through the use of “unit” solutions representing the stress distribution resulting from the application of a unit fluctuating pressure at one of the MSLs at a particular frequency. [[⁽³⁾]]

This report describes the overall methodology used to obtain the unit solutions in the frequency domain and how to assemble them into a stress response for a given combination of pressure signals in the MSLs. This is followed by details of the BFN1 steam dryer finite element model including the elements used and overall resolution, treatment of connections between elements, the hydrodynamic model, the implementation of structural damping and key idealizations/assumptions inherent to the model. Post-processing procedures are also reviewed including the computation of maximum and alternating stress intensities, identification of high stress locations, adjustments to stress intensities at welds, and evaluation of stress ratios used to establish compliance with the ASME Code. The results in terms of stress intensity distributions and stress ratios are presented next, together with PSDs of the dominant stress components.

2. Methodology

2.1 Overview

Based on previous analysis undertaken at Quad Cities Units 1 and 2, the steam dryer can experience strong acoustic loads due to the fluctuating pressures in the MSLs connected to the steam dome containing the dryer. C.D.I. has developed an acoustic circuit model (ACM) that, given a collection of strain gage measurements [5] of the fluctuating pressures in the MSLs, predicts the acoustic pressure field anywhere inside the steam dome and on the steam dryer [1,2,4]. The ACM is formulated in frequency space and contains two major components that are directly relevant to the ensuing stress analysis of concern here. [[

(1)

(2)

⁽³⁾]]

[[

(3)

(4)

(5)

⁽³⁾]]

[[

(6)

⁽³⁾]]

2.2 [[
[[

(4) and (5)

⁽³⁾]]

(5)

(4),

⁽³⁾]]

[[

(3)]]

2.3 Computational Considerations

Focusing on the structural computational aspects of the overall approach, there are a number of numerical and computational considerations requiring attention. The first concerns the transfer of the acoustic forces onto the structure, particularly the spatial and frequency resolutions. The ANSYS finite element program inputs general distributed pressure differences using a table format. This consists of regular 3D rectangular (i.e., block) $n_x \times n_y \times n_z$ mesh where n_α is the number of mesh points in the i -th Cartesian direction and the pressure difference is provided at each mesh point (see Section 3.10). These tables are generated separately using a program that reads the loads provided from the ACM software, distributes these loads onto the finite element mesh using a combination of interpolation procedures on the surface and simple diffusion schemes off the surface (off-surface loads are required by ANSYS to ensure proper interpolation of forces), and written to ASCII files for input to ANSYS. A separate load file is written at each frequency for the real and imaginary component of the complex force.

The acoustic field is stored at 5 Hz intervals from 0 to 250 Hz. While a 5 Hz resolution is sufficient to capture frequency dependence of the acoustic field (i.e., the pressure at a point varies gradually with frequency), it is too coarse for representing the structural response especially at low frequencies. For 1% critical structural damping, one can show that the frequency spacing needed to resolve a damped resonant peak at natural frequency, f_n , to within 5% accuracy is $\Delta f = 0.0064 \times f_n$. Thus for $f_n = 10$ Hz where the lowest structural response modes occur, a frequency interval of 0.064 Hz or less is required. In our calculations we require that 5% maximum error be maintained over the range from $f_n = 5$ Hz to 250 Hz resulting in a finest frequency interval of 0.0321 Hz at the low frequency end (this adequately resolves all structural modes up to 250 Hz). Since there are no structural modes between 0 to 5 Hz, a 0.5 Hz spacing is used over this range with minimal (less than 5%) error. The unit load, $\hat{f}_n(\omega, \mathbf{R})$, at any frequency, ω_k , is obtained by linear interpolation of the acoustic solutions at the two nearest frequencies, ω_i and ω_{i+1} , spaced 5 Hz apart. Linear interpolation is sufficient since the pressure load varies slowly over the 5 Hz range (linear interpolation of the structural response would not be acceptable over this range since it varies much more rapidly over the same interval).

Solution Management

[[

(3)]]

[[

(3)]]

Structural Damping

In harmonic analysis one has a broader selection of damping models than in transient simulations. A damping factor, z , of 1% critical damping is used in the structural analysis. In transient simulations, this damping can only be enforced exactly at two frequencies (where the damping model is “pinned”). Between these two frequencies the damping factor can be considerably smaller, for example 0.5% or less depending on the pinning frequencies. Outside the pinning frequencies, damping is higher. With harmonic analysis it is straightforward to enforce very close to 1% damping over the entire frequency range. In this damping model, the damping matrix, \mathbf{D} , is set to

$$\mathbf{D} = \frac{2z}{\omega} \mathbf{K} \quad (7)$$

where \mathbf{K} is the stiffness matrix and ω the forcing frequency. One can show that with this model the damping factor varies between 0.995% and 1.005% which is a much smaller variation than using the pinned model required in transient simulation.

Load Frequency Rescaling

One way to evaluate the sensitivity of the stress results to approximations in the structural modeling and applied loads is to rescale the frequency content of the applied loads. In this procedure the nominal frequencies, ω_k , are shifted to $(1+\lambda)\omega_k$, where the frequency shift, λ , ranges between $\pm 10\%$, and the response recomputed for the shifted loads. The objective of the frequency shifting can be explained by way of example. Suppose that in the actual dryer a strong structural-acoustic coupling exists at a particular frequency, ω^* . This means that the following conditions hold simultaneously: (i) the acoustic signal contains a significant signal at ω^* ; (ii) the structural model contains a resonant mode of natural frequency, ω_n , that is near ω^* ; and (iii) the associated structural mode shape is strongly coupled to the acoustic load (i.e., integrating the product of the mode shape and the surface pressure over the steam dryer surface produces a significant modal force). Suppose now that because of discretization errors and modeling idealizations that the predicted resonance frequency differs from ω^* by a small amount (e.g., 1.5%). Then condition (ii) will be violated and the response amplitude therefore significantly

diminished. By shifting the load frequencies one re-establishes condition (ii) when $(1 + \lambda)\omega^*$ is near ω_n . The other two requirements also hold and a strong structural acoustic interaction is restored.

[[(6)

(3)]]

Evaluation of Maximum and Alternating Stress Intensities

Once the unit solutions have been obtained, the most intensive computational steps in the generation of stress intensities are: (i) the FFTs to evaluate stress time histories from (5); and (ii) the calculation of alternating stress intensities. [[

[8],

(3)]]

The high computational penalty incurred in calculating the alternating stress intensities is due to the fact that this calculation involves comparing the stress tensors at every pair of points in the stress history. This comparison is necessary since in general the principal stress directions can vary during the response, thus for N samples in the stress history, there will be $(N-1)N/2$ such pairs or, for $N=64K$ (the number required to accurately resolve the spectrum up to 250 Hz in 0.01 Hz intervals), 2.1×10^9 calculations per node each requiring the determination of the roots to a cubic polynomial. [[

(3)]]

3. Finite Element Model Description

A description of the ANSYS model of the Browns Ferry Unit 1 steam dryer follows.

3.1 Steam Dryer Geometry

A geometric representation of the Browns Ferry steam dryer was developed from available drawings (provided by TVA and included in the design record file, DRF-TVA-250B) within the Workbench module of ANSYS. The completed model is shown in Figure 1. This model includes the following modifications made to the Browns Ferry Unit 1 steam dryer on-site and additional modifications proposed for EPU operation. These are as follows:

On-Site Modifications

- (i) The 0.5 inch thick old outer hoods were cut away and replaced with 1 inch thick outer hoods.
- (ii) Channel-shaped hood assemblies composed of 1 inch thick plates were added to the outer hoods.
- (iii) The vertical hood supports located underneath the hood were cut away following the replacement with the thicker outer hood and exterior hood reinforcement assemblies.
- (iv) The top tie rods were replaced with thicker new ones. The gussets on the top of the outer hoods supporting the steam dam plate were cut away to facilitate installation of the new tie bars and possibly alleviate local stresses.
- (v) The cover plates were replaced by new ones that are 1 in thick.
- (vi) The outermost sections (the parts between the upper support ring and outer vane bank) of the supporting beam spanning the dryer were removed.

Previous analysis [3] showed significant stresses at the welds where the thicker tie bars (item (iv)) connect to the top cover plates which would result in alternating stress ratios at EPU below the target level of 2.0. Therefore, additional design modifications have been proposed to reduce these stresses to target levels. These changes are as follows:

Additional Modifications Proposed For EPU Operation

- (vii) Remove the thicker tie bars connecting to the inner hoods (i.e., those connecting the inner to inner hoods and those connecting the inner to middle hoods) and replace them with ones having tapered and flared ends to more evenly distribute loads at the end connections.
- (viii) Similarly, replace the thicker tie bars connecting to the outer hoods with the modified ones having flared and tapered ends. However, rather than completely removing these existing tie bars, part of each one is retained to support the lock gusset and restrain motion of the steam dam. The portion extending between the steam dam to the middle hood is removed.
- (ix) Add three additional gussets to support each of the two steam dams.

These additional modifications have been incorporated into the BFN1 steam dryer model and are reflected in the results presented in this report. The modified areas are shown in Figure 2 and Figure 3.

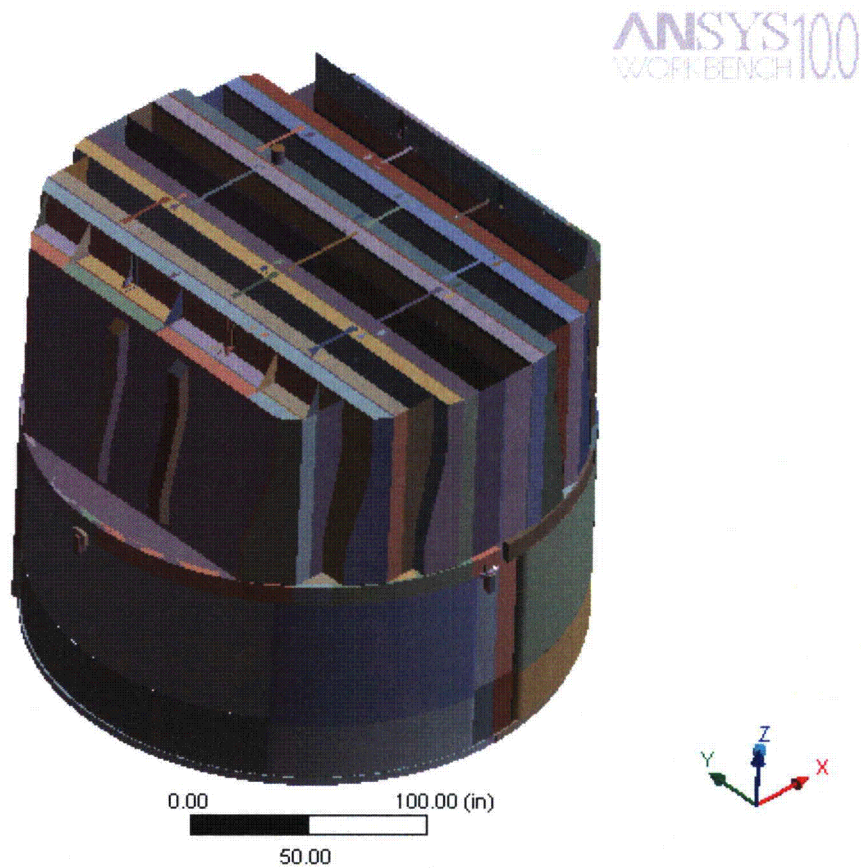


Figure 1. Overall geometry of the Browns Ferry Unit 1 steam dryer model.

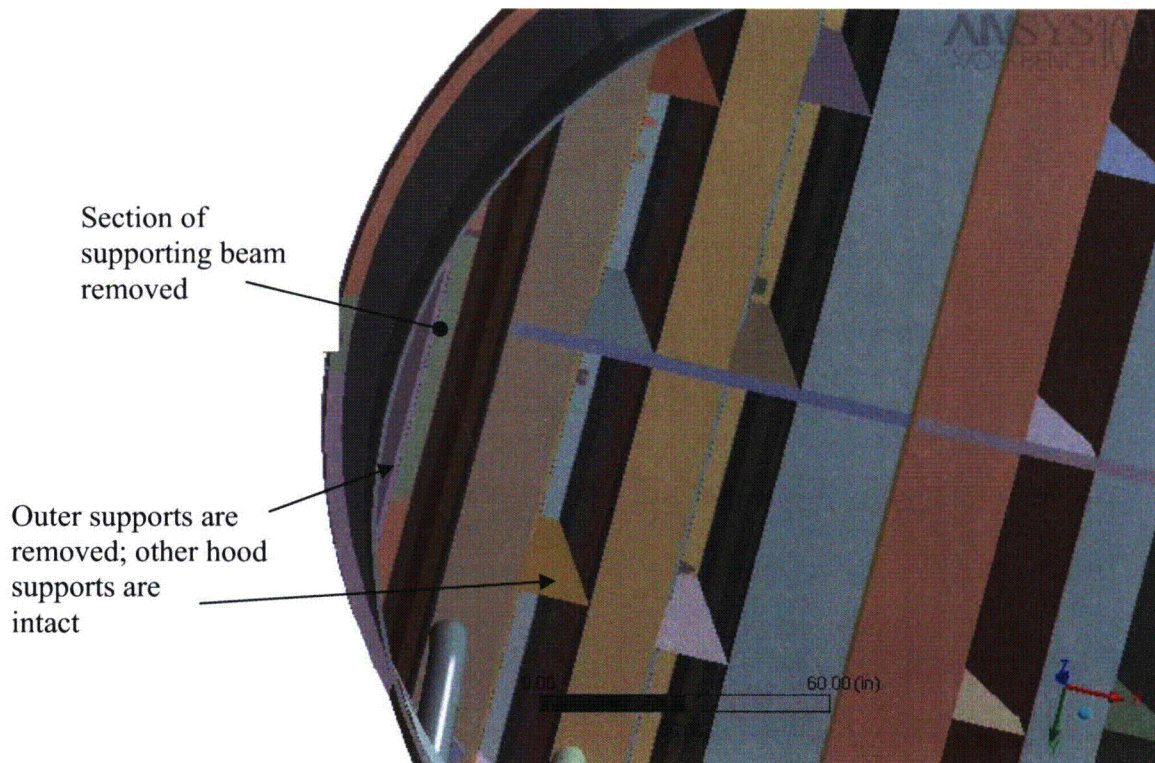
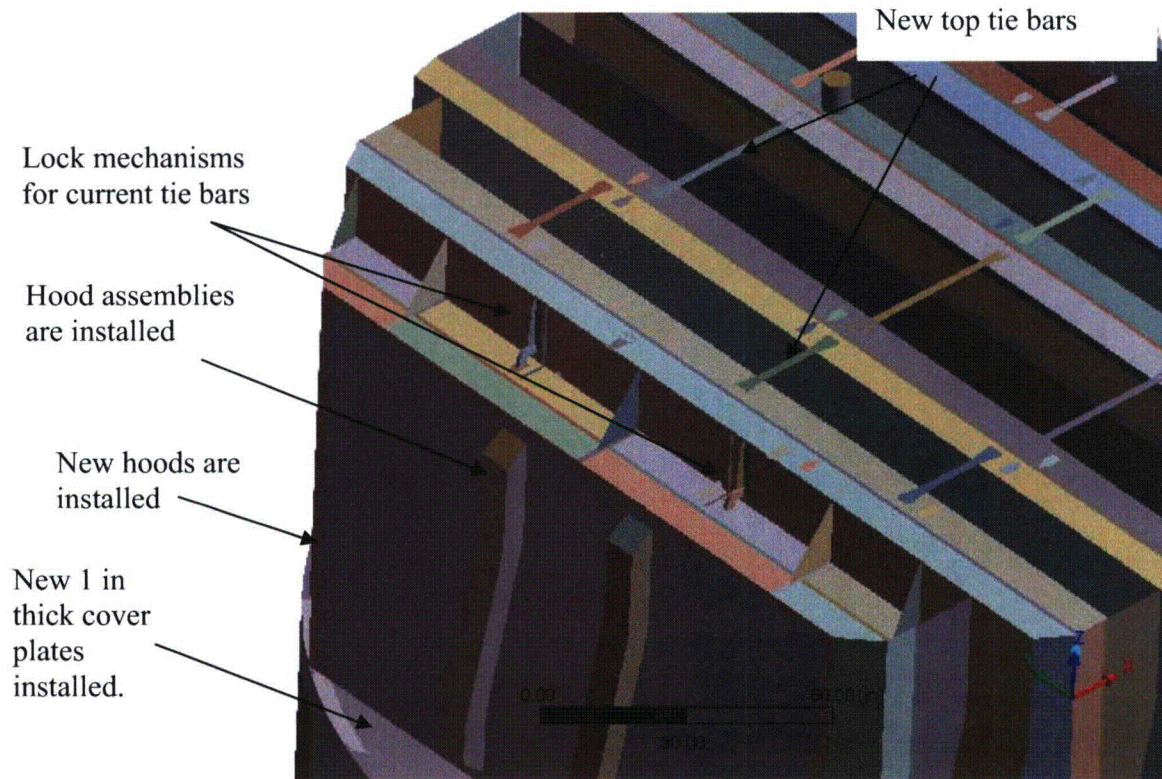


Figure 2. On-site modifications accounted for in the model and associated geometrical details.

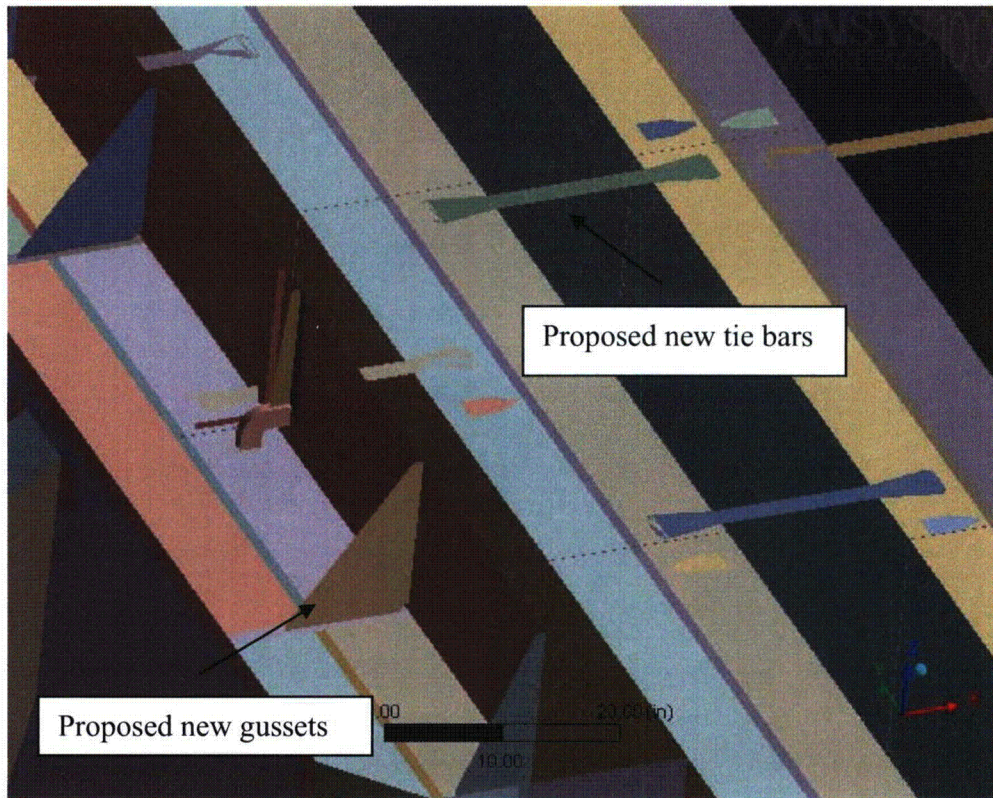


Figure 3. Proposed BFN1 modifications involving tie bars and additional steam dam gussets to improve stress margins at EPU.

3.2 Material Properties

The steam dryer is constructed from Type 304 stainless steel and has an operating temperature of 550°F. Properties used in the analysis are summarized below in Table 1.

Table 1. Material properties.

	Young's Modulus (10 ⁶ psi)	Density (lbm/in ³)	Poisson's Ratio
structural steel	25.55	0.284	0.3
structural steel with added water inertia	25.55	1.055	0.3

The structural steel modulus is taken from Appendix A of the ASME Code for Type 304 Stainless Steel at an operating temperature 550°F. The effective properties of perforated plates and submerged parts are discussed in Sections 3.4 and 3.6. Note that the increased effective density for submerged components is only used in the harmonic analysis. When calculating the stress distribution due to the static dead weight load, the unmodified density of steel (0.284 lbm/in³) is used throughout.

3.3 Model Simplifications

The following simplifications were made to achieve reasonable model size while maintaining good modeling fidelity for key structural properties:

- Perforated plates were approximated as continuous plates using modified elastic properties designed to match the static and modal behaviors of the perforated plates. The perforated plate structural modeling is summarized in Section 3.4 and Appendix C of [3].
- The drying vanes were replaced by point masses attached to the corresponding trough bottom plates and vane bank top covers. The bounding perforated plates, vane bank end plates, and vane bank top covers were explicitly modeled (see Section 3.5).
- The added mass properties of the lower part of the skirt below the reactor water level were obtained using a separate hydrodynamic analysis (see Section 3.6).
- [[⁽³⁾]]
- Four steam dryer support brackets that are located on the reactor vessel and spaced at 90° intervals were explicitly modeled (see Section 3.9).
- Most welds were replaced by node-to-node connections; interconnected parts share common nodes along the welds. In other locations the constraint equations between nodal degrees of freedom were introduced as described in Section 3.9.

3.4 Perforated Plate Model

The perforated plates were modeled as solid plates with adjusted elastic and dynamic properties. Properties of the perforated plates were assigned according to the type and size of perforation. Based on [9], for an equilateral square pattern with given hole size and spacing, the effective moduli of elasticity were found.

The adjusted properties for the perforated plates are shown in Table 2 as ratios to material properties of structural steel, provided in Table 1. Locations of perforated plates are classified by steam entry / exit vane bank side and vertical position.

Tests were carried out to verify that this representation of perforated plates by continuous ones with modified elastic properties preserves the modal properties of the structure. These tests are summarized in Appendix C of [3] and compare the predicted first modal frequency for a cantilevered perforated plate against an experimentally measured value. The prediction was obtained for a 40% open area plate (the maximum open area ratio of the perforated plates at BFN1, as seen in Table 2) using the analytical formula for a cantilevered plate and the modified Young's modulus and Poisson's ratio given by O'Donnell [9]. The measured and predicted frequencies are in close agreement, differing by less than 3%.

[[

[10,11],

[12]

[3]

⁽³⁾]]

[[

Figure 4. [[

⁽³⁾]]

Table 2. Material properties of perforated plates.

[[

(3)]]

3.5 Vane Bank Model

The vane bank assemblies consist of many vertical angled plates that are computationally expensive to model explicitly, since a prohibitive number of elements would be required. These parts have significant weight which is transmitted through the surrounding structure, so it is important to capture their gross inertial properties. Here the vane banks are modeled as a collection of point masses located at the center of mass for each vane bank section (Figure 4). The following masses were used for the vane bank sections, based on data found on provided drawings:

inner banks, 1575 lbm, 4 sections per bank;

middle banks, 1450 lbm, total 4 sections per bank; and
outer banks, 1515 lbm, 3 sections per bank.

These masses were applied to the base plates and vane top covers using the standard ANSYS point mass modeling option, element MASS21. ANSYS automatically distributes the point mass inertial loads to the nodes of the selected structure. The distribution algorithm minimizes the sum of the squares of the nodal inertial forces, while ensuring that the net forces and moments are conserved. Vane banks are not exposed to main steam lines directly, but rather shielded by the hoods.

The collective stiffness of the vane banks is expected to be small compared to the surrounding support structure and is neglected in the model. In the static case it is reasonable to expect that this constitutes a conservative approach, since neglecting the stiffness of the vane banks implies that the entire weight is transmitted through the adjacent vane bank walls and supports. In the dynamic case the vane banks exhibit only a weak response since (i) they have large inertia so that the characteristic acoustically-induced forces divided by the vane masses and inertias yield small amplitude motions, velocities and accelerations; and (ii) they are shielded from acoustic loads by the hoods, which transfer dynamic loads to the rest of the structure. Thus, compared to the hoods, less motion is anticipated on the vane banks so that approximating their inertial properties with equivalent point masses is justified. Nevertheless, the bounding parts, such as perforated plates, side panels, and top covers, are retained in the model. Errors associated with the point mass representation of the vane banks are compensated for by frequency shifting of the applied loads.

3.6 Water Inertia Effect on Submerged Panels

Water inertia was modeled by an increase in density of the submerged structure to account for the added hydrodynamic mass. This added mass was found by a separate hydrodynamic analysis (included in DRF-TVA-250B supporting this report) to be 0.1928 lbm/in² on the submerged skirt area. This is modeled by effectively increasing the material density for the submerged portions of the skirt. Since the skirt is 0.25 inches thick, the added mass is equivalent to a density increase of 0.771 lbm/in³. This added water mass was included in the ANSYS model by appropriately modifying the density of the submerged structural elements when computing harmonic response. For the static stresses, the unmodified density of steel is used throughout.

3.7 Structural Damping

Structural damping was defined as 1% of critical damping for all frequencies. This damping is consistent with guidance given on pg. 10 of NRC RG-1.20 [13].

3.8 Mesh Details and Element Types

Shell elements were employed to model the skirt, hoods, perforated plates, side and end plates, trough bottom plates, reinforcements, base plates and cover plates. Specifically, the four-node, Shell Element SHELL63, was selected to model these structural components. This element models bending and membrane stresses, but omits transverse shear. The use of shell elements is appropriate for most of the structure where the characteristic thickness is small compared to the other plate dimensions. For thicker structures, such as the upper and lower

support rings, solid brick elements were used to provide the full 3D stress. Tie bars at dryer vane bank mid-height were modeled with BEAM188 beam elements. The elements SURF154 are used to assure proper application of pressure loading to the structure. Mesh details and element types are shown in Table 3 and Table 4, respectively.

The mesh is generated automatically by ANSYS with refinement near edges. The maximum allowable mesh spacing is specified by the user. Here a 2.5 inch maximum allowable spacing is specified everywhere except in the following areas: drain pipes (2 inch maximum spacing); perforated plates (2 inches); and the curved portions of the drain channels (1.5 inches). Details of the finite element mesh are shown in Figure 6. Numerical experiments carried out using the ANSYS code applied to simple analytically tractable plate structures with dimensions and mesh spacings similar to the ones used for the steam dryer, confirm that the natural frequencies are accurately recovered (less than 1% errors for the first modes). These errors are compensated for by the use of frequency shifting.

3.9 Connections Between Structural Components

Most connections between parts are modeled as node-to-node connections. This is the correct manner (i.e., within the finite element framework) of joining elements away from discontinuities. At joints between shells, this approach omits the additional stiffness provided by the extra weld material. Also, locally 3D effects are more pronounced. The latter effect is accounted for using weld factors. The deviation in stiffness due to weld material is negligible, since weld dimensions are on the order of the shell thickness. The consequences upon modal frequencies and amplitude are, to first order, proportional to t/L where t is the thickness and L a characteristic shell length. The errors committed by ignoring additional weld stiffness are thus small and readily compensated for by performing frequency shifts.

When joining shell and solid elements, however, the problem arises of properly constraining the rotations, since shell element nodes contain both displacement and rotational degrees of freedom at every node whereas solid elements model only the translations. A node-to-node connection would effectively appear to the shell element as a simply supported, rather than (the correct) cantilevered restraint and significantly alter the dynamic response of the shell structure.

To address this problem, constraint equations are used to properly connect adjacent shell- and solid-element modeled structures. Basically, all such constraints express the deflection (and rotation for shell elements) of a node, \mathbf{R}_1 , on one structural component in terms of the deflections/rotations of the corresponding point, \mathbf{P}_2 , on the other connected component. Specifically, the element containing \mathbf{P}_2 is identified and the deformations at \mathbf{P}_2 determined by interpolation between the element nodes. The following types of shell-solid element connections are used in the steam dryer model including the following:

1. Connections of shell faces to solid faces (Figure 7a). While only displacement degrees of freedom are explicitly constrained, this approach also implicitly constrains the rotational degrees of freedom when multiple shell nodes on a sufficiently dense grid are connected to the same solid face.
2. Connections of shell edges to solids (e.g., connection of the bottom of closure plates with the upper ring). Since solid elements do not have rotational degrees of freedom, the

coupling approach consisted of having the shell penetrate into the solid by one shell thickness and then constraining both the embedded shell element nodes (inside the solid) and the ones located on the surface of the solid structure (see Figure 7b). Numerical tests involving simple structures showed that this approach and penetration depth reproduce both the deflections and stresses of the same structure modeled using only solid elements or ANSYS' bonded contact technology. Continuity of rotations and displacements is achieved.

The use of constraint conditions rather than the bonded contacts advocated by ANSYS for connecting independently meshed structural components confers better accuracy and useful numerical advantages to the structural analysis of the steam dryer including better conditioned and smaller matrices. The smaller size results from the fact that equations and degrees of freedom are eliminated rather than augmented (in Lagrange multiplier-based methods) by additional degrees of freedom. Also, the implementation of contact elements relies on the use of very high stiffness elements (in penalty function-based implementations) or results in indefinite matrices (Lagrange multiplier implementations) with poorer convergence behavior compared to positive definite matrices.

The upper support ring rests on four support blocks which resist vertical and lateral displacement. Because the contact region between the blocks and upper support ring is small, the ring is considered free to rotate about the radial axis. Specifically nodal constraints (zero relative displacement) are imposed over the contact area between the steam dryer upper support ring and the support blocks. Two nodes on each support block are fixed as indicated in Figure 8. One node is at the center of the support block surface facing the vessel and the other node is 0.5" offset inside the block towards the steam dryer, half way to the nearest upper support ring node. This arrangement approximates the nonlinear contact condition where the ring can tip about the block.

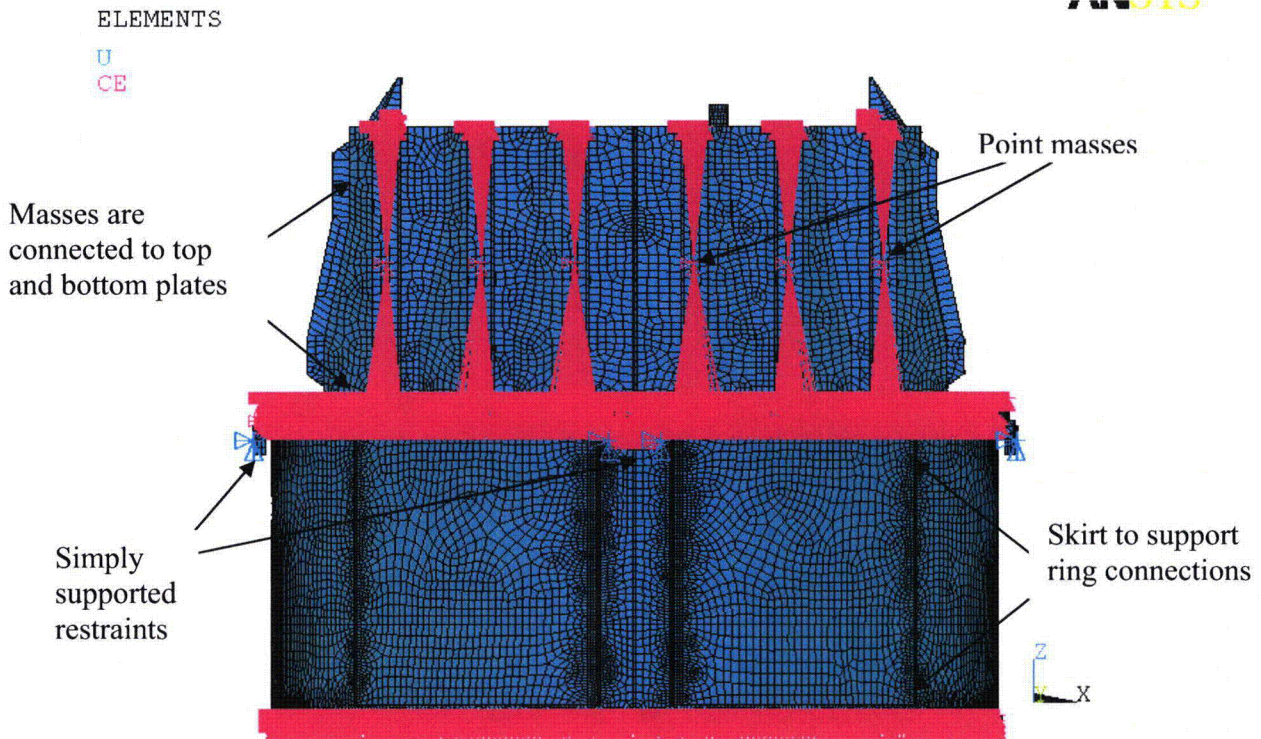


Figure 5. Point masses representing the vanes. The pink shading represents where constraint equations between nodes are applied.

Table 3. FE Model Summary.

Description	Quantity
Total Nodes ¹	133,622
Total Elements	119,408

1. Not including additional damper nodes and elements.

Table 4. Listing of Element Types.

Generic Element Type Name	Element Name	ANSYS Name
20-Node Quadratic Hexahedron	SOLID186	20-Node Hexahedral Structural Solid
10-Node Quadratic Tetrahedron	SOLID187	10-Node Tetrahedral Structural Solid
4-Node Elastic Shell	SHELL63	4-Node Elastic Shell
Mass Element	MASS21	Structural Mass
Pressure Surface Definition	SURF154	3D Structural Surface Effect
Beam element	BEAM188	3-D Finite Strain Beam
Damper element	COMBIN14	Spring-Damper

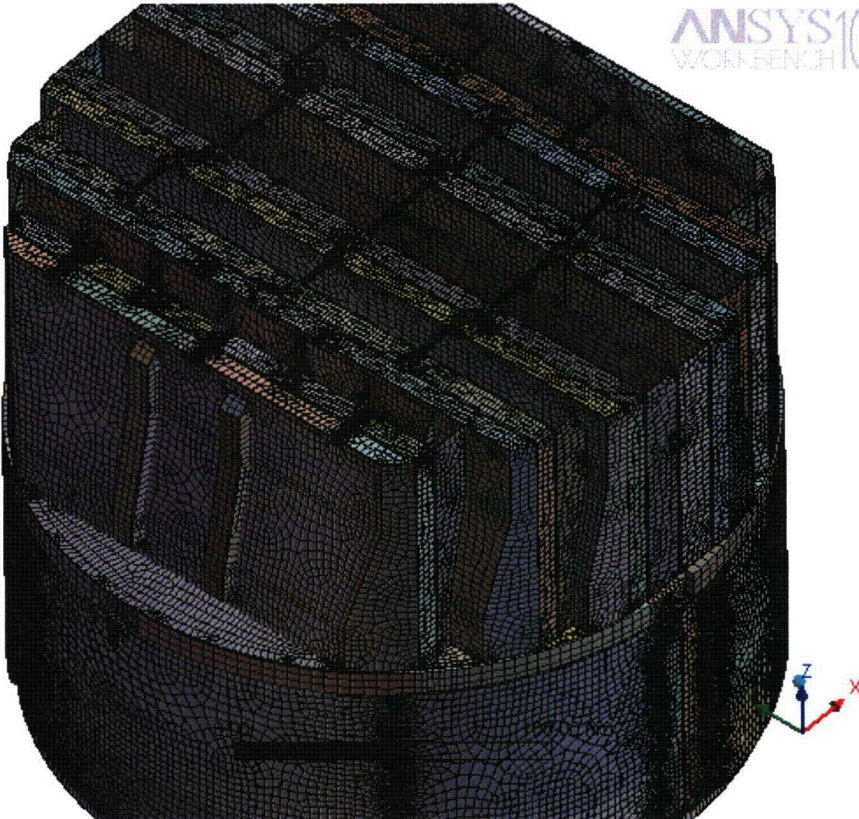


Figure 6a. Mesh overview.

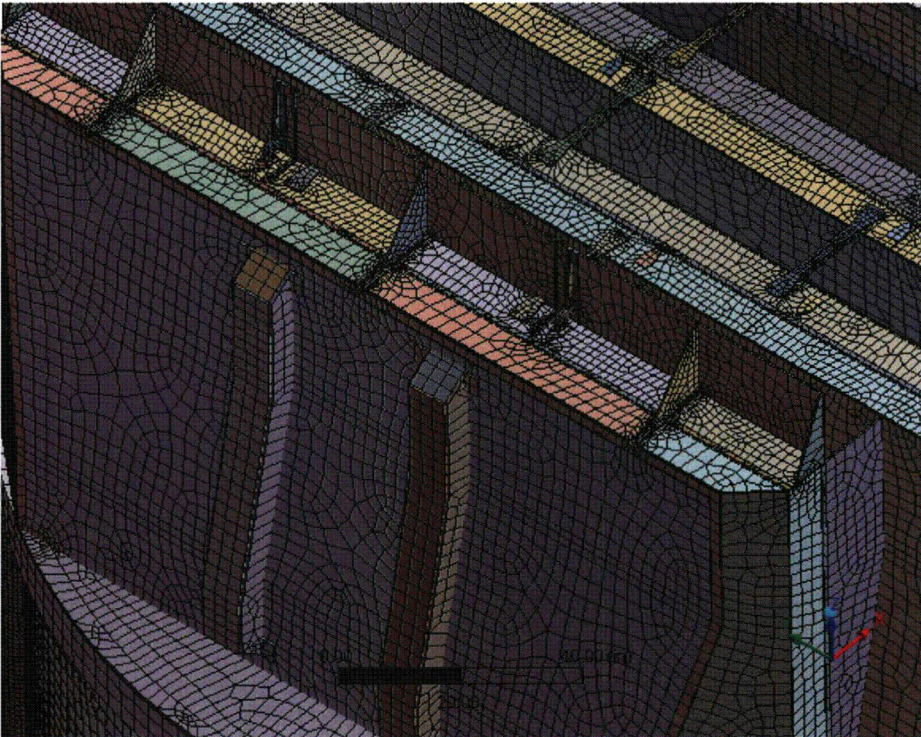


Figure 6b. Close-up of mesh showing hoods and hood assemblies.

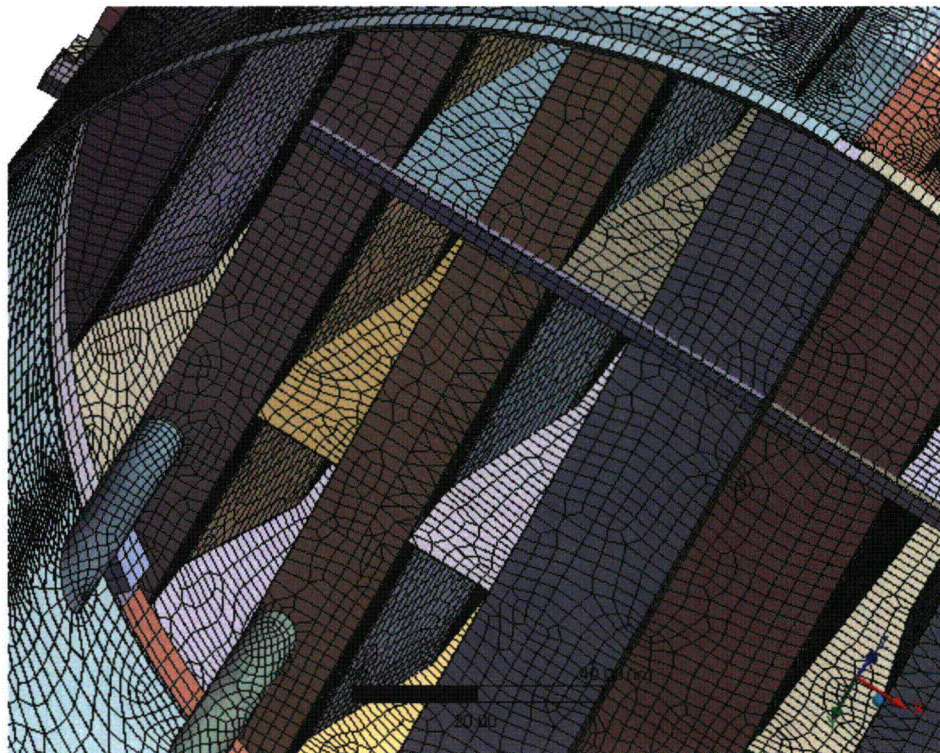


Figure 6c. Close-up of mesh showing drain pipes and hood supports; supporting beams and base plates.

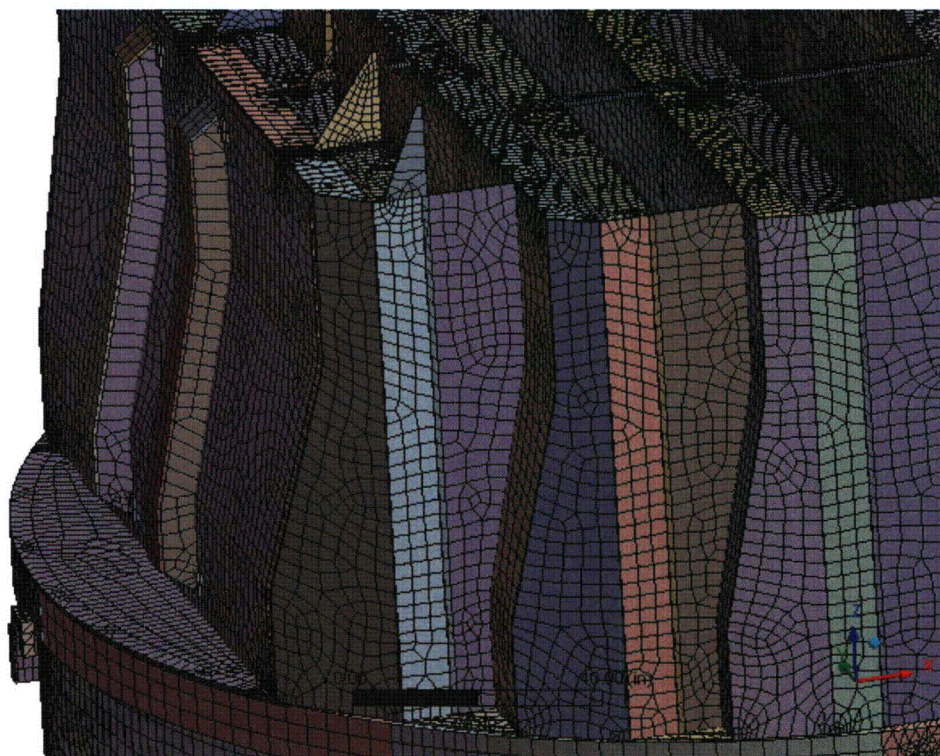


Figure 6d. Close-up of mesh showing node-to-node connections between various plates.

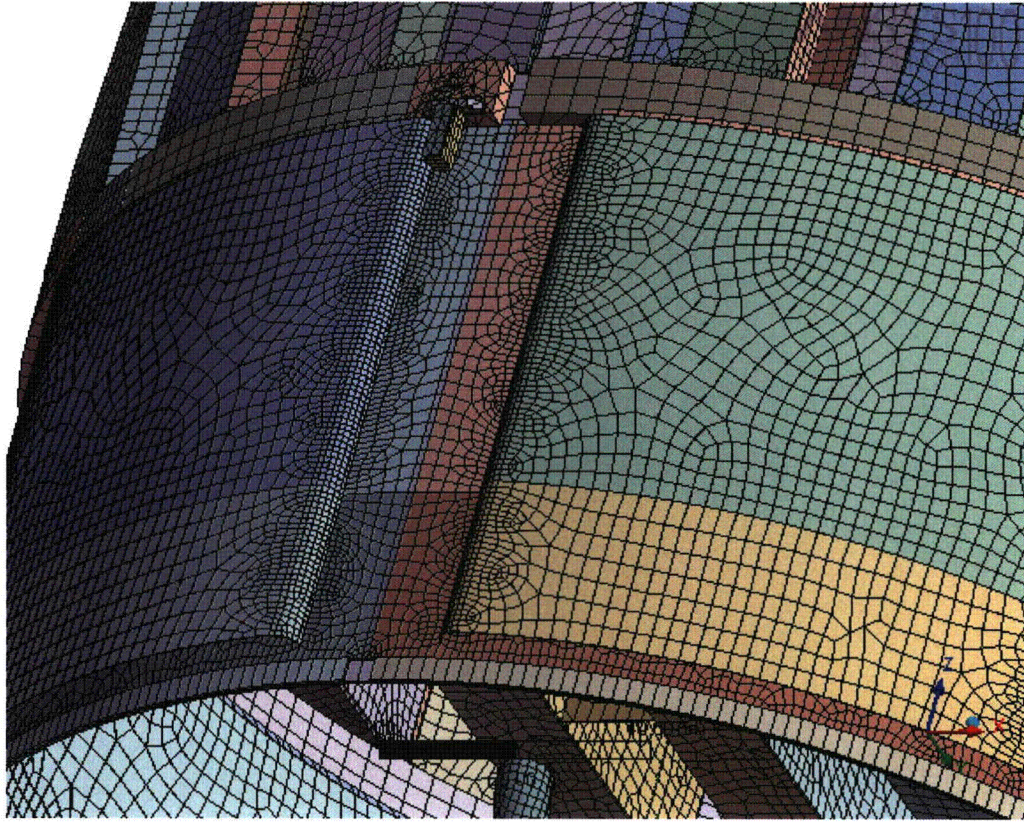


Figure 6e. Close-up of mesh showing node-to-node connections between the skirt and drain channels.

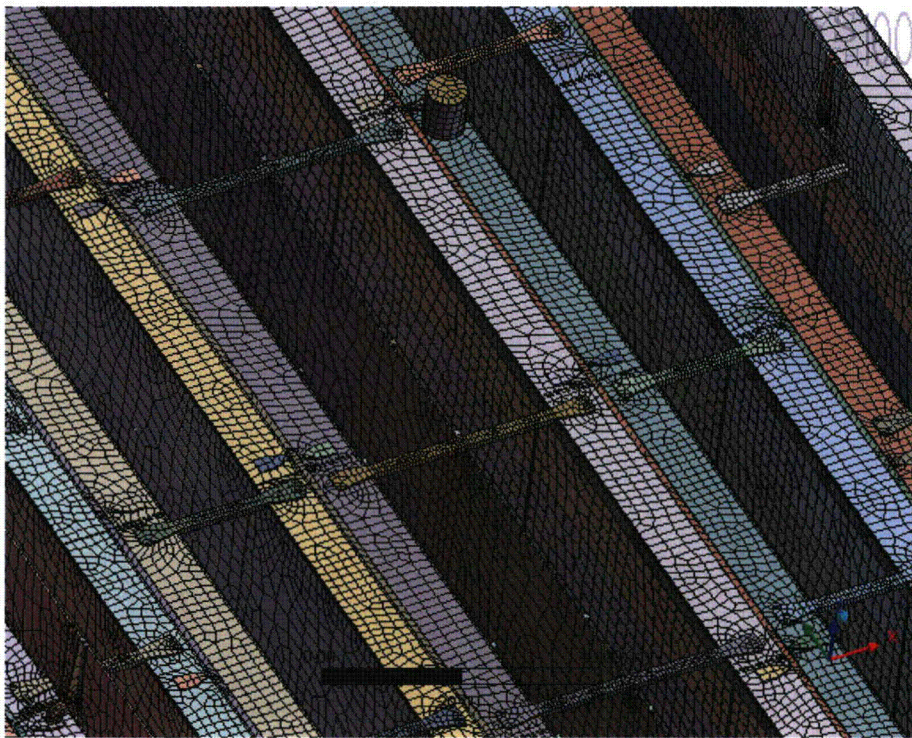
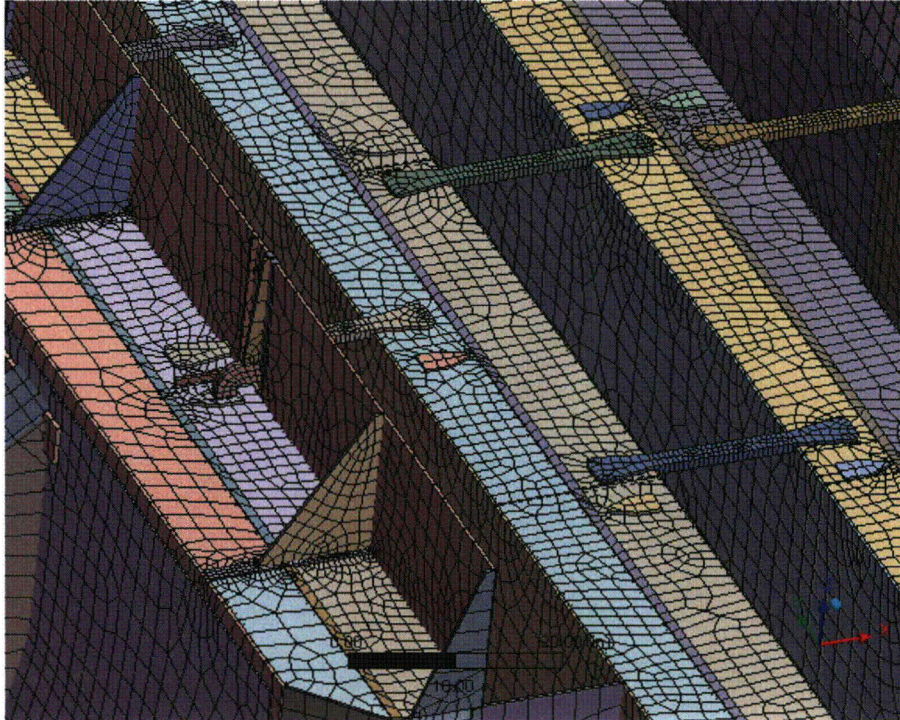


Figure 6f. Close-up view of tie bars connecting vane cover plates and adjacent to the steam dam.

Shell nodes DOF are related to solid element shape functions

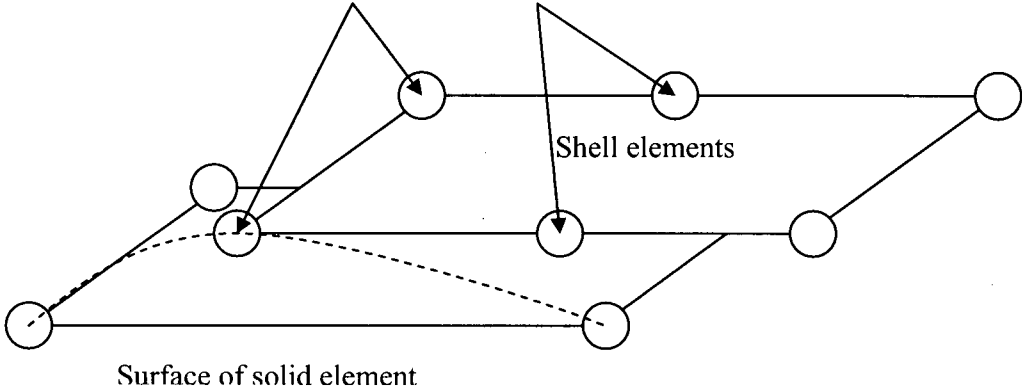


Figure 7a. Face-to-face shell to solid connection.

Shell nodes DOF are related to solid element shape functions

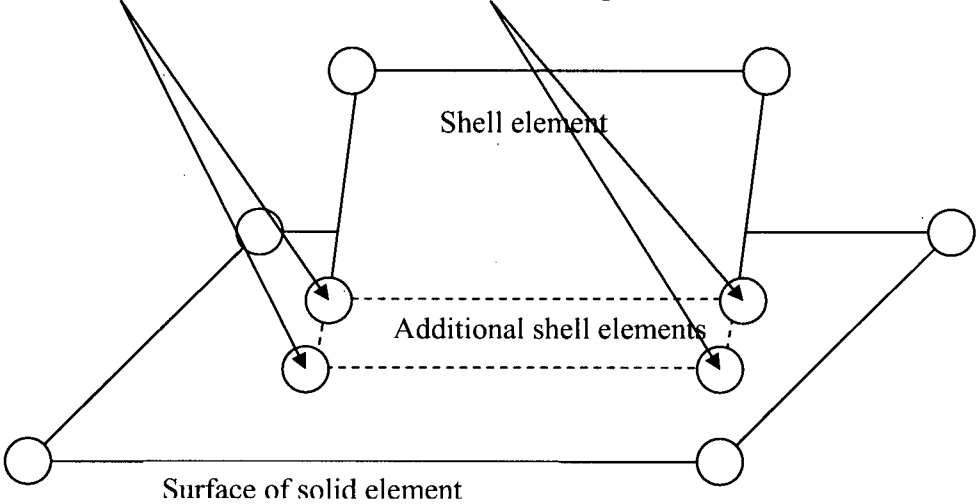


Figure 7b. Shell edge-to-solid face connection.

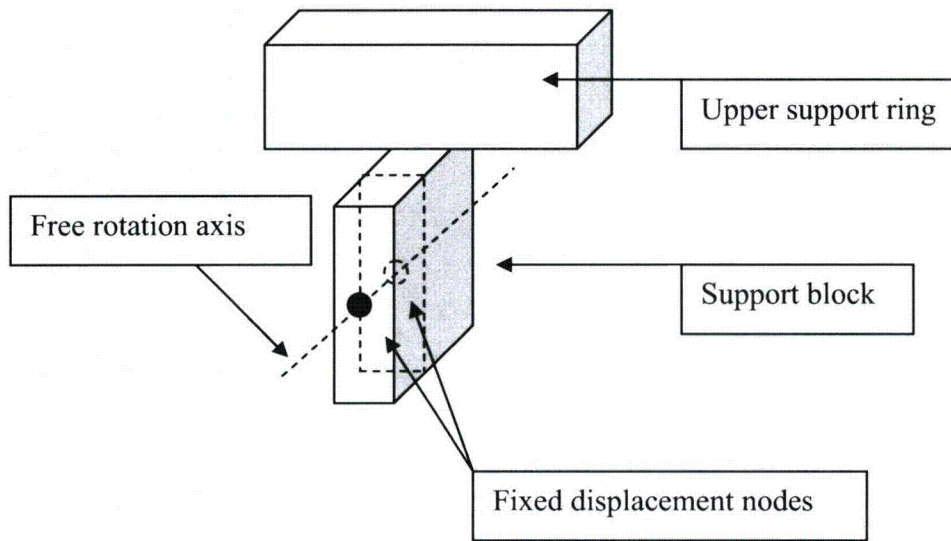


Figure 8. Boundary conditions. Inside node is half way between outer surface of support block and upper support ring.

3.10 Pressure Loading

The harmonic loads are produced by the pressures acting on the exposed surfaces of the steam dryer. At every frequency and for each MSL, the pressure distribution corresponding to a unit pressure at the MSL inlet is represented on a three-inch grid lattice grid (i.e., a mesh whose lines are aligned with the x-, y- and z-directions) that is superimposed over the steam dryer surface. This grid is compatible with the "TableLoads" format used by ANSYS to "paint" general pressure distributions upon structural surfaces. The pressures are obtained from the Helmholtz solver routine in the acoustic analysis [1].

In general, the lattice nodes do not lie on the surface, so that to obtain the pressure differences at the surface, it is necessary to interpolate the pressure differences stored at the lattice nodes. This is done using simple linear interpolation between the eight forming nodes of the lattice cell containing the surface point of interest. Inspection of the resulting pressures at selected nodes shows that these pressures vary in a well-behaved manner between the nodes with prescribed pressures. Graphical depictions of the resulting pressures and comparisons between the peak pressures in the original nodal histories and those in the final surface load distributions produced in ANSYS, all confirm that the load data are interpolated accurately and transferred correctly to ANSYS.

The harmonic pressure loads are only applied to surfaces above the water level, as indicated in Figure 9. In addition to the pressure load, the static loading induced by the weight of the steam dryer is analyzed separately. The resulting static and harmonic stresses are linearly combined to obtain total values which are then processed to calculate maximum and alternating stress intensities for assessment in Section 5.

[[

[2]
(3)]] This is useful since revisions in the loads model do not necessitate recalculation of the unit stresses.



NODES

PRES-NORM

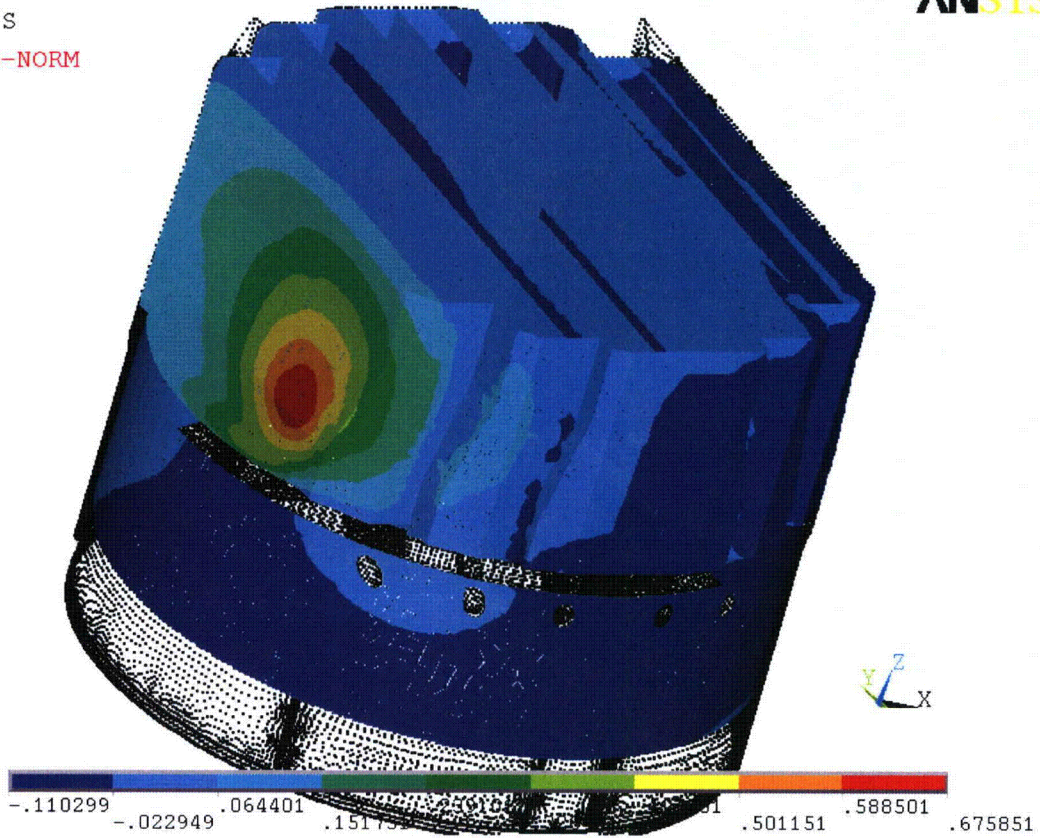


Figure 9a. Real part of unit pressure loading MSL C (in psid) on the steam dryer at 50.2 Hz. No loading is applied to the submerged surface.



NODES
PRES-NORM

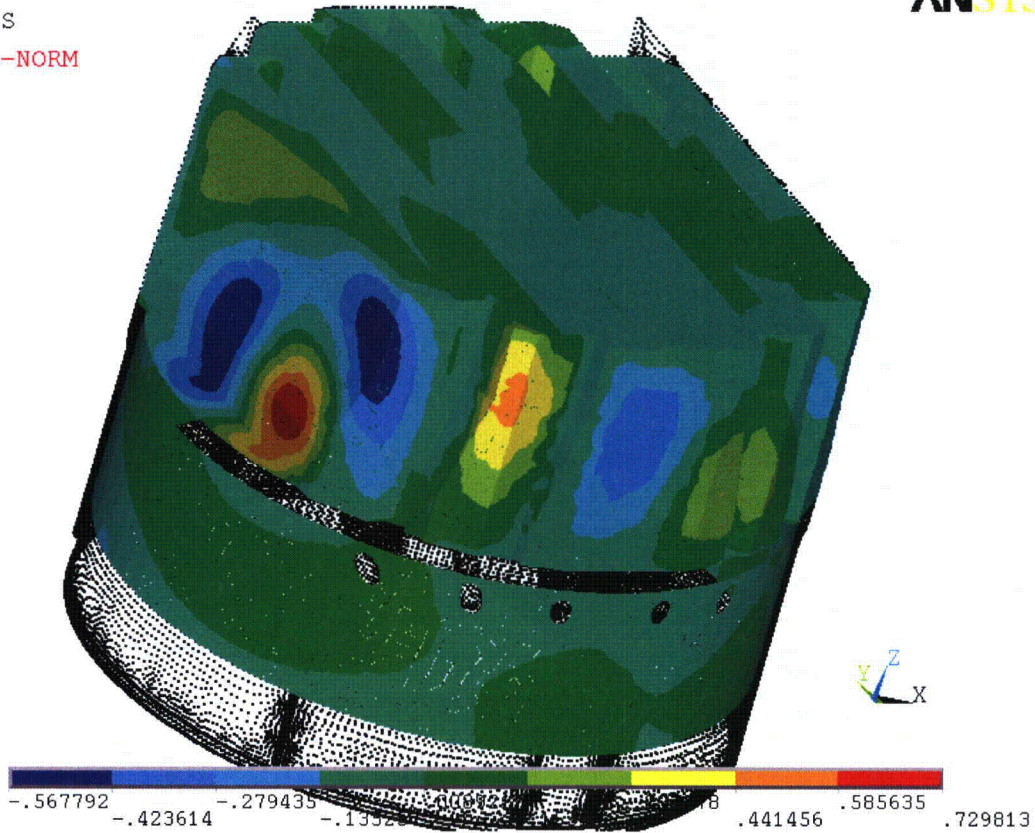


Figure 9b. Real part of unit pressure loading MSL C (in psid) on the steam dryer at 200.9 Hz. No loading is applied to the submerged surface.

4. Structural Analysis

The solution is decomposed into static and harmonic parts, where the static solution produces the stress field induced by the supported structure subjected to its own weight and the harmonic solution accounts for the harmonic stress field due to the unit pressure of given frequency in one of the main steam lines. All solutions are linearly combined, with amplitudes provided by signal measurements in each steam line, to obtain the final displacement and stress time histories. This decomposition facilitates the prescription of the added mass model accounting for hydrodynamic interaction and allows one to compare the stress contributions arising from static and harmonic loads separately. Proper evaluation of the maximum membrane and membrane+bending stresses requires that the static loads due to weight be accounted for. Hence both static and harmonic analyses are carried out.

4.1 Static Analysis

The results of the static analysis are shown in Figure 10. The locations with highest stress include the upper support ring areas near the support brackets with stress intensity 5,831 psi.

4.2 Harmonic Analysis

The harmonic pressure loads were applied to the structural model at all surface nodes described in Section 3.10. Typical stress intensity distributions over the structure are shown in Figure 11. Stresses were calculated for each frequency, and results from static and harmonic calculations were combined.

To evaluate maximum stresses, the stress harmonics including the static component are transformed into a time history using FFT, and the maximum and alternating stress intensities for the response, evaluated. According to ASME B&PV Code, Section III, Subsection NG-3216.2 the following procedure was established to calculate alternating stresses. For every node, the stress difference tensors, $\sigma'_{nm} = \sigma_n - \sigma_m$, are considered for all possible pairs of the stresses σ_n and σ_m at different time levels, t_n and t_m . Note that all possible pairs require consideration, since there are no "obvious" extrema in the stress responses. However, in order to contain computational cost, extensive screening of the pairs takes place (see Section 2.3), so that pairs known to produce alternating stress intensities less than 1,500 psi are rejected. For each remaining stress difference tensor, the principal stresses S_1, S_2, S_3 are computed and the maximum absolute value among principal stress differences, $S_{nm} = \max\{|S_1 - S_2|, |S_1 - S_3|, |S_2 - S_3|\}$, obtained. The alternating stress at the node is then one-half the maximum value of S_{nm} taken over all combinations (n,m), i.e., $S_{alt} = \frac{1}{2} \max_{n,m} \{S_{nm}\}$. This alternating stress is compared against allowable values, depending on the node location with respect to welds.



NODAL SOLUTION

STEP=1

SUB =1

TIME=1

USUM (AVG)

RSYS=0

DMX =.059243

SMN =.001387

SMX =.059243

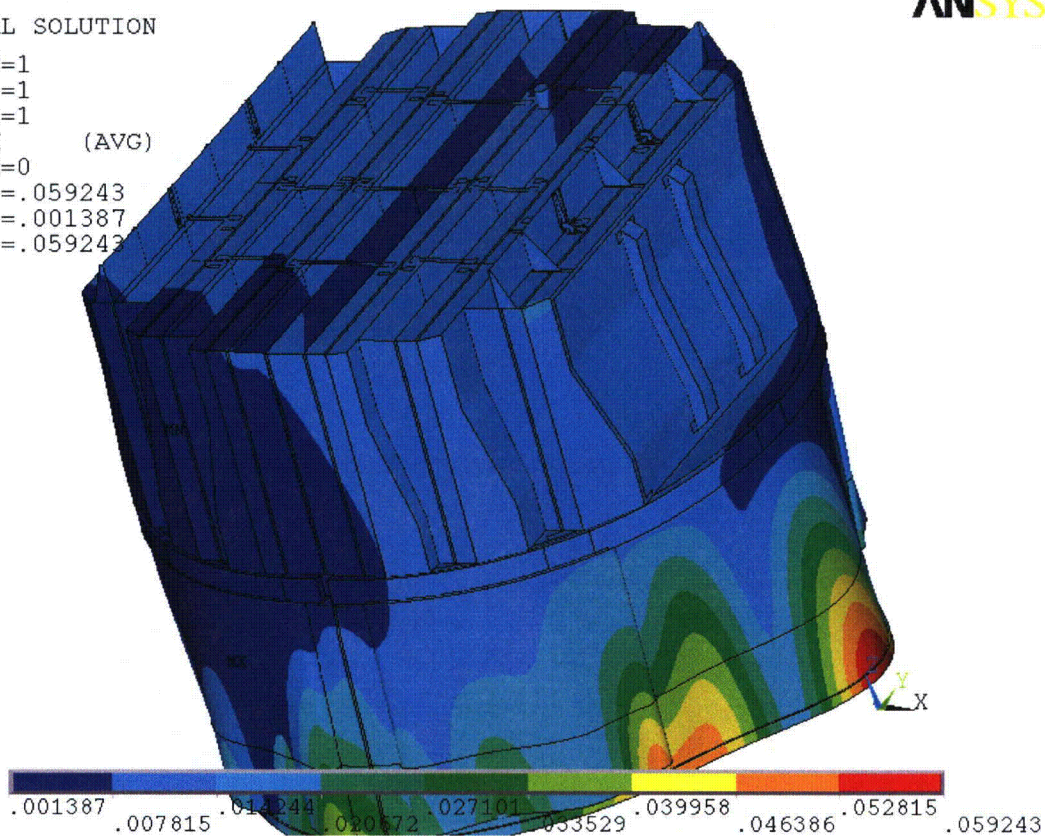


Figure 10a. Overview of static calculations showing displacements (in inches). Maximum displacement (DMX) is 0.06 inches. Note that displacements are amplified for visualization.



```
NODAL SOLUTION
STEP=1
SUB =1
TIME=1
SINT      (AVG)
DMX =.059243
SMN =.427543
SMX =5831
```

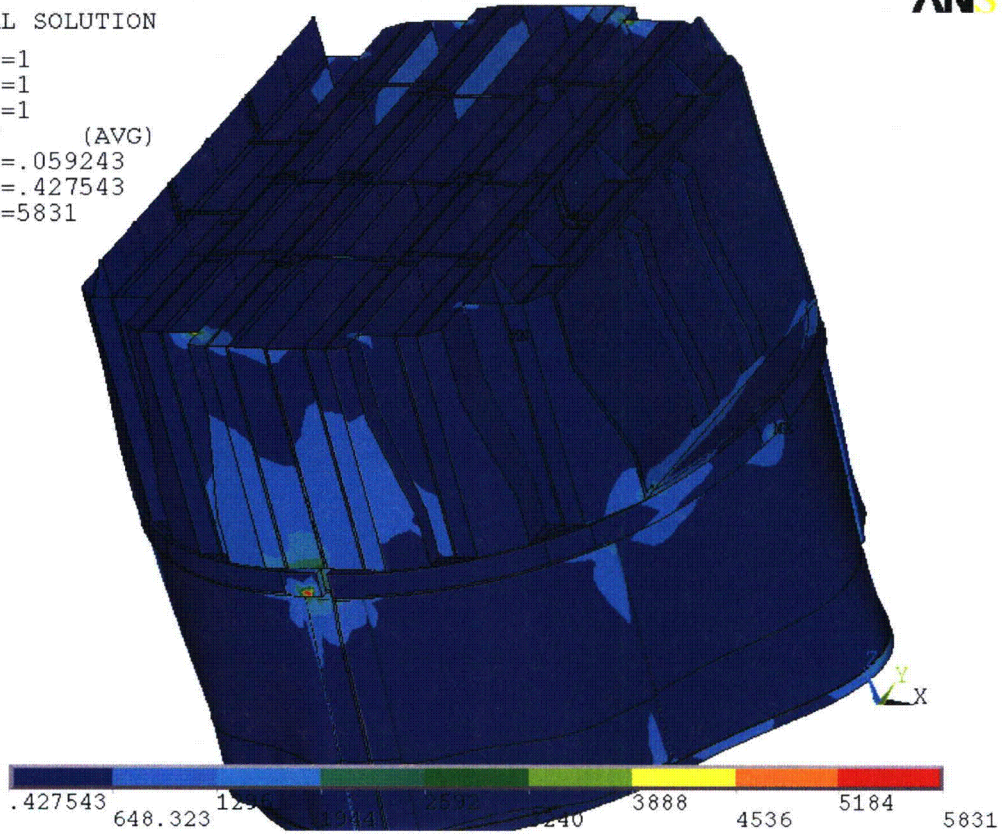


Figure 10b. Overview of static calculations showing stress intensities (in psi). Maximum stress intensity (SMX) is 5,831 psi. Note that displacements are amplified for visualization.



NODAL SOLUTION

STEP=307
SUB =1
FREQ=50.207
REAL ONLY
SINT (AVG)
DMX =.088935
SMN =1.9
SMX =8877

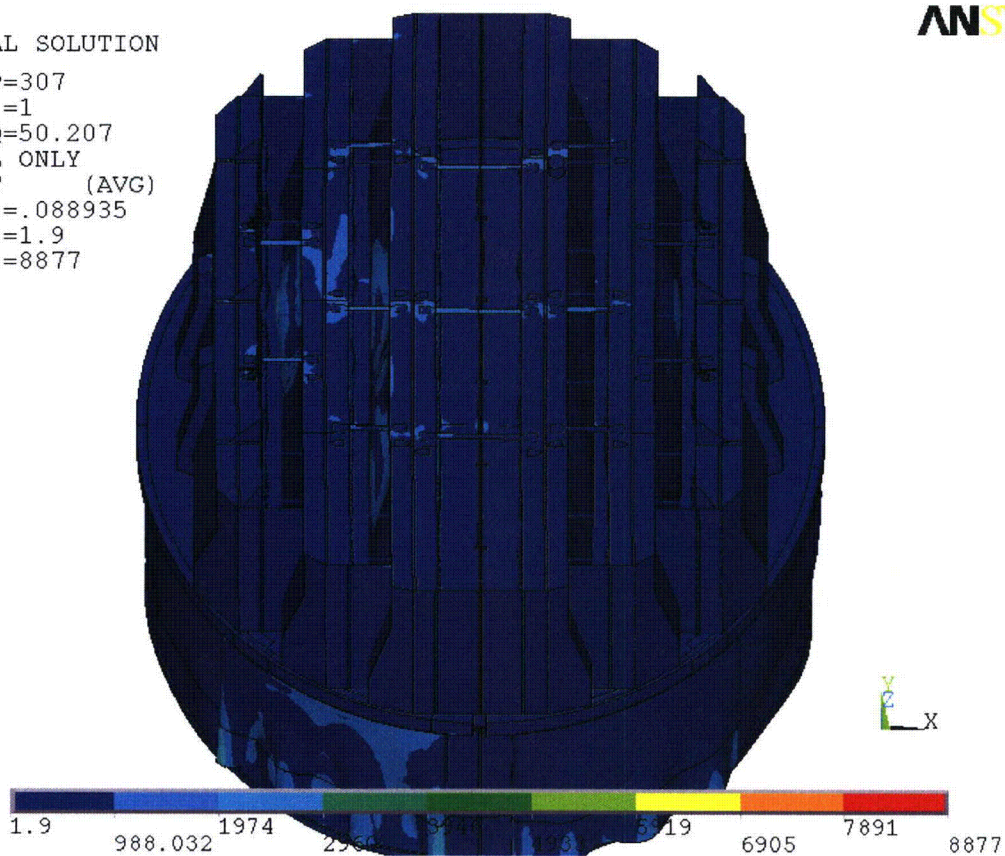


Figure 11a. Overview of harmonic calculations showing real part of stress intensities (in psi) along with displacements. Unit loading MSL C at 50.2 Hz.



NODAL SOLUTION

STEP=251

SUB =1

FREQ=200.885

REAL ONLY

SINT (AVG)

DMX =.007797

SMN =.20593

SMX =3718

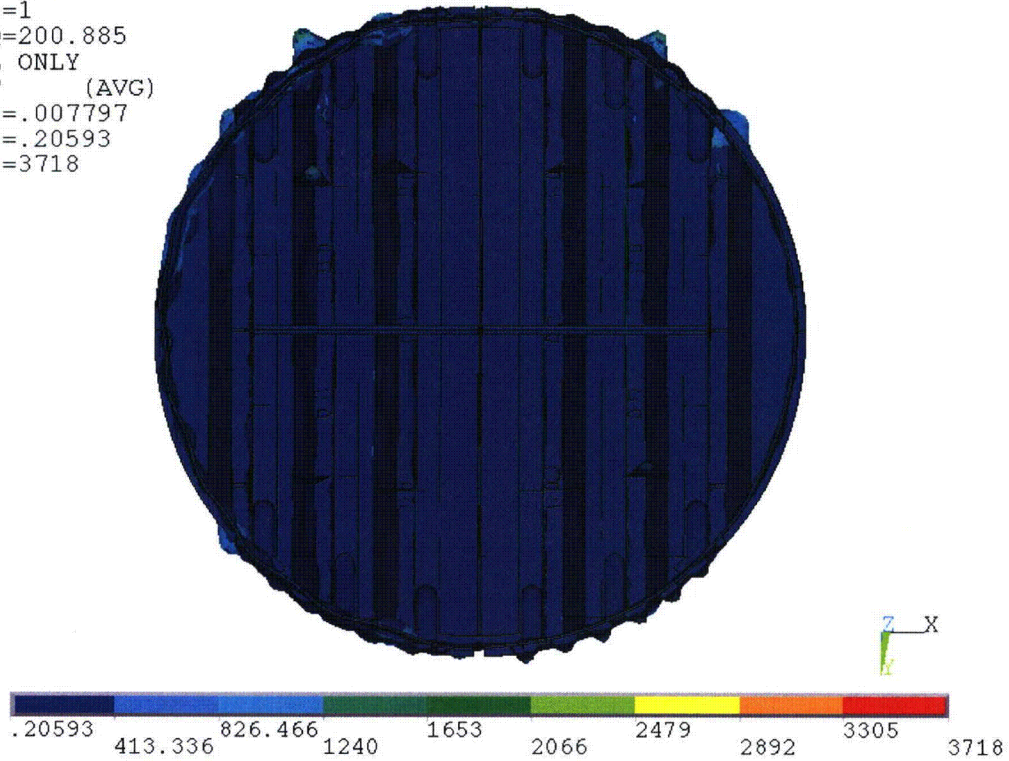


Figure 11b. Overview of harmonic calculations showing real part of stress intensities (in psi) along with displacements. Unit loading MSL C at 200.9 Hz.

4.3 Post-Processing

The static and transient stresses computed at every node with ANSYS were exported into files for subsequent post-processing. These files were then read into separate customized software to compute the maximum and alternating stresses at every node. The maximum stress was defined for each node as the largest stress intensity occurring during the time history. Alternating stresses were calculated according to the ASME standard described above. For shell elements the maximum stresses were calculated separately at the mid-plane, where only membrane stress is present, and at top/bottom of the shell, where bending stresses are also present.

For nodes that are shared between several structural components or lie on junctions, the maximum and alternating stress intensities are calculated as follows. First, the nodal stress tensor is computed separately for each individual component by averaging over all finite elements meeting at the node and belonging to the same structural component. The time histories of these stress tensors are then processed to deduce the maximum and alternating stress intensities for each structural component. Finally, for nodes shared across multiple components, the highest of the component-wise maximum and alternating stresses is recorded as the "nodal" stress. This approach prevents averaging of stresses across components and thus yields conservative estimates for nodal stresses at the weld locations where several components are joined together.

The maximum stresses are compared against allowable values which depend upon the stress type (membrane, membrane+bending, alternating – P_m , P_m+P_b , S_{alt}) and location (at a weld or away from welds). These allowables are specified in the following section. For solid elements the most conservative allowable for membrane stress, P_m , is used, although bending stresses are nearly always present also. The structure is then assessed in terms of stress ratios formed by dividing allowables by the computed stresses at every node. Stress ratios less than unity imply that the associated maximum and/or alternating stress intensities exceed the allowable levels. Post-processing tools calculate the stress ratios, identifying the nodes with low stress ratios and generating files formatted for input to the 3D graphics program, TecPlot, which provides more general and sophisticated plotting options than currently available in ANSYS.

4.4 Computation of Stress Ratios for Structural Assessment

The ASME B&PV Code, Section III, subsection NG provides different allowable stresses for different load combinations and plant conditions. The stress levels of interest in this analysis are for the normal operating condition, which is the Level A service condition. The load combination for this condition is:

$$\text{Normal Operating Load Combination} = \text{Weight} + \text{Pressure} + \text{Thermal}$$

The weight and fluctuating pressure contributions have been calculated in this analysis and are included in the stress results. The static pressure differences and thermal expansion stresses are small, since the entire steam dryer is suspended inside the reactor vessel and all surfaces are exposed to the same conditions. Seismic loads only occur in Level B and C cases, and are not considered in this analysis.

Allowable Stress Intensities

The ASME B&PV Code, Section III, subsection NG shows the following (Table 5) for the maximum allowable stress intensity (S_m) and alternating stress intensity (S_a) for the Level A service condition. The allowable stress intensity values for type 304 stainless steel at operating temperature 550°F are taken from Table I-1.2 and Fig. I-9.2.2 of Appendix I of Section III, in the ASME B&PV Code. The calculation for different stress categories is performed in accordance with Fig. NG-3221-1 of Division I, Section III, subsection NG.

Table 5. Maximum Allowable Stress Intensity and Alternating Stress Intensity for all areas other than welds. The notation P_m represents membrane stress; P_b represents stress due to bending; Q represents secondary stresses (from thermal effects and gross structural discontinuities, for example); and F represents additional stress increments (due to local structural discontinuities, for example).

Type	Notation	Service Limit	Allowable Value (psi)
<i>Maximum Stress Allowables:</i>			
General Membrane	P_m	S_m	18,300
Membrane + Bending	$P_m + P_b$	$1.5 S_m$	27,450
Primary + Secondary	$P_m + P_b + Q$	$3.0 S_m$	54,900
<i>Alternating Stress Allowable:</i>			
Peak = Primary + Secondary + F	S_{alt}	S_a	13,600

When evaluating welds, either the calculated or allowable stress was adjusted, to account for stress concentration factor and weld quality. Specifically:

- For maximum allowable stress intensity, the allowable value is decreased by multiplying its value in Table 5 by 0.55.
- For alternating stress intensity, the calculated weld stress intensity is multiplied by a weld stress intensity (fatigue) factor of 1.8, before comparison to the S_a value given above.

The weld factors of 0.55 and 1.8 were selected based on the observable quality of the shop welds and liquid penetrant NDE testing of all welds (excluding tack and intermittent welds, which were subject to 5X visual inspection) during fabrication. These factors are consistent with fatigue strength reduction factors recommended by the Welding Research Council, [14], and stress concentration factors at welds, provided in [15] and [16]. In addition, critical welds are subject to periodical visual inspections in accordance with the requirements of GE SIL 644 SIL and BWR VIP-139 [17]. Therefore, for weld stress intensities, the allowable values are shown in Table 6.

These factors (0.55 and 1.8) also conservatively presume that the structure is joined using fillet welds unless specified otherwise. Since fillet welds correspond to larger stress concentration factors than other types of welds, this assumption is a conservative one.

Table 6. Weld Stress Intensities.

Type	Notation	Service Limit	Allowable Value (psi)
<i>Maximum Stress Allowables:</i>			
General Membrane	Pm	0.55 Sm	10,065
Membrane + Bending	Pm + Pb	0.825 Sm	15,098
Primary + Secondary	Pm + Pb + Q	1.65 Sm	30,195
<i>Alternating Stress Allowables:</i>			
Peak = Primary + Secondary + F	S _{alt}	Sa	13,600

Comparison of Calculated and Allowable Stress Intensities

The classification of stresses into general membrane or membrane + bending types was made according to the exact location, where the stress intensity was calculated; namely, general membrane, Pm, for middle surface of shell element, and membrane + bending, Pm + Pb, for other locations. For solid elements the most conservative, general membrane, Pm, allowable is used.

The structural assessment is carried out by computing stress ratios between the computed maximum and alternating stress intensities, and the allowable levels. Locations where any of the stresses exceed allowable levels will have stress ratios less than unity. Since computation of stress ratios and related quantities within ANSYS is time-consuming and awkward, a separate FORTRAN code was developed to compute the necessary maximum and alternating stress intensities, Pm, Pm+Pb, and S_{alt}, and then compare it to allowables. Specifically, the following quantities were computed at every node:

1. The maximum membrane stress intensity, Pm (evaluated at the mid-thickness location for shells),
2. The maximum membrane+bending stress intensity, Pm+Pb, (taken as the largest of the maximum stress intensity values at the bottom, top, and mid thickness locations, for shells),
3. The alternating stress, S_{alt}, (the maximum value over the three thickness locations is taken).
4. The stress ratio due to a maximum stress intensity assuming the node lies at a non-weld location (note that this is the minimum ratio obtained considering both membrane stresses and membrane+bending stresses):

$$SR-P(nw) = \min \{ Sm/Pm, 1.5 * Sm/(Pm+Pb) \}.$$
5. The alternating stress ratio assuming the node lies at a non-weld location,

$$SR-a(nw) = Sa / (1.1 * S_{alt}),$$
6. The same as 4, but assuming the node lies on a weld,

$$SR-P(w) = SR-P(nw) * f_{sw} * 0.55$$
7. The same as 5, but assuming the node lies on a weld,

$$SR-a(w) = SR-a(nw) * f_{sw} / 1.8.$$

where $f_{sw}=1$ at all welds (when justified, f_{sw} can be adjusted to reflect different weld types). Note that in steps 4 and 6, the minimum of the stress ratios based on P_m and P_m+P_b , is taken. The allowables listed in Table 5, $S_m=18,300$ psi and $S_a=13,600$ psi. The factors, 0.55 and 1.8, are the weld factors discussed above. The factor of 1.1 accounts for the differences in Young's moduli for the steel used in the steam dryer and the values assumed in alternating stress allowable. According to NG-3222.4 in subsection NG of Section III of the ASME Code, the effect of elastic modulus upon alternating stresses is taken into account by multiplying alternating stress S_{alt} at all locations by the ratio, $E/E_{model}=1.1$, where:

$$E = 28.3 \cdot 10^6 \text{ psi, as shown on Fig. I-9.2.2. ASME BP\&V Code}$$
$$E_{model} = 25.55 \cdot 10^6 \text{ psi (Table 1)}$$

The nodes with stress ratios lower than 4 are plotted in TecPlot (a 3D graphics plotting program widely used in engineering communities [18]) to establish whether they lie on a weld or not. The appropriate maximum and alternating stress ratios, SR-P and SR-a, are thus determined and a final listing of nodes having the smallest stress ratios is generated. These nodes are tabulated and depicted in the Results Sections.

4.5 Substructure Modeling

In order to maintain computational costs at a feasible level, the steam dryer model is predominantly comprised of shell elements. These elements are well suited for structures such as the steam dryer consisting of shell-like components and tend to produce conservative estimates of the stresses. In some cases however, such as welded junctions involving multiple components, shell element models can overestimate the nominal stress intensities in the vicinity of the junctions. In such cases a more refined analysis using solid elements to capture the complete 3D stress distribution, is warranted. Therefore, to efficiently analyze complex structures such as steam dryers, a standard engineering practice is to first analyze the structure using a shell-based model. If any locations with high stresses are identified these regions are examined in greater detail using 3D solid elements to obtain a more definitive stress prediction.

In the BFN1 steam dryer, two locations were identified as requiring a more refined stress analysis: (i) the bottom of the skirt/drain channel junction and (ii) the intersection between the bottom of the inner hood, hood support (stiffener) and base plate. The first location is characterized by a previously thickened continuous weld that wraps around the bottom of the drain channel and up along the interior of the channel. The second location involves the junction between three elements and experienced an alternating stress ratio of $SR-a=2.62$ in [3]. Although this stress ratio is comparatively high, it is nevertheless of concern because it is difficult to access.

These two locations were examined using detailed 3D solid element substructure models as reported in [19]. Based on these models, the nominal stress intensities computed by the 3D solid element model are lower than those obtained with the shell-based FEA used to analyze the complete steam dryer by factors of: (i) 0.58 for the bottom of the skirt/drain channel weld (a total of eight nodes) and (ii) 0.79 for the inner hood/hood support/base plate junction (a total of four nodes). The stress intensities predicted by the shell element-based analysis at these locations are therefore first multiplied by these factors to obtain more accurate

estimates of the nominal stresses. These are then multiplied by the 1.8 weld factor before comparing against allowables to obtain the alternating stress ratios.

5. Results

The stress intensities and associated stress ratios resulting from the Rev. 4 acoustic/hydrodynamic loads [2] with associated biases and uncertainties factored in, are presented below. The bias due to finite frequency discretization and uncertainty associated with the finite element model itself, are also factored in. In the following sections the highest maximum and alternating stress intensities are presented to indicate which points on the dryer experience significant stress concentration and/or modal response (Section 5.1). The lowest stress ratios obtained by comparing the stresses against allowable values, accounting for stress type (maximum and alternating) and location (on or away from a weld), are also reported (Section 5.2). Finally the frequency dependence of the stresses at nodes experiencing the lowest stress ratios is depicted in the form of accumulative PSDs (Section 5.3).

In each section results are presented both at nominal conditions (no frequency shift) and with frequency shift included. Unless specified otherwise, frequency shifts are generally performed at 2.5% increments. The tabulated stresses and stress ratios are obtained using a 'blanking' procedure that is designed to prevent reporting a large number of high stress nodes from essentially the same location on the structure. In the case of stress intensities this procedure is as follows. The relevant stress intensities are first computed at every node and then nodes sorted according to stress level. The highest stress node is noted and all neighboring nodes within 10 inches of the highest stress node and its symmetric images (i.e., reflections across the $x=0$ and $y=0$ planes) are "blanked" (i.e., excluded from the search for subsequent high stress locations). Of the remaining nodes, the next highest stress node is identified and its neighbors (closer than 10 inches) blanked. The third highest stress node is similarly located and the search continued in this fashion until all nodes are either blanked or have stresses less than half the highest value on the structure. For stress ratios, an analogous blanking procedure is applied. Thus the lowest stress ratio of a particular type in a 10" neighborhood and its symmetric images is identified and all other nodes in these regions excluded from listing in the table. Of the remaining nodes, the one with the lowest stress ratio is reported and its neighboring points similarly excluded, and so on until all nodes are either blanked or have a stress ratio higher than 4.

The measured CLTP strain gage signals contain significant contributions from non-acoustic sources such as sensor noise, MSL turbulence and pipe bending vibration that contribute to the hoop strain measurements. The ACM analysis does not distinguish between the acoustic and non-acoustic fluctuations in the MSL signals that could lead to sizeable, but fictitious acoustic loads and resulting stresses on the dryer. One way to remove these fictitious loads is to collect data with the system maintained at operating pressure (1000 psi) and temperature, but low (less than 20% of CLTP) flow. By operating the recirculation pumps at this condition, the background plant noise and vibrations remain present. At these conditions the acoustic loads are known to be negligible so that collected data, referred to as the 1000# data, originate entirely from non-acoustic sources such as sensor noise and mechanical vibrations. This information is valuable since it allows one to now distinguish between the acoustic and non-acoustic content in the CLTP signal and therefore modify the CLTP loads so that only the acoustic component is retained. For consistency, the 1000# strain gage signals are filtered in the same manner as the CLTP data and are fed into the ACM model to obtain the monopole and dipole signals at the MSL inlets. Since there is negligible flow, these signals are fictitious, i.e., the hoop strains

measured by the strain gages are not due to pressure fluctuations, but rather due to noise. However, under the supposition that these signals are acoustic in origin the hypothetical stresses due to these signals can nevertheless be computed.

The contribution of background noise in the Browns Ferry Unit 1 steam dryer was quantified by taking strain gage measurements at 9% power. Measurements taken for the BFN1 unit at increasing power levels indicate that the 9% signal measurements provide a conservative estimate of the noise at zero power [20]. At this level there are no significant acoustic sources. To compensate for the non-acoustic noise source represented in the 1000# data, the CLTP MSL inlet pressure signals are modified according to [20]:

$$P(f) = P_0(f) * \max \left[0.5, 1 - \frac{\bar{N}(f)}{\bar{P}_0(f)} \right] \quad (8)$$

where f is the frequency (in Hz), $P_0(f)$ is the MSL inlet pressure (monopole or dipole) at CLTP conditions before correction, $P(f)$ is the corresponding post-correction pressure and $\bar{N}(f)$ and $\bar{P}_0(f)$ are averaged pressure amplitudes associated with the 1000# data and CLTP data respectively. Specifically,

$$\bar{P}_0(f) = \frac{1}{2} \int_{f-1}^{f+1} |P_0(f)| df \quad (9)$$

where $|P_0(f)|$ denotes the absolute value of the complex quantity. Hence $\bar{P}_0(f)$ is the average amplitude of the CLTP pressure in the ± 1 Hz interval about frequency, f . The same definition, but using the 1000# pressure signal, is used for $\bar{N}(f)$. Note that this modification leaves the phase information in the original CLTP signal unchanged.

The applied load includes all biases and uncertainties for both the ACM (summarized in [2]) and the FEM. For the latter there are three main contributors to the bias and uncertainty. The first is an uncertainty (25.26%) that accounts for modeling idealizations (e.g., vane bank mass model), geometrical approximations and other discrepancies between the modeled and actual dryer such as neglecting of weld mass and stiffness in the FEA. The second contributor is a bias (9.53% - note that this has been increased from the 5.72% value previously used in [3]) accounting for discretization errors associated with using a finite size mesh, upon computed stresses. The third contributor is also a bias and compensates for the use of a finite discretization schedule in the construction of the unit solutions. The frequencies are spaced such that at 1% damping the maximum (worst case) error in a resonance peak is 5%. The average error for this frequency schedule is 1.72%.

5.1 General Stress Distribution and High Stress Locations

The maximum stress intensities obtained by post-processing the ANSYS stress histories for CLTP at nominal frequency and with frequency shift operating conditions are listed in Table 7. Contour plots of the stress intensities over the steam dryer structure are shown on Figure 12 (nominal frequency) and Figure 13 (maximum stress over all nine frequency shifts including

nominal). The figures are oriented to emphasize the high stress regions. Note that these stress intensities *do not* account for weld factors but include end-to-end bias and uncertainty and incorporate results from substructuring (see Section 4.5). Further, it should be noted that since the allowable stresses vary with location, stress intensities do not necessarily correspond to regions of primary structural concern. Instead, structural evaluation is more accurately made in terms of the stress ratios which compare the computed stresses to allowable levels with due account made for stress type and weld factors and also account for stress corrections obtained using high-detail substructure models. Comparisons on the basis of stress ratios are made in Section 5.2.

The maximum stress intensities in most areas are low (less than 500 psi, or 5% of the most conservative critical stress). For the membrane stresses (P_m) the high stress regions tend to occur at: (i) the restraint locations for the upper support ring and (ii) the upper edges of the closure plates. The first location is a very localized stress location and is believed to be significantly overestimated as a 'hot-spot' in the FEA. It experiences high stresses since the entire weight of the structure is transmitted through relatively small pads to the external structure. This stress is dominated by the static component. The closure plates experience high stresses since they restrain any motion of the adjacent vane banks. Other locations with $P_m > 2000$ psi include the bottom of the outer hood end plate, the bottoms of the hood/hood support/base plate junctions and the connections between the bottom support beam spanning the dryer, and the vane banks (see Figure 12b). Frequency shifting does not significantly alter the high P_m stress locations, again due to the dominance of the static (deadweight) load.

The membrane + bending stress ($P_m + P_b$) distributions evidence a stronger modal response. Modal excitations are most pronounced on the steam dams. Stress concentrations are observed at several locations coinciding with welds. The first pair of highest stress locations is the same as where for the highest membrane stresses and lies near the dryer supports. Note that these stresses occur in solid elements where no distinction is made between the membrane and bending stresses (this distinction is only appropriate for thin members such as shell and beam elements). The next set of locations (exemplified by the third entry in the table) involves the closure plate connections to the hoods or vane bank end plates. These stresses also appear to be dominated by the static component since alternating stresses are comparatively low. The drain channel/skirt welds show up as the 4th and 5th entries in Table 7b. These stresses contain a strong alternating stress contribution as discussed below. Other locations where $P_m + P_b$ stresses exceed the 1000 psi level include the bottom corners of the outer hood and the connections of the spanning support beam to the vane banks. These locations also had significant membrane stresses. Finally the regions about the upper ends of the reinforcement channels have significant $P_m + P_b$ stress intensities which are mostly due to vibratory response to the acoustic loads.

The alternating stress distributions in Figure 12 and Figure 13 indicate that these stresses are below 500 psi over most of the dryer. The submerged skirt, though not exposed to direct acoustic forcing, evidences a modal response due to coupling with the upper steam dryer structure subjected to acoustic loads. The highest alternating stress intensities occur on the welds joining the drain channel to the skirt. The particular nodes listed in the table are immediately above the lowest node on this weld. The stress intensity obtained with ANSYS for this lowest node is generally higher than that at weld nodes above it. However, as discussed in Section 4.5,

high resolution studies using a substructured model of this location shows that nominal stresses are actually lower by a factor of 0.58. Credit for this reduction is only taken for the bottom-most nodes. For the next nodes up along the weld, nominal stresses are also reduced, but no credit is taken for this stress reduction. Other nodes appearing in the Table 7b include: (i) the mid-plate (a non-weld location); (ii) the base of the old tie bar remnant that will be left in place to help support the steam dam; (iii) the connection between a mid-height tie bar to the perforated plate on the vane bank and (iv) the weld joining the top of the reinforcement channel to the outer hood. For locations (i)-(iv) the stress intensities when considering all frequency shifts are no higher than 12% above the values at zero shift. For the drain channel/skirt weld however, the highest stress intensity at zero shift is 1604 psi, so that the stress (2360 psi) at the +7.5% shift corresponds to a 47% increase.

Finally, for reference the highest stress intensities at any frequency shift for the locations in Table 7b are recomputed using the CLTP loads without noise removal and reported in Table 7c.

Table 7a. Locations with highest predicted stress intensities at CLTP conditions at zero frequency shift. Signal noise has been removed using 9% power data.

Stress Category	Location	Weld	Location (in) ^(a)			node ^(b)	Stress Intensities (psi)		
			x	y	z		P _m	P _m +P _b	S _{alt}
P _m	Upper Support Ring (USR)/Seismic Block/Support Part	No	122.1	-10	-9.5	122062	7701	7701	1756
"	USR part/Support/Support Part	No	7	122.3	-9.5	122280	6757	6757	1543
"	Top Cover Inner Hood/Middle Closure Plate/Inner Hood	Yes	31.5	108.4	88.9	95881	5763	6399	1100
"	Top Cover Middle Hood/Outer Closure Plate/Middle Hood	Yes	62.5	-85	88.9	90137	3915	4266	1521
"	Splice Bar/USR Part	Yes	-2.2	-119	0	122330	3825	3825	<500
P _m +P _b	USR/Seismic Block/Support Part	No	122.1	-10	-9.5	122062	7701	7701	1756
"	USR part/Support/Support Part	No	7	122.3	-9.5	122280	6757	6757	1543
"	Top Cover Inner Hood/Middle Closure Plate/Inner Hood	Yes	-31.5	-108.4	88.9	91141	5728	6594	975
"	Submerged Drain Channel/Skirt	Yes	-91	76.7	-99.5	98050	564	5237	1321
"	Top Cover Middle Hood/Outer Closure Plate/Middle Hood	Yes	62.5	-85	88.9	90137	3915	4266	1521
S _{alt}	Remaining tie bar (outer hood)/tie bar base	Yes	81.5	31.4	88.9	132385	2252	2252	2126
"	Mid Plate	No	0	-3.9	88.2	23883	183	2209	2032
"	Outer Hood/Hood Mod	Yes	93.5	-20	86.9	89590	120	2146	1925
"	Mid Bottom Perf Plate Exit/Mid Top Perf. Plate Exit/Tie Bar	Yes	-77	9.6	62.9	107135	426	1903	1837
"	Upper Support Ring/Seismic Block/Support Part	No	122.1	-10	-9.5	122062	7701	7701	1756

Notes for Table 7 and Table 8.

- (a) Spatial coordinates are in a reference frame whose origin is located at the intersection of the steam dryer centerline and the plane containing the base plates (this plane also contains the top of the upper support ring and the bottom edges of the hoods). The y-axis is parallel to the hoods, the x-axis is normal to the hoods pointing from MSL C/D to MSL A/B, and the z-axis is vertical, positive up.
- (b) Node numbers are retained for further reference.
- (c) In accordance with [19], the nominal stress intensities at the drain channel/skirt junction are multiplied by 0.58.
- (d) In accordance with [19], the nominal stress intensities at the inner hood/hood support/middle base plate junction are multiplied by 0.79.

Table 7b. Locations with highest predicted stress intensities taken over all frequency shifts at CLTP conditions. Signal noise has been removed using 9% power data.

Stress Category	Location	Weld	Location (in)(a)			node(b)	Stress Intensities (psi)			% Freq. Shift
			x	y	z		Pm	Pm+Pb	S _{alt}	
Pm	USR/Seismic Block/Support Part	No	122.1	-10	-9.5	122062	7821	7821	1997	2.5
"	USR part/Support/Support Part	No	7	122.3	-9.5	122280	6945	6945	1934	2.5
"	Top Cover Inner Hood/Middle Closure Plate/Inner Hood	Yes	31.5	108.4	88.9	95881	6017	6630	1297	7.5
"	Top Cover Middle Hood/Outer Closure Plate/Middle Hood	Yes	-62.5	85	88.9	90897	4171	4657	2058	10
"	Splice Bar/USR Part	Yes	-2.2	-119	0	122330	3984	3984	<500	2.5
Pm+Pb	USR/Seismic Block/Support Part	No	122.1	-10	-9.5	122062	7821	7821	1997	2.5
"	USR part/Support/Support Part	No	7	122.3	-9.5	122280	6945	6945	1934	2.5
"	Top Cover Inner Hood/Middle Closure Plate/Inner Hood	Yes	-31.5	-108.4	88.9	91141	5939	6855	1298	5
"	Submerged Drain Channel/Skirt	Yes	-91	76.7	-99.5	98050	638	5595	1704	10
"	Submerged Drain Channel/Skirt	Yes	11.5	-118.4	-99.5	98860	503	4874	2360	5
S _{alt}	Submerged Drain Channel/Skirt	Yes	11.5	-118.4	-99.5	98860	503	4874	2360	7.5
"	Mid Plate	No	0	-3.9	88.2	23883	188	2437	2189	-5
"	Remaining tie bar (outer hood)/tie bar base	Yes	81.5	31.4	88.9	132385	2252	2252	2126	0
"	Mid Bottom Perf Exit/Mid Top Perf. Plate Exit/Tie Bar	Yes	77	9.6	62.9	106852	425	2191	2118	7.5
"	Outer Hood/Hood Mod/Mod Base/Channel Cap	Yes	93.5	22.6	84.3	111407	671	2158	2090	7.5

See Table 7a for notes (a)-(d).

Table 7c. Highest stress intensities at any frequency shift for the nodes listed in Table 7b computed using the unfiltered CLTP loads (i.e., signal noise has *not* been removed).

Stress Category	Location	Weld	Location (in) (a)			node(b)	Stress Intensities (psi)			% Freq. Shift
			x	y	z		Pm	Pm+Pb	S _{alt}	
Pm	USR/Seismic Block/Support Part	No	122.1	-10	-9.5	122062	8311	8311	2400	7.5
"	USR part/Support/Support Part	No	7	122.3	-9.5	122280	7136	7136	2134	2.5
"	Top Cover Inner Hood/Middle Closure Plate/Inner Hood	Yes	31.5	108.4	88.9	95881	6390	7104	1603	7.5
"	Top Cover Middle Hood/Outer Closure Plate/Middle Hood	Yes	-62.5	85	88.9	90897	4813	5538	2751	5
"	Splice Bar/USR Part	Yes	-2.2	-119	0	122330	4069	4069	586	2.5
Pm+Pb	Upper Support Ring/Seismic Block/Support Part	No	122.1	-10	-9.5	122062	8311	8311	2400	7.5
"	USR part/Support/Support Part	No	7	122.3	-9.5	122280	7136	7136	2134	2.5
"	Top Cover Inner Hood/Middle Closure Plate/Inner Hood	Yes	-31.5	-108.4	88.9	91141	6335	7274	1752	5
"	Submerged Drain Channel/Skirt	Yes	-91	76.7	-99.5	98050	735	5965	2102	10
"	Submerged Drain Channel/Skirt	Yes	11.5	-118.4	-99.5	98860	664	5640	3005	5
S _{alt}	Submerged Drain Channel/Skirt	Yes	11.5	-118.4	-99.5	98860	664	5640	3005	5
"	Mid Plate	No	0	-3.9	88.2	23883	203	3538	3195	-5
"	Remaining tie bar (outer hood)/tie bar base	Yes	81.5	31.4	88.9	132385	3508	3508	3339	0
"	Mid Bottom Perf Exit/Mid Top Perf. Plate Exit/Tie Bar	Yes	77	9.6	62.9	106852	508	2818	2716	7.5
"	Outer Hood/Hood Mod/Mod Base/Channel Cap	Yes	93.5	22.6	84.3	111407	818	2627	2507	0

See Table 7a for notes (a)-(d).

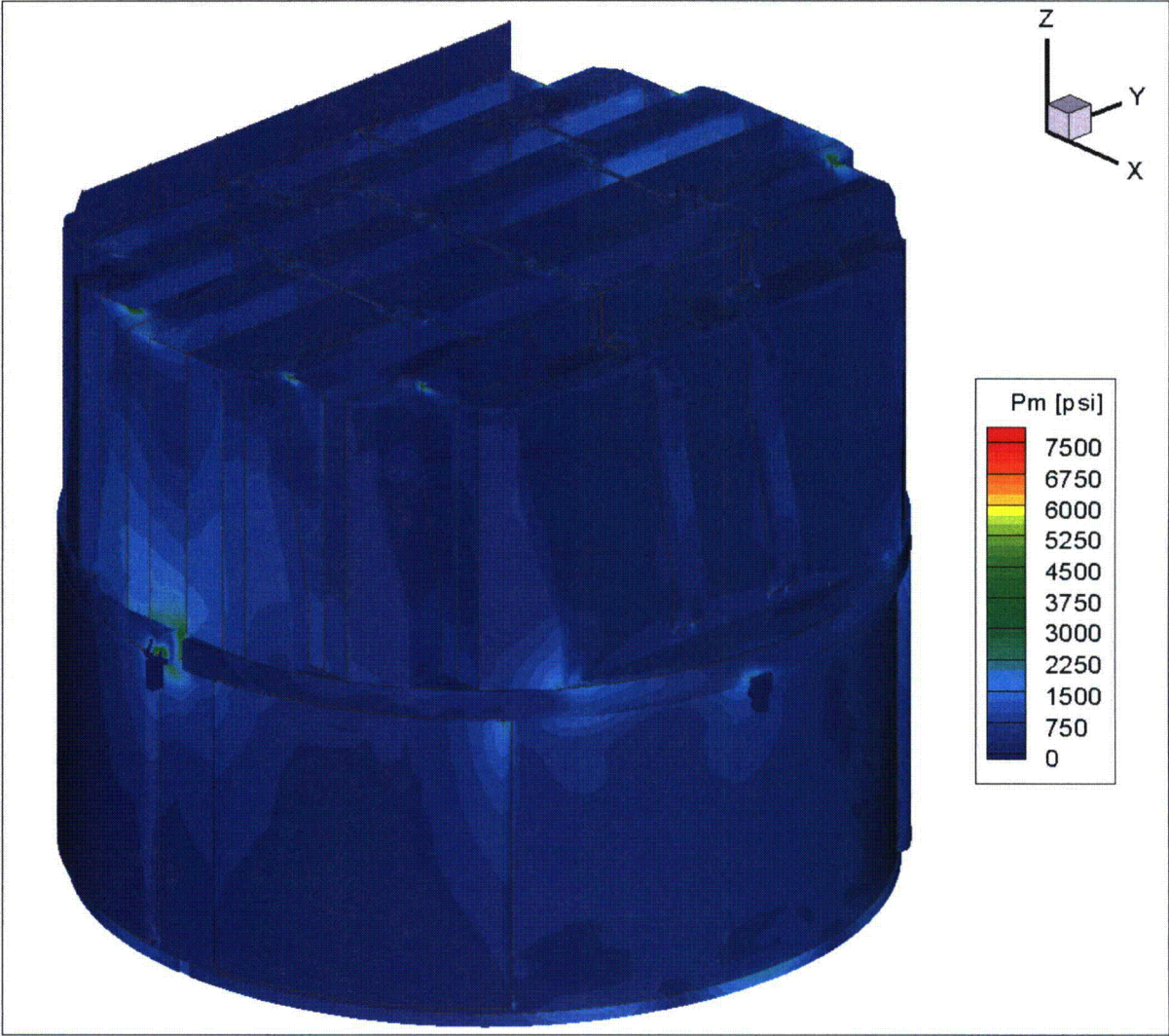


Figure 12a. Contour plot of maximum membrane stress intensity, P_m , for CLTP load. The maximum stress intensity is 7,701 psi. First view.

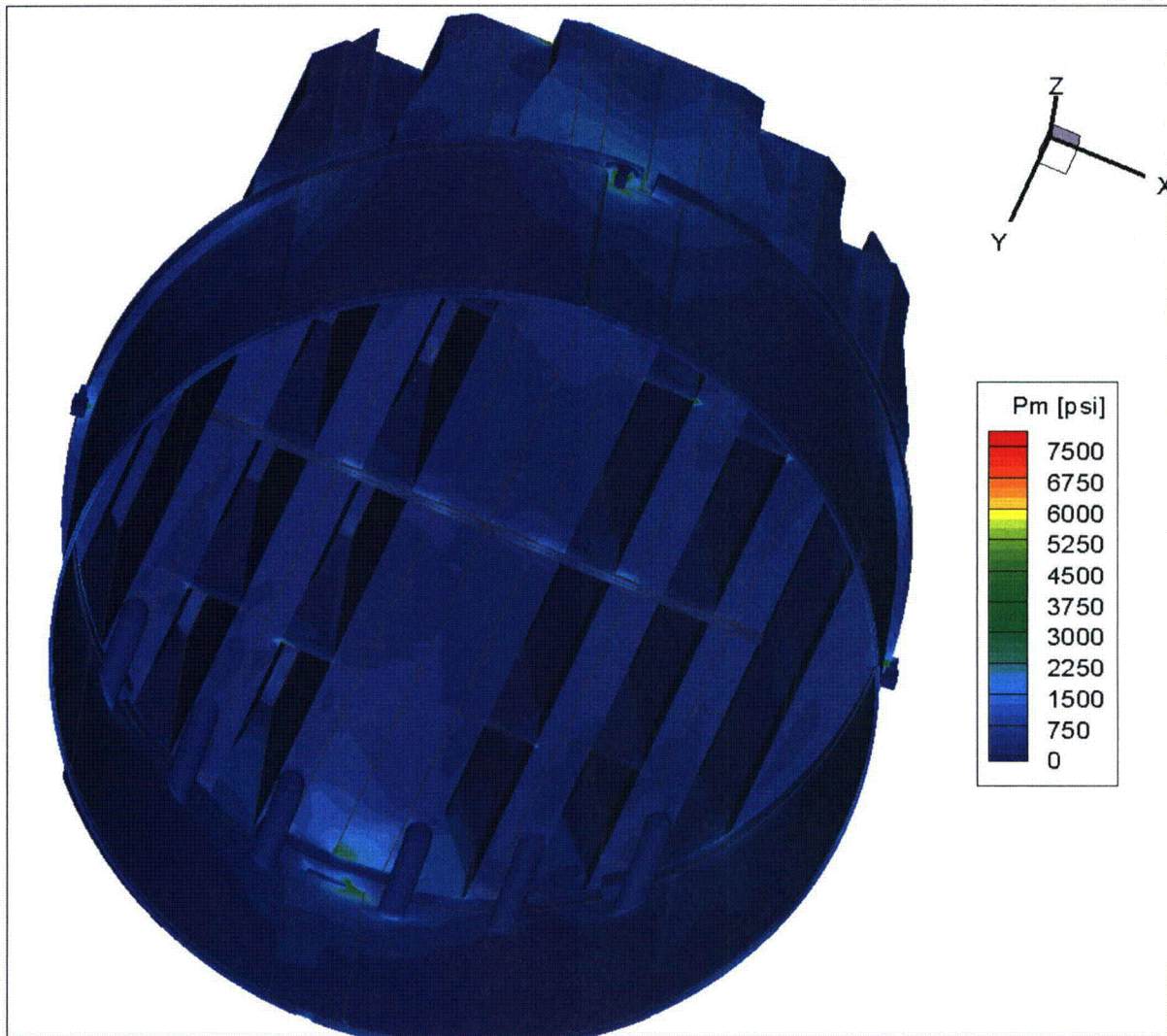


Figure 12b. Contour plot of maximum membrane stress intensity, P_m , for CLTP load. Second view from below.

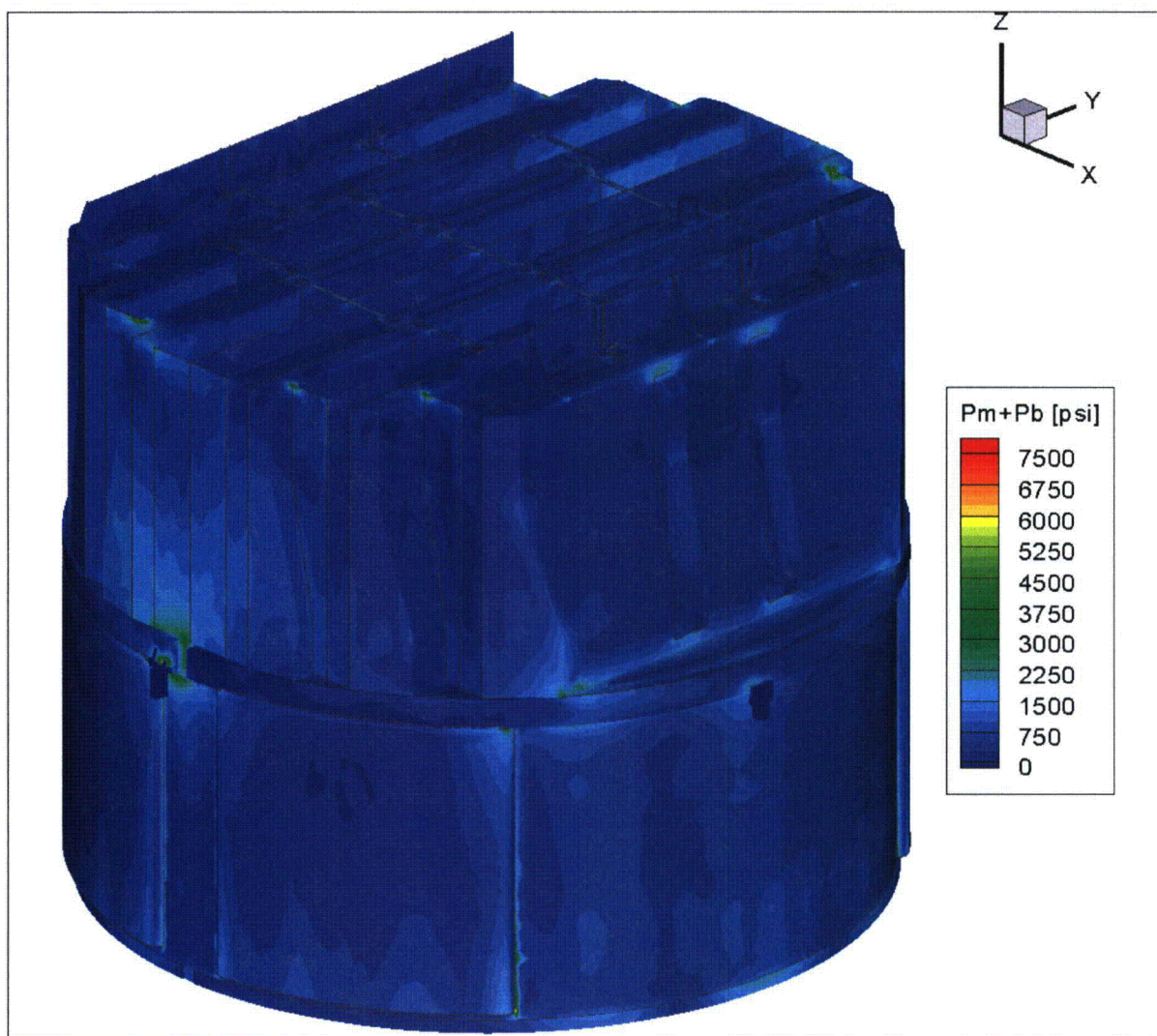


Figure 12c. Contour plot of maximum membrane+bending stress intensity, P_m+P_b , for CLTP load. The maximum stress intensity is 7,701 psi. First view.

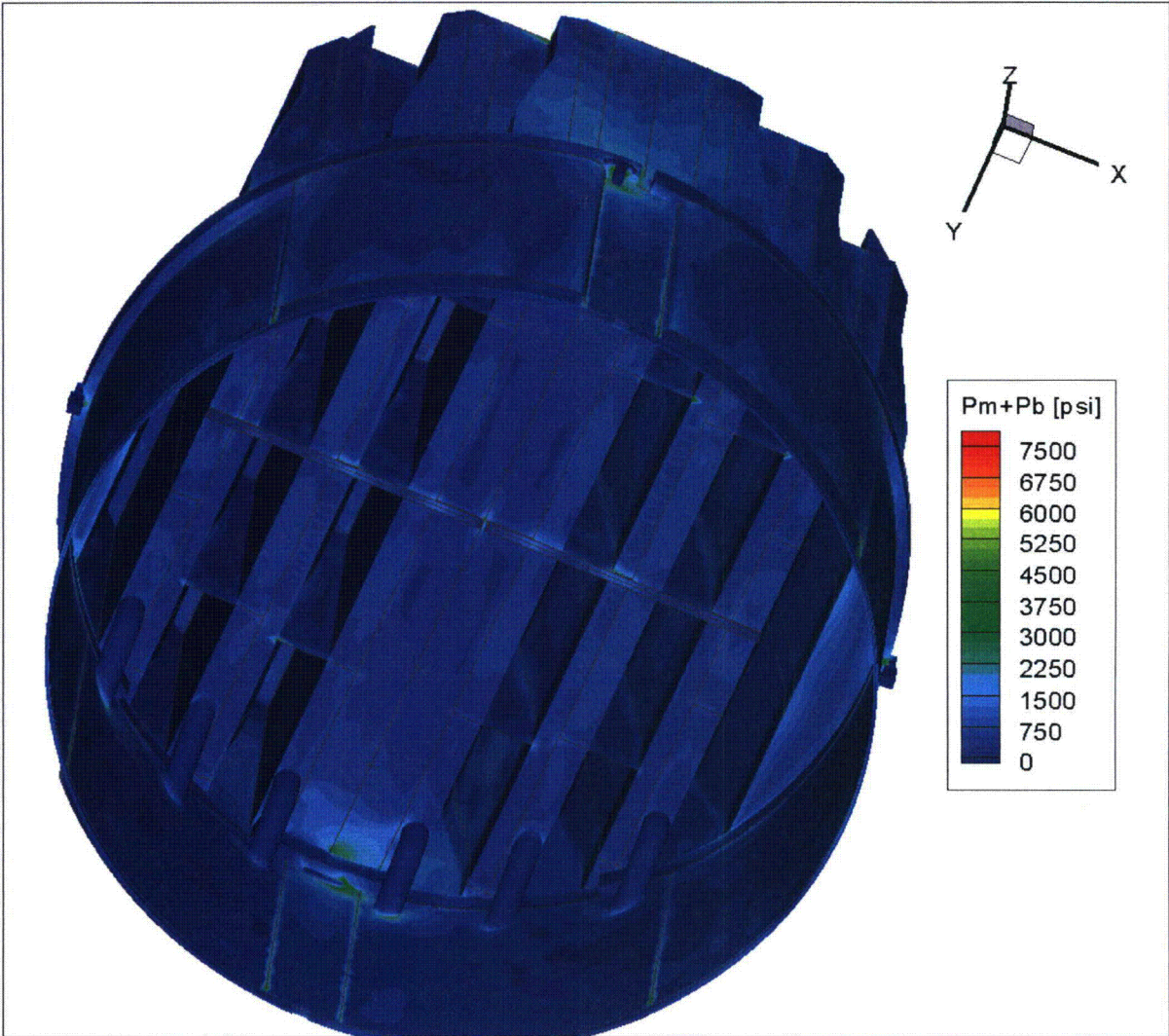


Figure 12d. Contour plot of maximum membrane+bending stress intensity, P_m+P_b , for CLTP load. Second view from below.

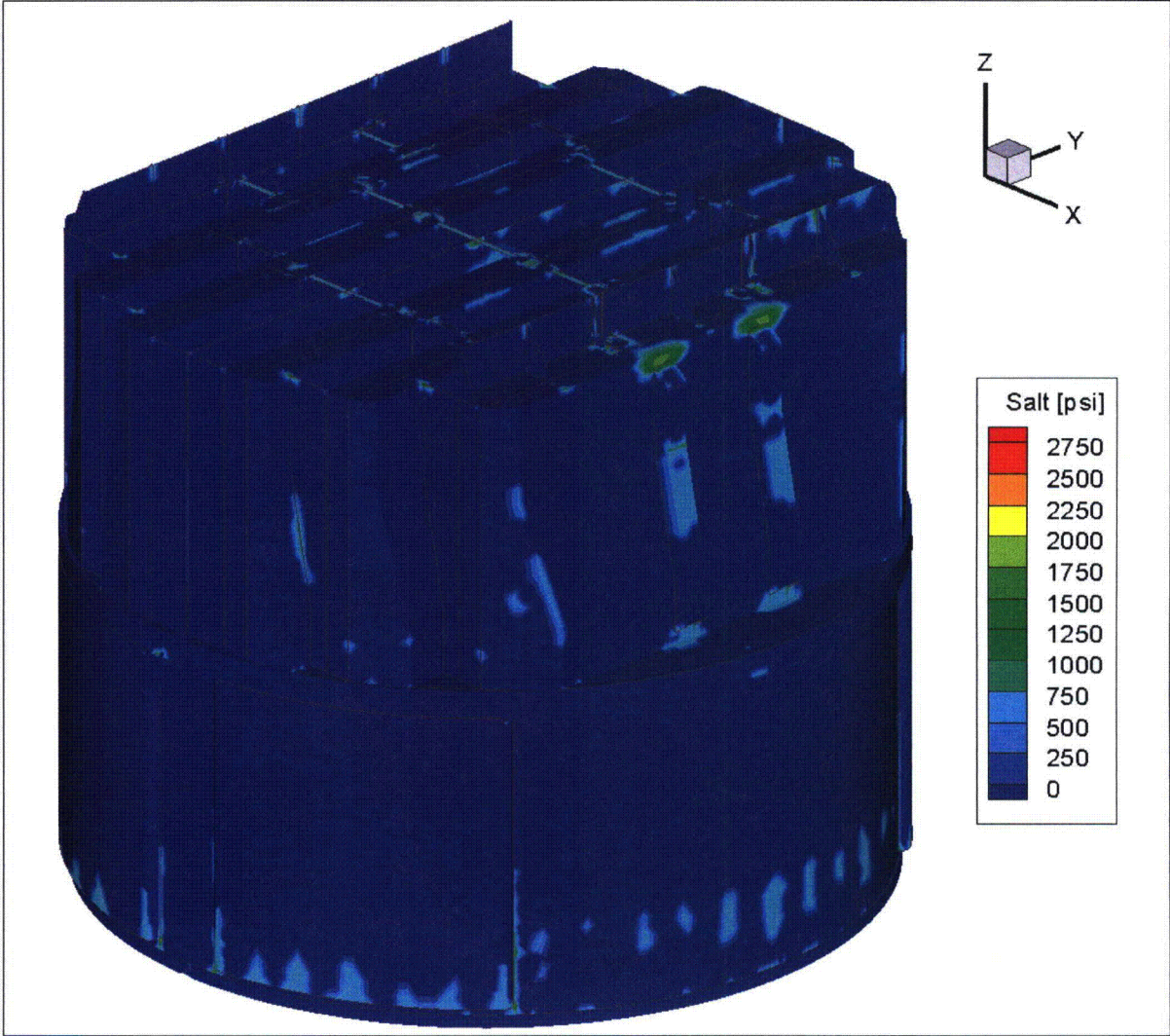


Figure 12e. Contour plot of alternating stress intensity, S_{alt} , for CLTP load. The maximum alternating stress intensity is 2,126 psi.

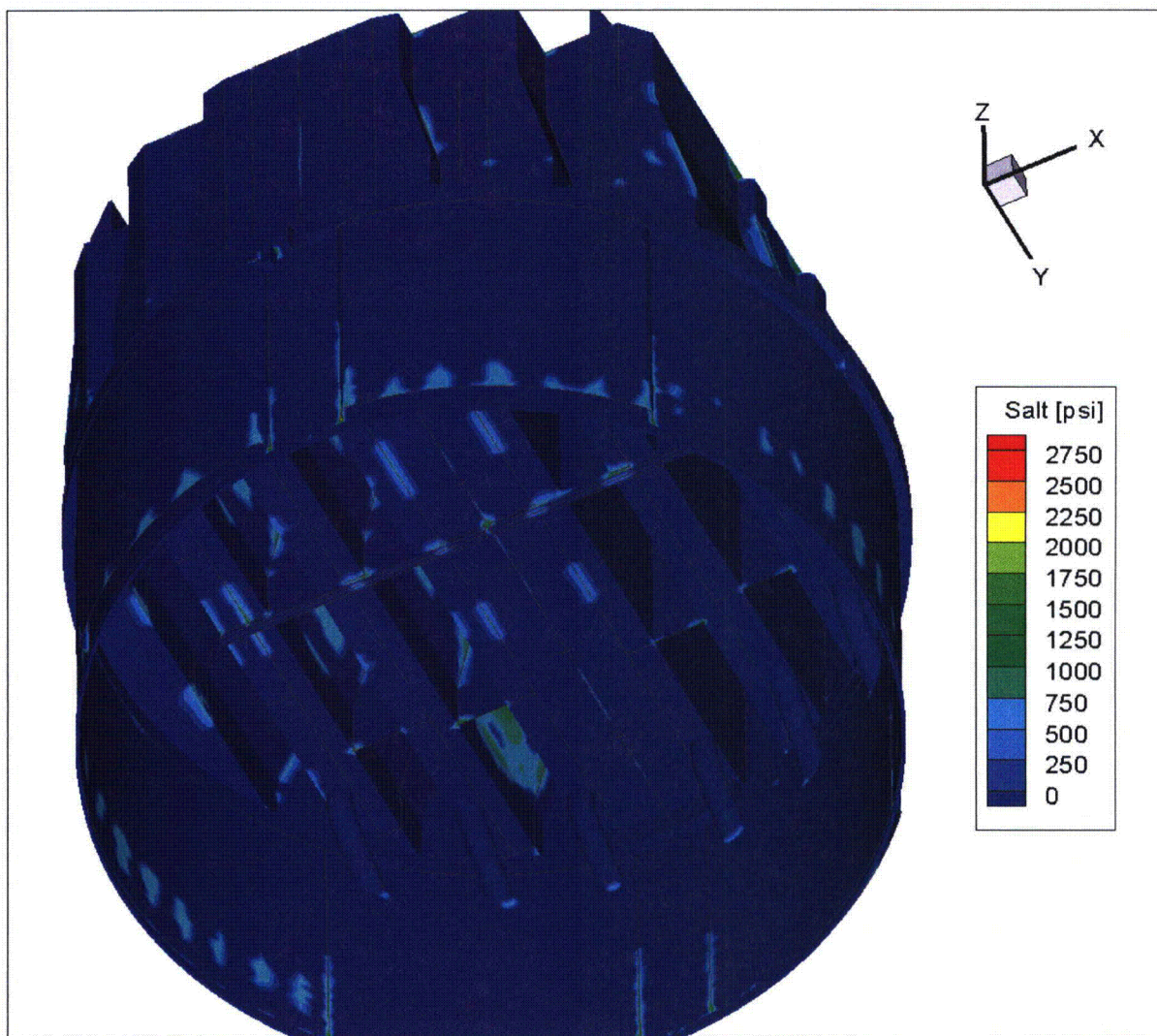


Figure 12f. Contour plot of alternating stress intensity, S_{alt} , for CLTP load. Second view from below.

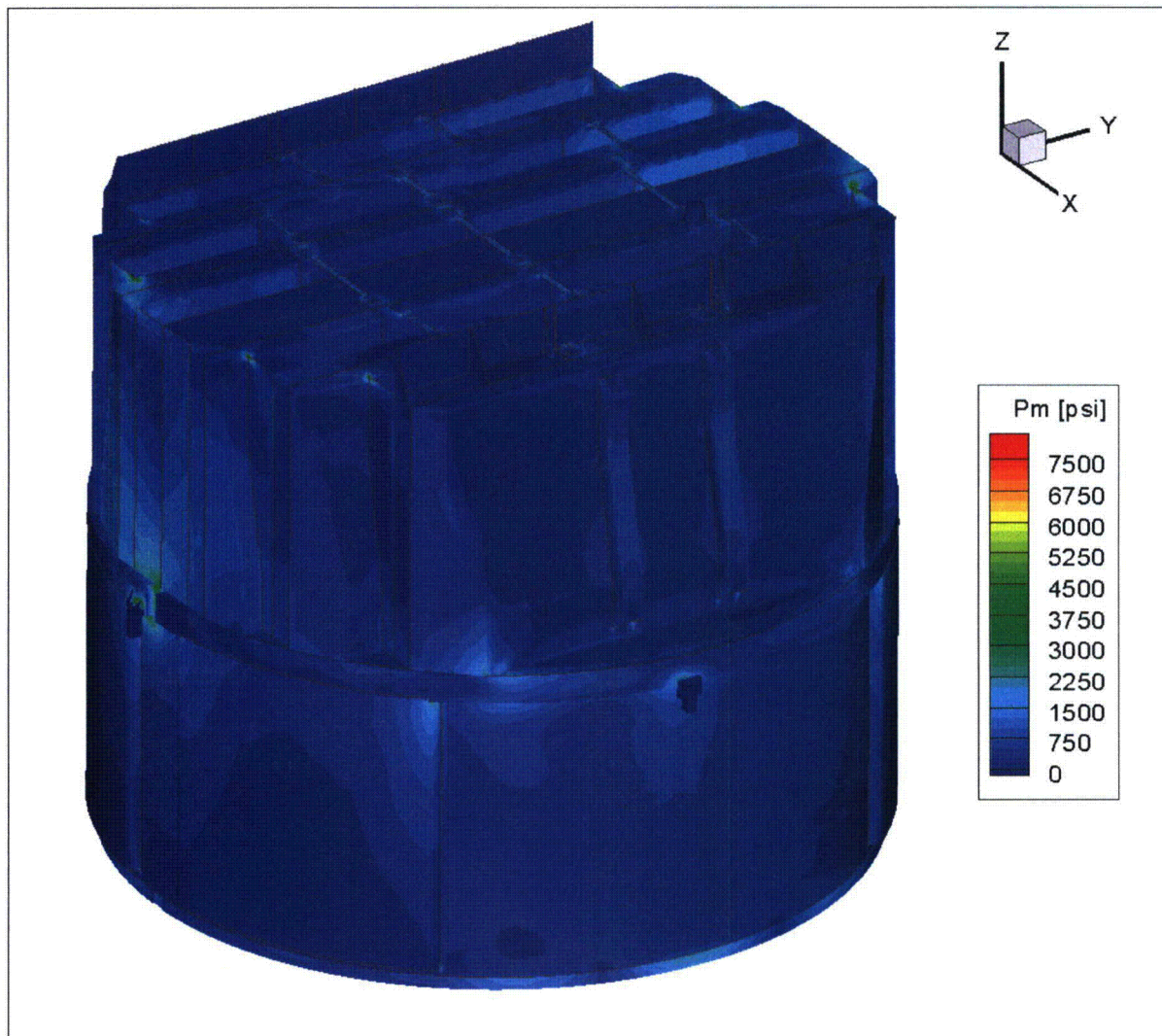


Figure 13a. Contour plot of maximum membrane stress intensity, P_m , for CLTP operation with frequency shifts. The recorded stress at a node is the maximum value taken over all frequency shifts. The maximum stress intensity is 7,821 psi.

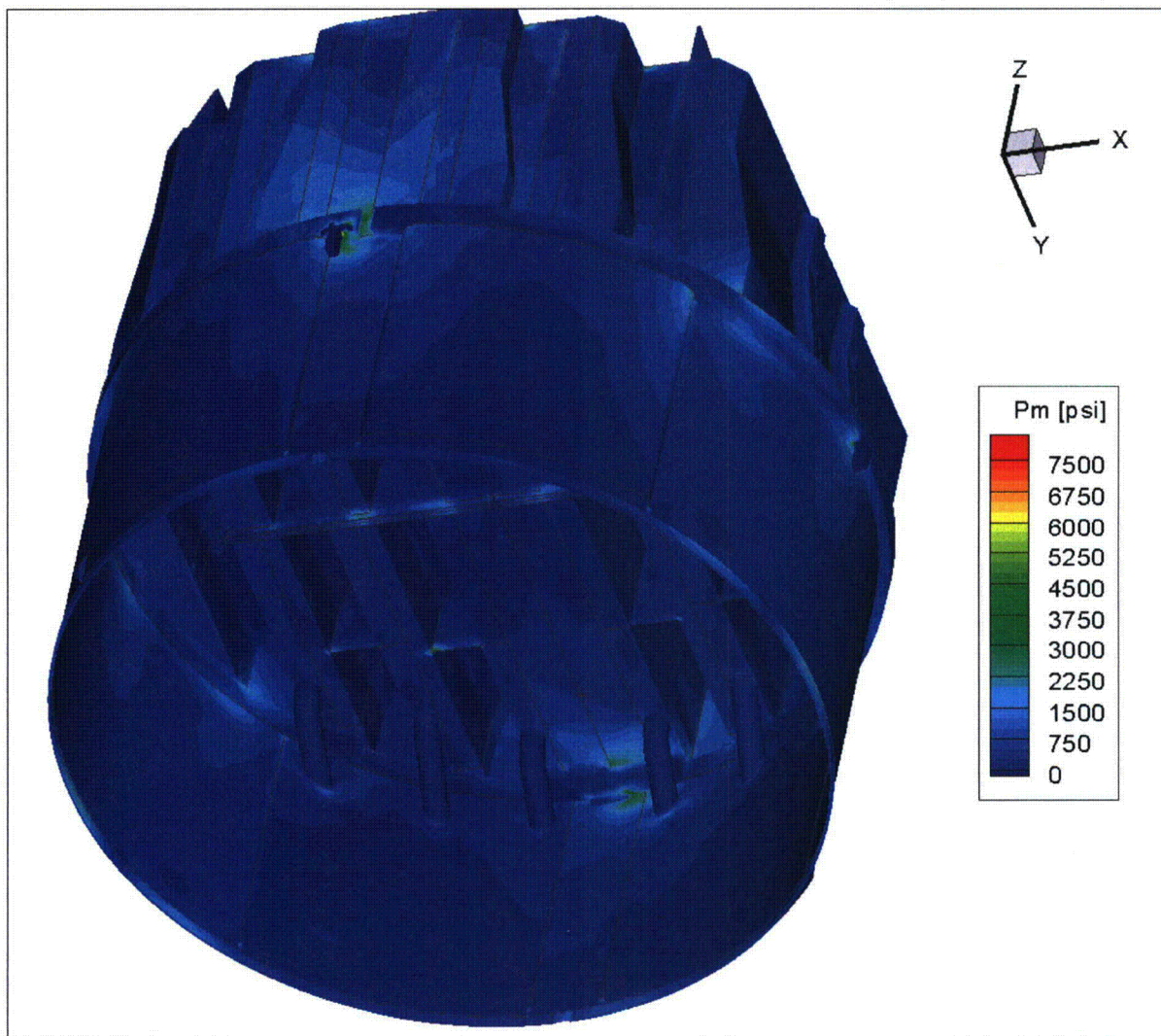


Figure 13b. Contour plot of maximum membrane stress intensity, P_m , for CLTP operation with frequency shifts. The recorded stress at a node is the maximum value taken over all frequency shifts. Second view from below.

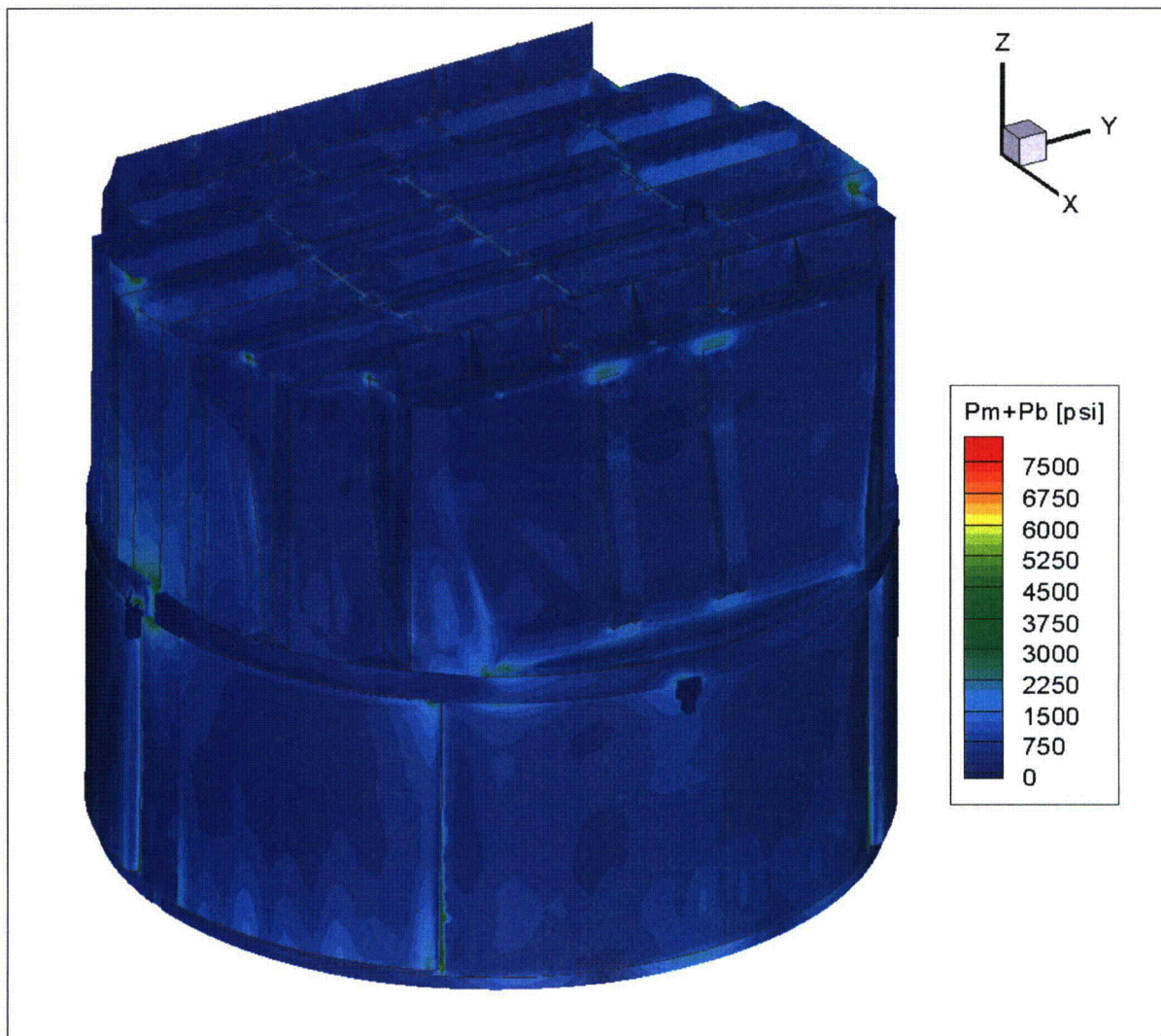


Figure 13c. Contour plot of maximum membrane+bending stress intensity, P_m+P_b , for CLTP operation with frequency shifts. The recorded stress at a node is the maximum value taken over all frequency shifts. The maximum stress intensity is 7,821 psi. First view.

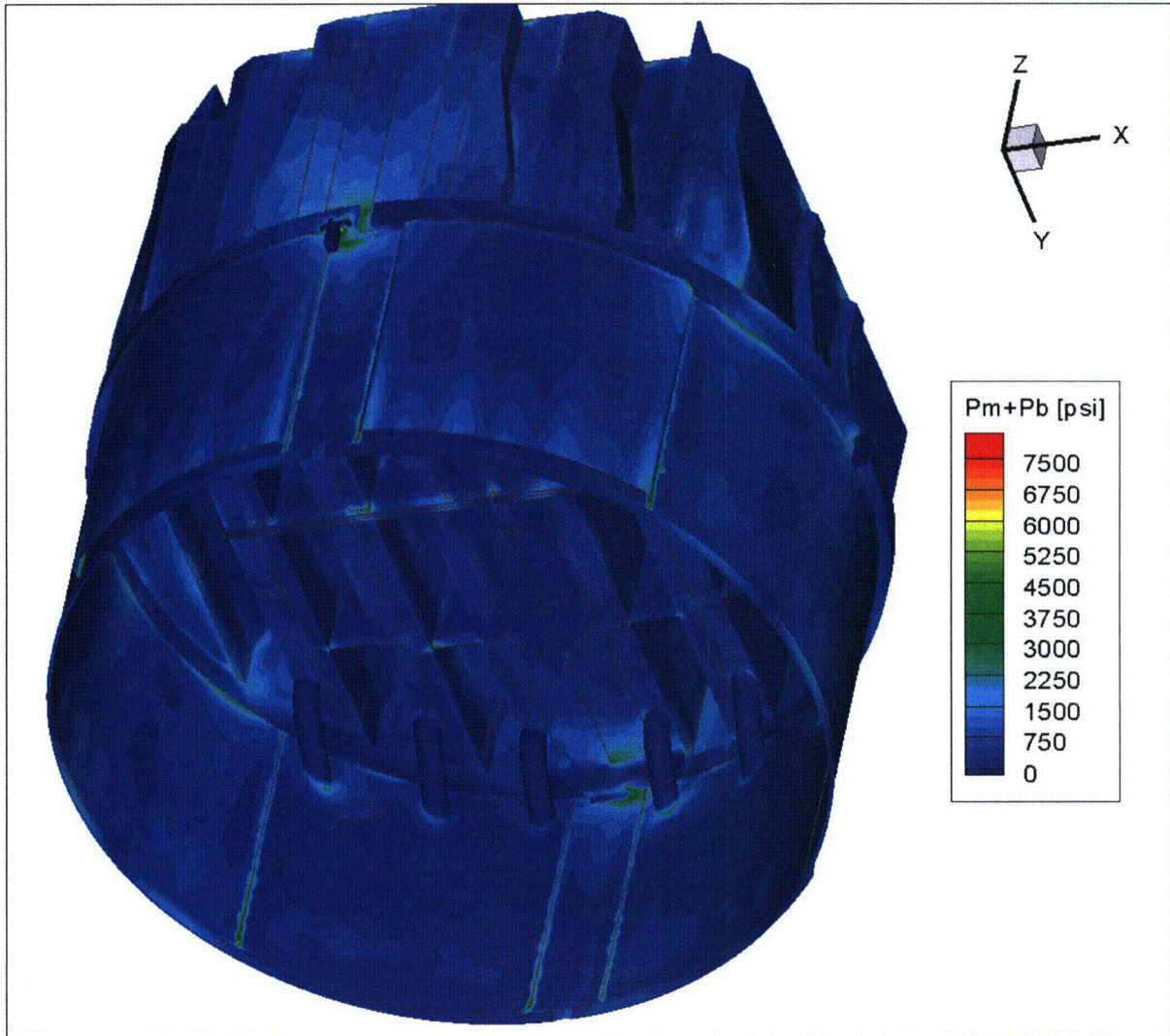


Figure 13d. Contour plot of maximum membrane+bending stress intensity, P_m+P_b , for CLTP operation with frequency shifts. This second view from beneath reveals high stress and modal response of interior hood supports.

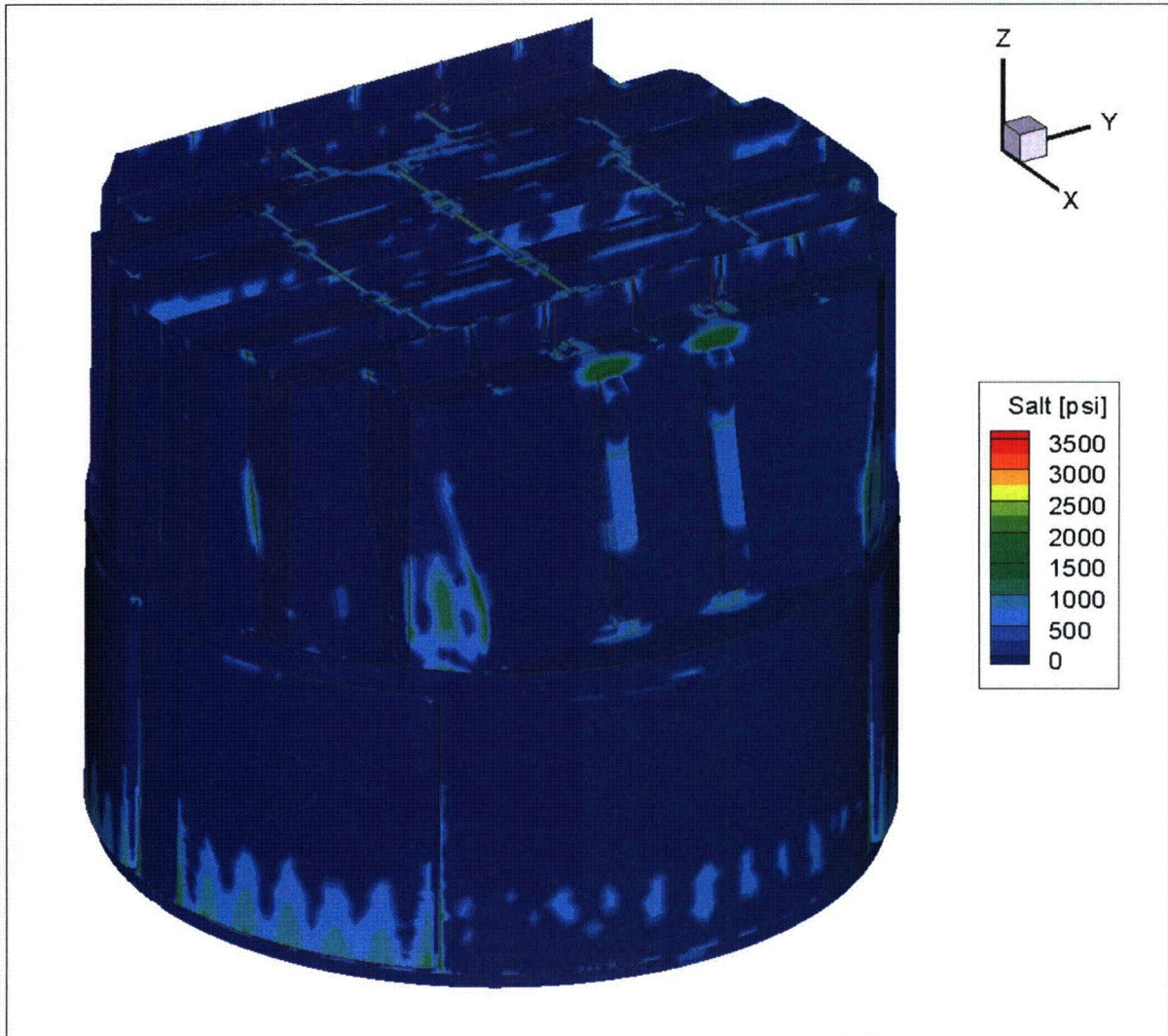


Figure 13e. Contour plot of alternating stress intensity, S_{alt} , for CLTP operation with frequency shifts. The recorded stress at a node is the maximum value taken over all frequency shifts. The maximum alternating stress intensity is 2,360 psi.

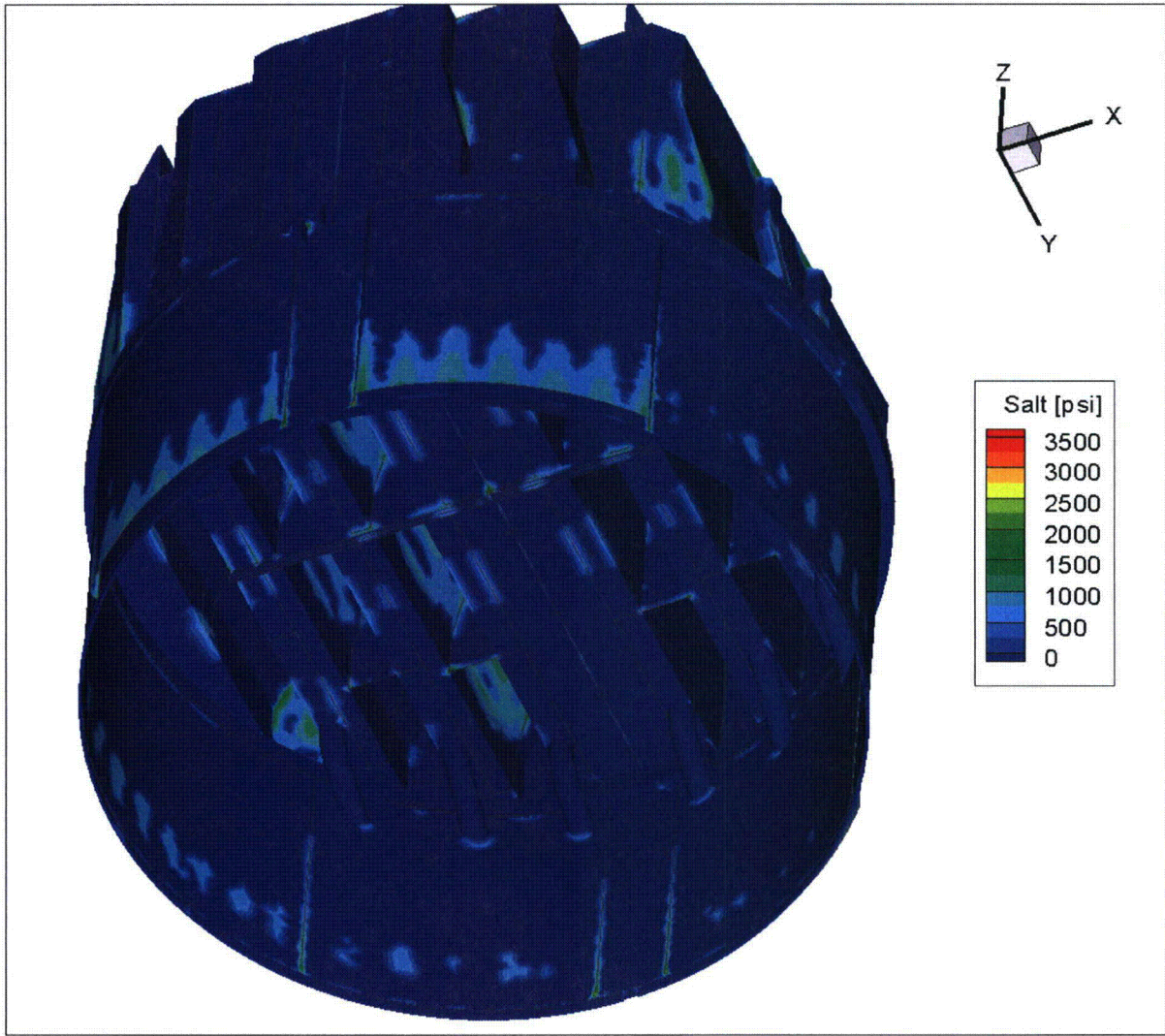


Figure 13f. Contour plot of alternating stress intensity, S_{alt} , for CLTP operation with frequency shifts. The recorded stress at a node is the maximum value taken over all frequency shifts. Second view from below.

5.2 Load Combinations and Allowable Stress Intensities

The stress ratios computed for CLTP at nominal frequency and with frequency shifting are listed in Table 8. The stress ratios are grouped according to type (SR-P for maximum membrane and membrane+bending stress, SR-a for alternating stress) and location (away from welds or on a weld). The tabulated nodes are also depicted in Figure 14 (no frequency shift) and Figure 15 (all frequency shifts included). The plots corresponding to maximum stress intensities depict all nodes with stress ratios $SR-P \leq 4$, whereas the plots of alternating stress ratios display all nodes with $SR-a \leq 5$.

For CLTP operation at nominal frequency the minimum alternating stress ratio is $SR-a=3.23$, and occurs on the weld joining the base of the tie bar to the tie bar base on the top cover plate of the outer vane bank. This tie bar is left in place to support the steam dam. When all frequency shifts are included the minimum alternating stress reduces by 11% to $SR-a=2.91$. The minimum alternating stress ratio location shifts to the drain channel/skirt weld. The top five alternating stress locations in Table 8b are discussed briefly in the previous section and are within expectations. The 6th and 7th nodes in the table correspond to nodes whose computed stresses have been revised to reflect the results from detailed substructure analysis [19]. The minimum stress ratio due to maximum stress intensity, $SR-P=1.75$, occurs on the middle closure plate connecting to the inner hood; it reduces to 1.67 when all frequency shifts are included. All of these locations lie on welds.

Compared to previous stress analysis of the BFN1 steam dryer, the addition of the modified tie bars with widened and tapered ends has eliminated virtually all of the high stress areas previously associated with old tie bar bases resulting in stress ratios $SR-a > 4.5$ for the welds on the ends of these tie bars.

Finally, the highest stress intensities (and lowest stress ratios) at any frequency shift for the locations in Table 8b are recomputed using the CLTP loads without noise removal and reported in Table 8c.

In summary, the lowest alternating stress ratio (and the only one below $SR-a < 3.0$) occurs near the bottom of the drain channel/skirt weld at the +7.5% frequency shift. The lowest value at any frequency shift is $SR-a=2.91$ indicating that stresses are well below allowable levels. The lowest stress ratio associated with a maximum stress is $SR-P=1.67$. This value is dominated by the static component and is only weakly altered by acoustic loads. Since acoustic loads scale roughly with the square of the steam flow, it is reasonable to anticipate that under EPU conditions (where steam flow increases by 15%) the stresses would increase by approximately $(115\%)^2=1.32$. Under this assumption the minimum alternating stress ratio would reduce from 2.91 to $2.91/1.32=2.20$, which given that the applied loads already account for all end-to-end biases and uncertainties, still contains sufficient margin for sustained EPU operation.

Table 8a. Locations with minimum stress ratios for CLTP conditions with no frequency shift. Signal noise is removed using 9% power data. Stress ratios are grouped according to stress type (maximum – SR-P; or alternating – SR-a) and location (away from a weld or at a weld). Bold text indicates minimum stress ratio of any type on the structure. Locations are depicted in Figure 14.

Stress Ratio	Weld	Location	Location (in.) (a)			node(b)	Stress Intensity (psi)			Stress Ratio		
			x	y	z		Pm	Pm+Pb	S _{alt}	SR-P	SR-a	
SR-P	No	1. USR/Seismic Block/Support Part	122.1	-10	-9.5	122062	7701	7701	1756	2.38	7.04	
	"	2. USR part/Support/Support Part	7	122.3	-9.5	122280	6757	6757	1543	2.71	8.01	
SR-a	No	<i>NONE SR-a > 5 at all non weld nodes</i>										
SR-P	Yes	1. Top Cover Inner Hood/Middle Closure Plate/Inner Hood	31.5	108.4	88.9	95881	5763	6399	1100	1.75	6.24	
"	"	2. Top Cover Middle Hood/Outer Closure Plate/Middle Hood	62.5	-85	88.9	90137	3915	4266	1521	2.57	4.52	
"	"	3. Splice Bar/USR Part	-2.2	-119	0	122330	3825	3825	<500	2.63	>13	
"	"	4. Straddle	6.1	118.8	-12.5	120708	3729	3729	<500	2.7	>13	
"	"	5. Middle Cover Plate/Hood Support/Inner Hood(d)	39.8	-59.8	0	104843	3531	3679	1599	2.85	4.30	
"	"	6. Submerged Drain Channel /Skirt	-91	76.7	-99.5	98050	564	5237	1321	2.88	5.2	
"	"	7. Outer Cover Plate/Hood Support/Middle Hood	70.8	-54.6	0	101377	2788	3132	1664	3.61	4.13	
"	"	8. Submerged Drain Channel/Skirt(c)	-91	76.7	-100.5	98024	876	4026	1241	3.75	5.54	

See Table 7a for notes (a)-(d).

Table 8a (cont.). Locations with minimum stress ratios for CLTP conditions with no frequency shift. Signal noise is removed using 9% power data. Stress ratios are grouped according to stress type (maximum – SR-P; or alternating – SR-a) and location (away from a weld or at a weld). Bold text indicates minimum stress ratio of any type on the structure. Locations are depicted in Figure 14.

Stress Ratio	Weld	Location	Location (in.) (a)			node(b)	Stress Intensity (psi)			Stress Ratio	
			x	y	z		Pm	Pm+Pb	S _{alt}	SR-P	SR-a
SR-a	Yes	1. Remaining tie bar (outer hood)/tie bar base	81.5	31.4	88.9	132385	2252	2252	2126	4.47	3.23
"	"	2. Outer Hood/Hood Mod	93.5	-20	86.9	89590	120	2146	1925	7.04	3.57
"	"	3. Mid Bottom Perf Exit/Mid Top Perf Exit/Tie Bar	-77	9.6	62.9	107135	426	1903	1837	7.93	3.74
"	"	4. Outer Cover Plate/Hood Support/Middle Hood	70.8	-54.6	0	101377	2788	3132	1664	3.61	4.13
"	"	5. Submerged Drain Channel/Skirt	11.5	-118.4	-99.5	98860	385	3933	1604	3.84	4.28
"	"	6. Middle Cover Plate/Hood Support/Inner Hood(d)	39.8	-59.8	0	104843	3531	3679	1599	2.85	4.30
"	"	7. Top Cover Middle Hood/Tie Bar Base Thin	-55.5	31.4	88.9	89960	371	1569	1538	9.62	4.47
"	"	8. Submerged Drain Channel/Skirt(c)	-11.5	118.4	-100.5	98156	695	3019	1525	5.00	4.51

See Table 7a for notes (a)-(d).

Table 8b. Locations with minimum stress ratios at CLTP conditions with frequency shifts. Signal noise is removed using 9% power data. Stress ratios at every node are recorded as the lowest stress ratio identified during the frequency shifts. Stress ratios are grouped according to stress type (maximum – SR-P; or alternating – SR-a) and location (away from a weld or at a weld). Bold text indicates minimum stress ratio of any type on the structure. Locations are depicted in Figure 15.

Stress Ratio	Weld	Location	Location (in.) (a)			node(b)	Stress Intensity (psi)			Stress Ratio		% Freq. Shift
			x	y	z		Pm	Pm+Pb	S _{alt}	SR-P	SR-a	
SR-P	No	1. USR/Seismic Block/Support Part	122.1	-10	-9.5	122062	7821	7821	1997	2.34	6.19	2.5
		2. USR part/Support/Support Part	7	122.3	-9.5	122280	6945	6945	1934	2.64	6.39	2.5
SR-a	No	<i>NONE SR-a > 5 at all non weld nodes</i>										
SR-P	Yes	1. Top Cover Inner Hood/Middle Closure Plate/Inner Hood	31.5	108.4	88.9	95881	6017	6630	1297	1.67	5.3	7.5
"	"	2. Top Cover Middle Hood/Outer Closure Plate/Middle Hood	-62.5	85	88.9	90897	4171	4657	2058	2.41	3.34	10
"	"	3. Splice Bar/USR Part	-2.2	-119	0	122330	3984	3984	<500	2.53	>13	2.5
"	"	4. Middle Cover Plate/Hood Support/Inner Hood ^(d)	39.8	-59.8	0	104843	3943	3954	1996	2.55	3.44	7.5
"	"	5. Splice Bar/Straddle	-6	-117.8	-9.5	122087	3799	3799	643	2.65	10.68	2.5
"	"	6. Submerged Drain Channel/Skirt	-91	76.7	-99.5	98050	638	5595	1704	2.7	4.03	10
"	"	7. Submerged Drain Channel/Skirt	11.5	-118.4	-99.5	98860	503	4874	2360	3.1	2.91	5
"	"	8. Submerged Drain Channel/Skirt ^(c)	-91	76.7	-100.5	98024	1009	4476	1553	3.37	4.42	10

See Table 7a for notes (a)-(d).

Table 8b (cont.). Locations with minimum stress ratios at CLTP conditions with frequency shifts. Signal noise is removed using 9% power data. Stress ratios at every node are recorded as the lowest stress ratio identified during the frequency shifts. Stress ratios are grouped according to stress type (maximum – SR-P; or alternating – SR-a) and location (away from a weld or at a weld). Bold text indicates minimum stress ratio of any type on the structure. Locations are depicted in Figure 15.

Stress Ratio	Weld	Location	Location (in.) (a)			node(b)	Stress Intensity (psi)			Stress Ratio		% Freq. Shift
			x	y	z		Pm	Pm+Pb	S _{alt}	SR-P	SR-a	
SR-a	Yes	1. Submerged Drain Channel/Skirt	11.5	-118.4	-99.5	98860	503	4874	2360	3.1	2.91	7.5
"	"	2. Remaining tie bar (outer hood)/tie bar base	81.5	31.4	88.9	132385	2252	2252	2126	4.47	3.23	0
"	"	3. Mid Bottom Perf. Plate Exit/Mid Top Perf. Plate Exit/Tie Bar	77	9.6	62.9	106852	425	2191	2118	6.89	3.24	7.5
"	"	4. Outer Hood/Hood Mod/Mod Base/Channel Cap	93.5	22.6	84.3	111407	671	2158	2090	7	3.29	7.5
"	"	5. Top Cover Middle Hood/Outer Closure Plate/Middle Hood	-62.5	85	88.9	90897	4171	4657	2058	2.41	3.34	10
"	"	6. Submerged Drain Channel/Skirt(c)	-11.5	118.4	-100.5	98156	772	3563	2056	4.24	3.34	10
"	"	7. Middle Cover Plate/Hood Support/Inner Hood(d)	39.8	-59.8	0	104843	3943	3954	1996	2.55	3.44	7.5

See Table 7a for notes (a)-(d).

Table 8c. Minimum stress stress ratios at any frequency shift for the nodes listed in Table 8b computed using the unfiltered CLTP loads (i.e., signal noise has not been removed). Locations are depicted in Figure 15.

Stress Ratio	Weld	Location	Location (in.) (a)			node(b)	Stress Intensity (psi)			Stress Ratio		% Freq. Shift
			x	y	z		Pm	Pm+Pb	S _{alt}	SR-P	SR-a	
SR-P	No	1. USR/Seismic Block/Support Part	122.1	-10	-9.5	122062	8311	8311	2400	2.20	5.15	7.5
		2. USR part/Support/Support Part	7	122.3	-9.5	122280	7136	7136	2134	2.56	5.79	2.5
SR-a	No											
SR-P	Yes	1. Top Cover Inner Hood/Middle Closure Plate/Inner Hood	31.5	108.4	88.9	95881	6390	7104	1603	1.58	4.28	7.5
"	"	2. Top Cover Middle Hood/Outer Closure Plate/Middle Hood	-62.5	85	88.9	90897	4813	5538	2751	2.09	2.50	5
"	"	3. Splice Bar/USR Part	-2.2	-119	0	122330	4069	4069	586	2.47	11.72	2.5
"	"	4. Middle Cover Plate/Hood Support/Inner Hood(d)	39.8	-59.8	0	104843	5839	5868	2703	1.72	2.54	5
"	"	5. Splice Bar/Straddle	-6	-117.8	-9.5	122087	3902	3902	752	2.58	9.14	2.5
"	"	6. Submerged Drain Channel/Skirt	-91	76.7	-99.5	98050	735	5965	2102	2.53	3.27	10
"	"	7. Submerged Drain Channel/Skirt	11.5	-118.4	-99.5	98860	664	5640	3005	2.68	2.29	5
"	"	8. Submerged Drain Channel/Skirt(c)	-91	76.7	-100.5	98024	2018	8641	2277	1.75	3.02	10
SR-a	Yes	1. Submerged Drain Channel/Skirt	11.5	-118.4	-99.5	98860	664	5640	3005	2.68	2.29	5
"	"	2. Remaining tie bar (outer hood)/tie bar base	81.5	31.4	88.9	132385	3508	3508	3339	2.87	2.06	0
"	"	3. Mid Bottom Perf. Plate Exit/Mid Top Perf. Plate Exit/Tie Bar	77	9.6	62.9	106852	508	2818	2716	5.36	2.53	7.5
"	"	4. Outer Hood/Hood Mod/Mod Base/Channel Cap	93.5	22.6	84.3	111407	818	2627	2507	5.75	2.74	0
"	"	5. Top Cover Middle Hood/Outer Closure Plate/Middle Hood	-62.5	85	88.9	90897	4813	5538	2751	2.09	2.50	10
"	"	6. Submerged Drain Channel/Skirt(c)	-11.5	118.4	-100.5	98156	1964	7163	2561	2.11	2.69	10
"	"	7. Middle Cover Plate/Hood Support/Inner Hood(d)	39.8	-59.8	0	104843	5839	5868	2703	1.72	2.54	7.5

See Table 7a for notes (a)-(d).

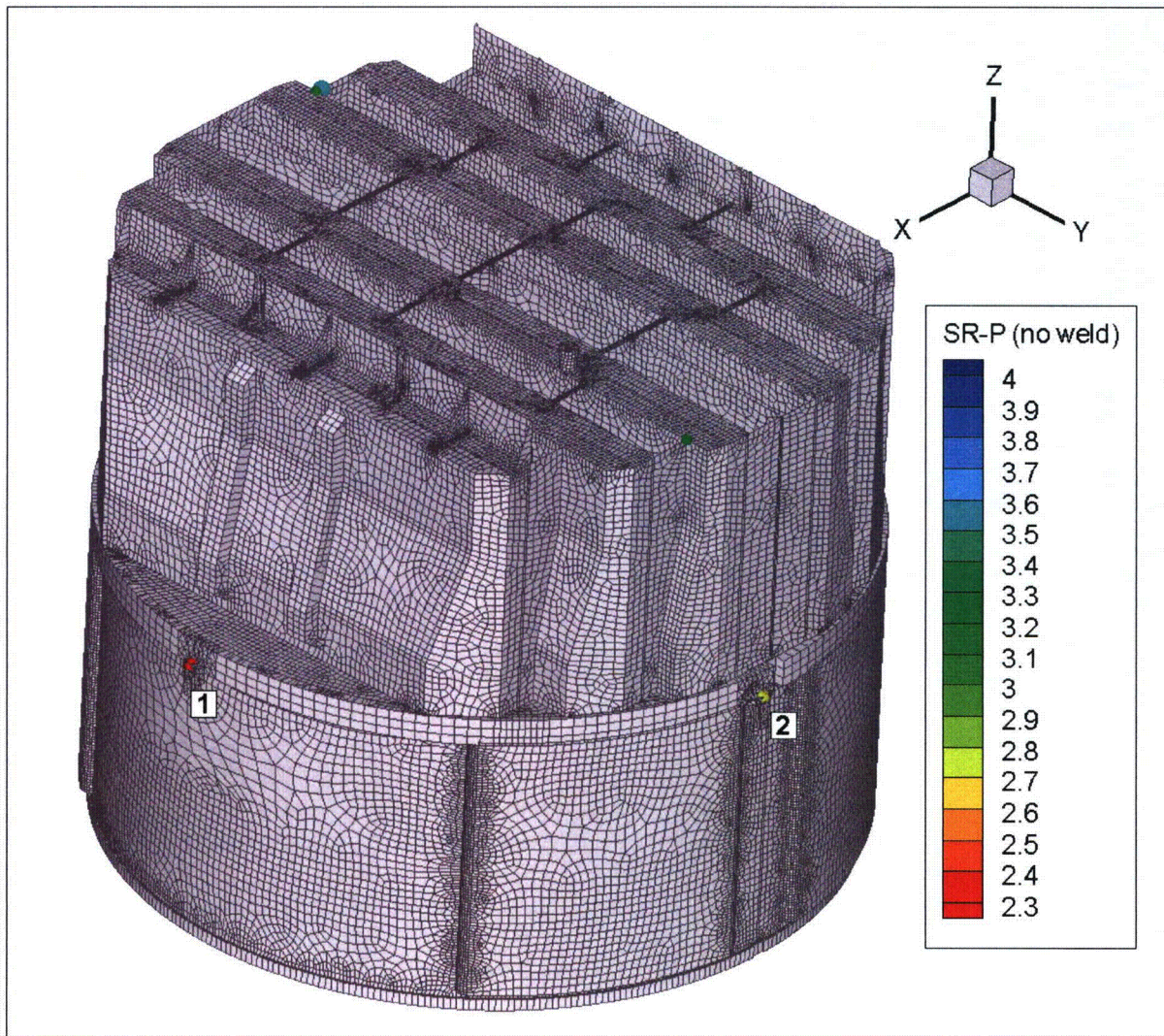


Figure 14a. Location of smallest maximum stress ratios, $SR-P \leq 4$, at non-welds for nominal CLTP operation. Number refers to the enumerated locations for SR-P values at non-welds in Table 8a.

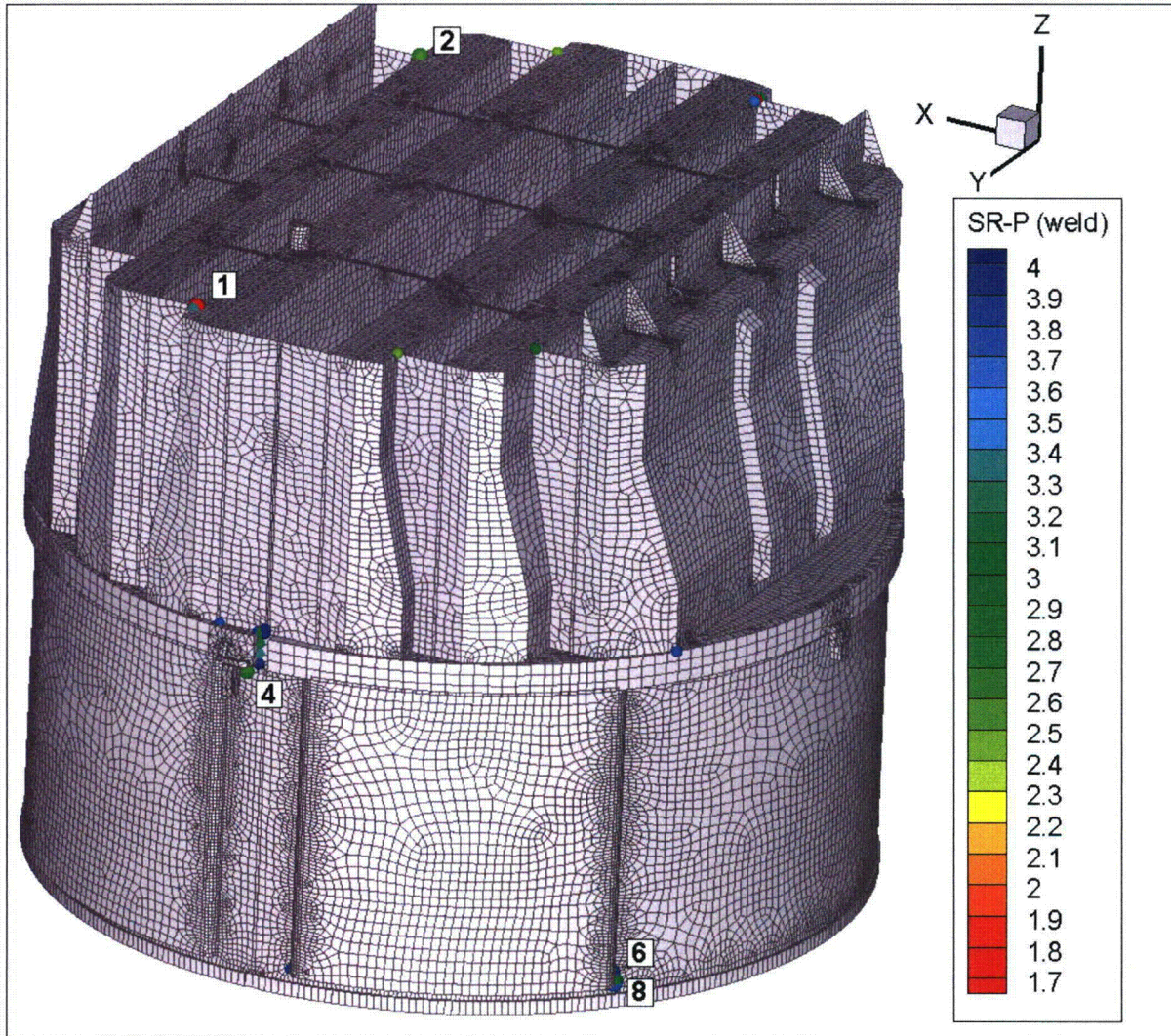


Figure 14b. Locations of smallest maximum stress ratios, $SR-P \leq 4$, at welds for nominal CLTP operation. Numbers refer to the enumerated locations for SR-P values at welds in Table 8a. First view showing locations 1, 2, 4, 6 and 8.

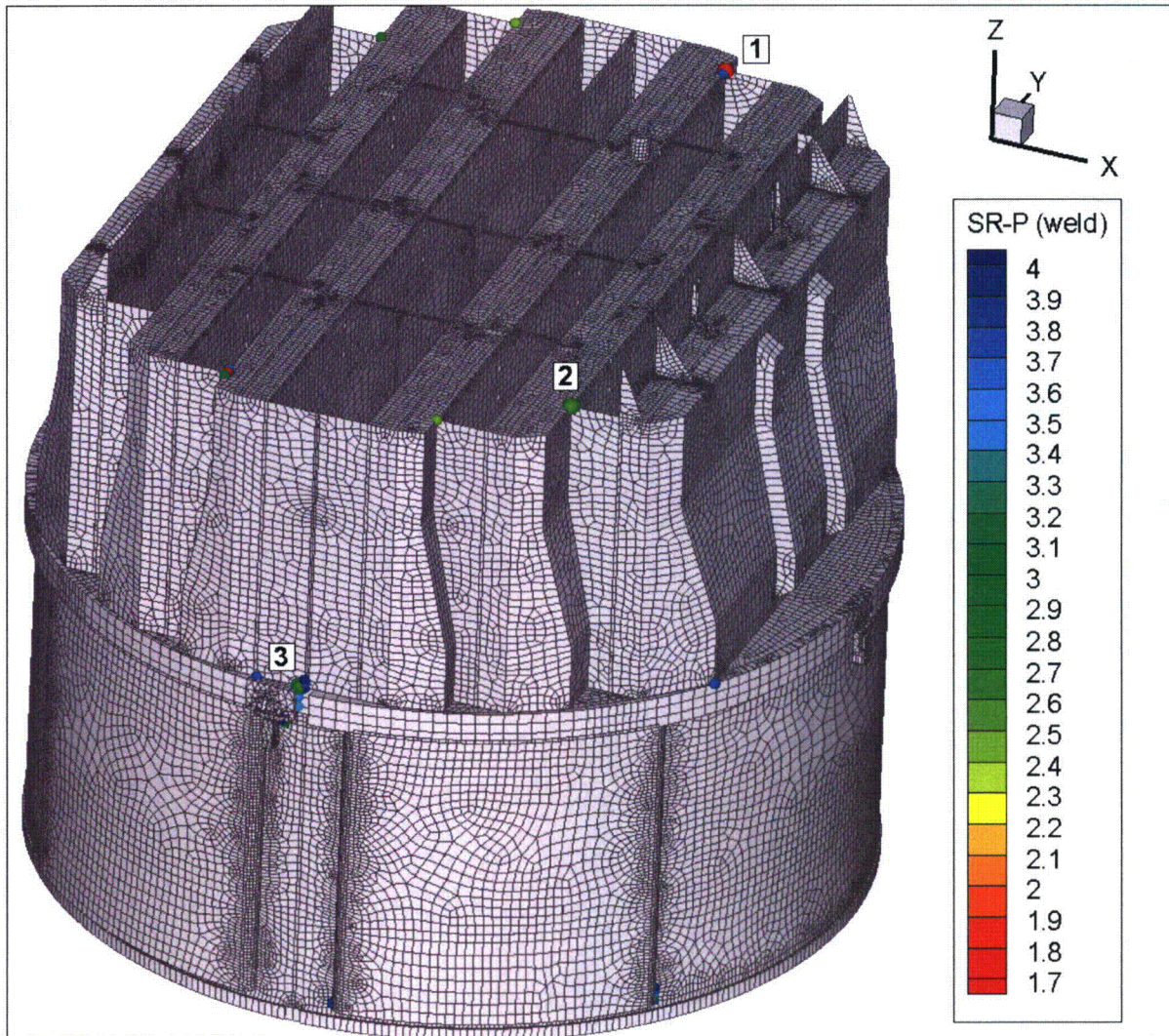


Figure 14c. Locations of smallest maximum stress ratios, $SR-P \leq 4$, at welds for nominal CLTP operation. Numbers refer to the enumerated locations for SR-P values at welds in Table 8a. Second view showing locations 1-3.

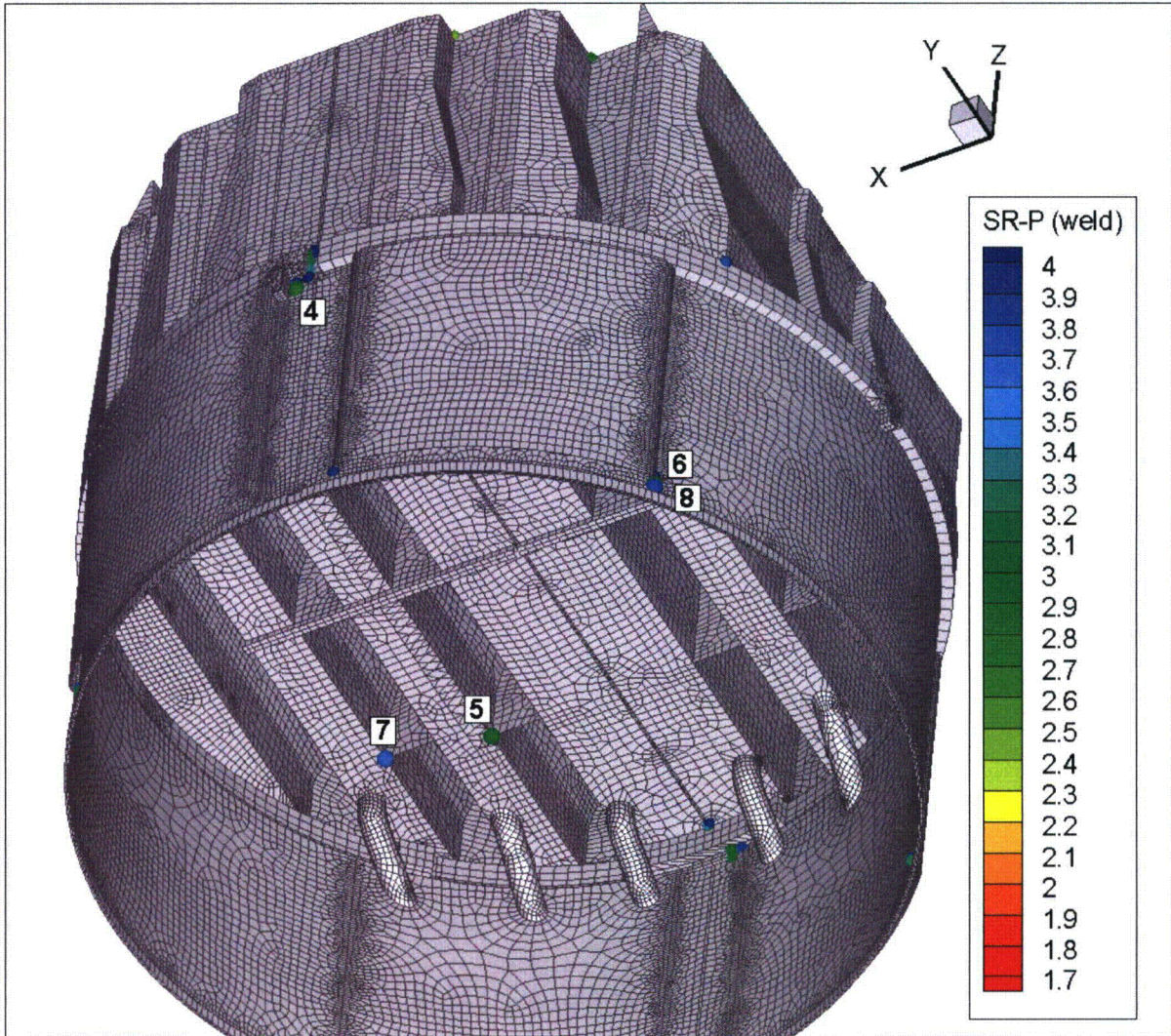


Figure 14d. Locations of smallest maximum stress ratios, $SR-P \leq 4$, at welds for nominal CLTP operation. Numbers refer to the enumerated locations for SR-P values at welds in Table 8a. Third view showing locations 4-8.

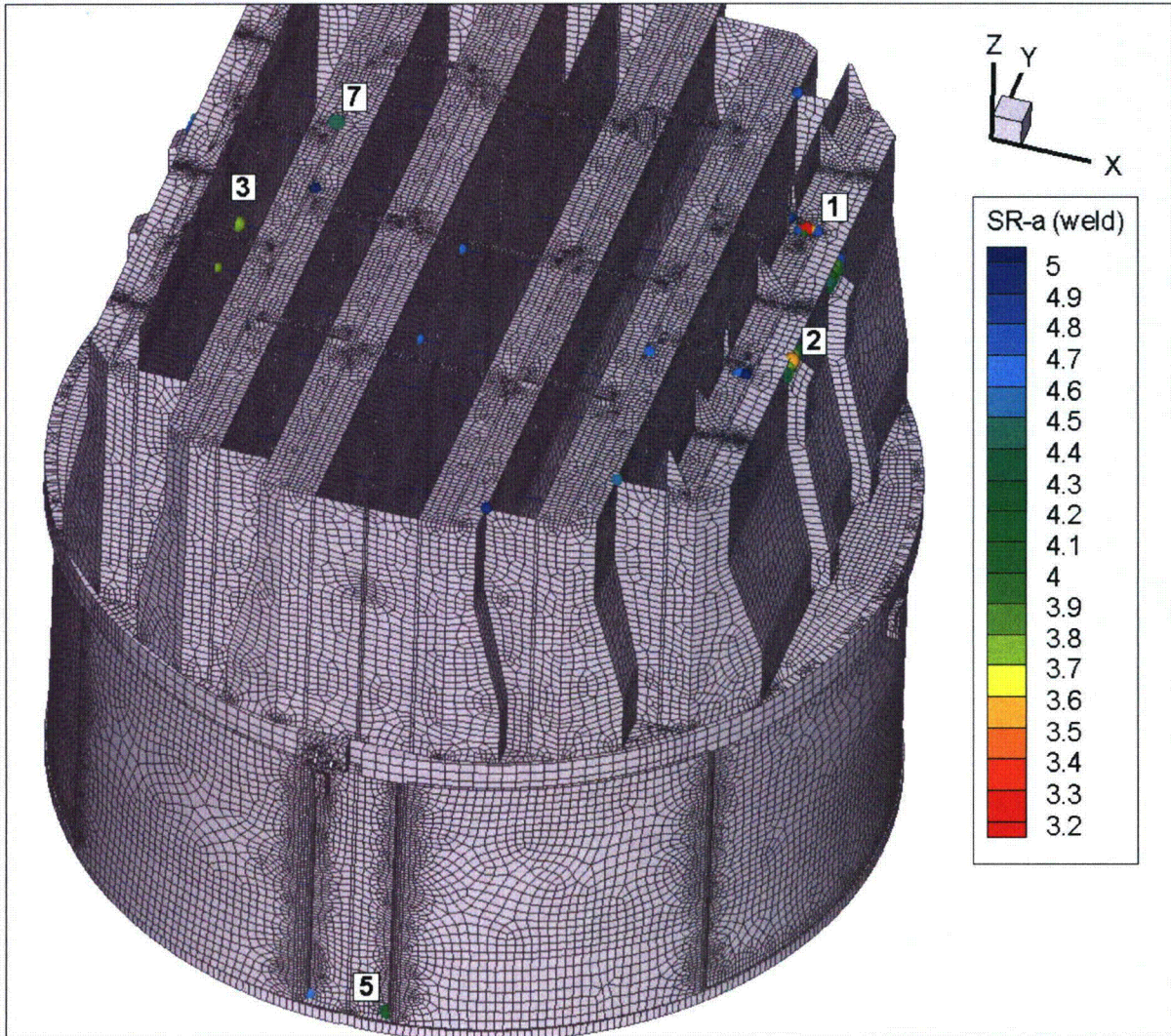


Figure 14e. Locations of minimum alternating stress ratios, $SR-a \leq 5$, at welds for nominal CLTP operation. Numbers refer to the enumerated locations for SR-a values at welds in Table 8a. First view showing locations 1-3, 5 and 7.

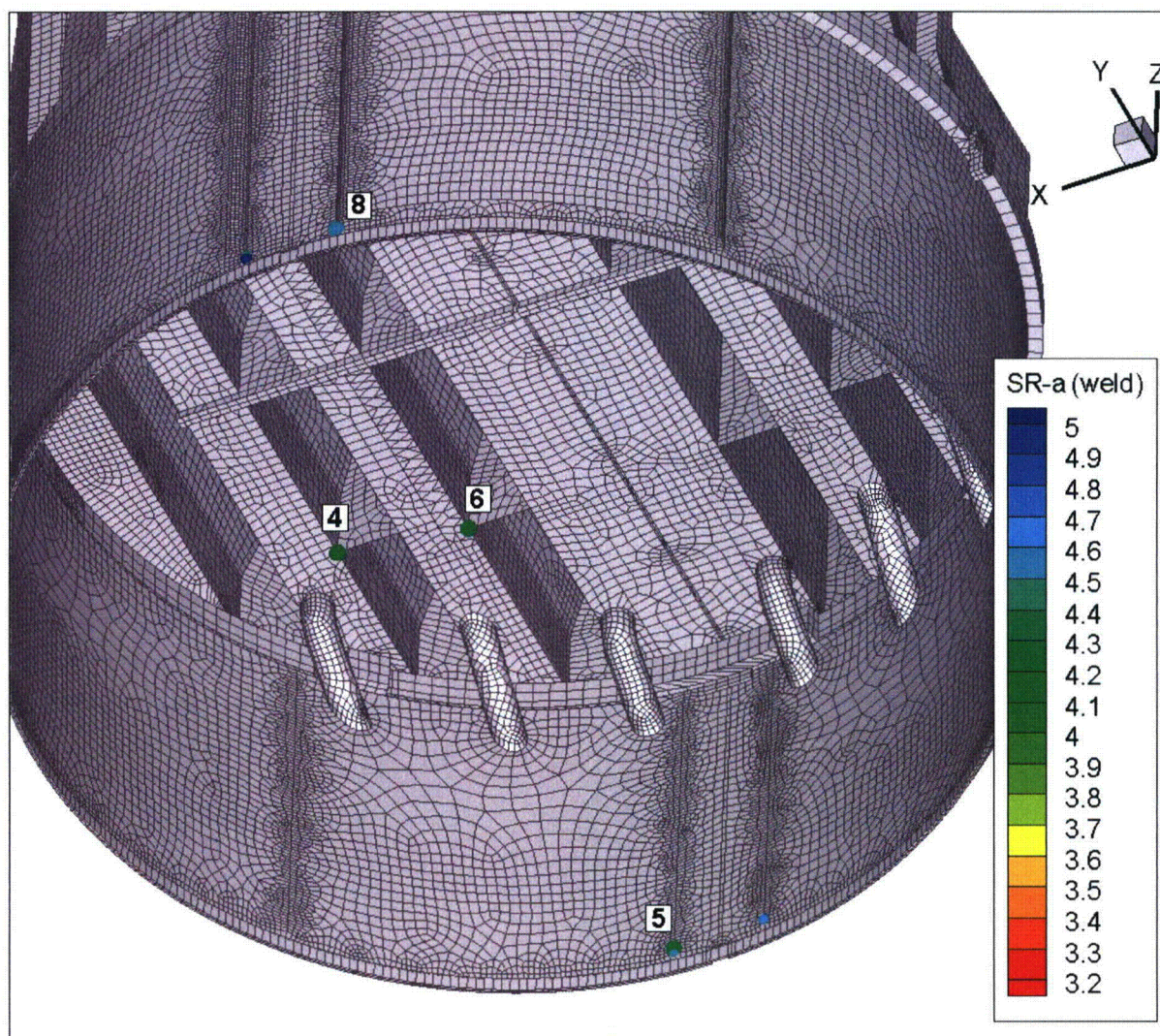


Figure 14f. Locations of minimum alternating stress ratios, $SR-a \leq 5$, at welds for nominal CLTP operation. Numbers refer to the enumerated locations for SR-a values at welds in Table 8a. Second view showing locations 4-6 and 8.

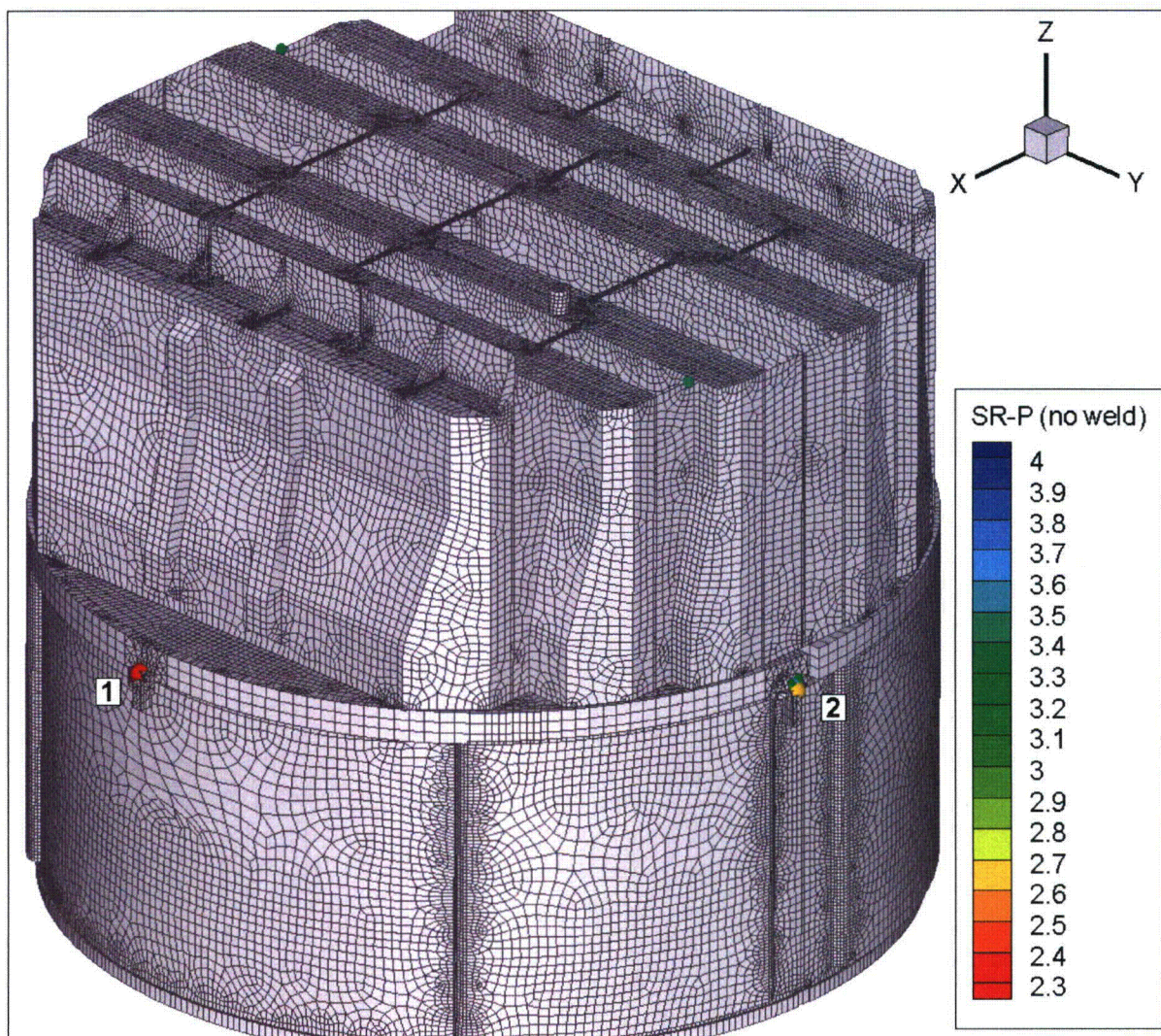


Figure 15a. Location of minimum stress ratios, $SR-P \leq 4$, associated with maximum stress intensities at non-welds for CLTP operation with frequency shifts. The recorded stress ratio is the minimum value taken over all frequency shifts. The number refers to the enumerated location for SR-P values at non-welds in Table 8b.

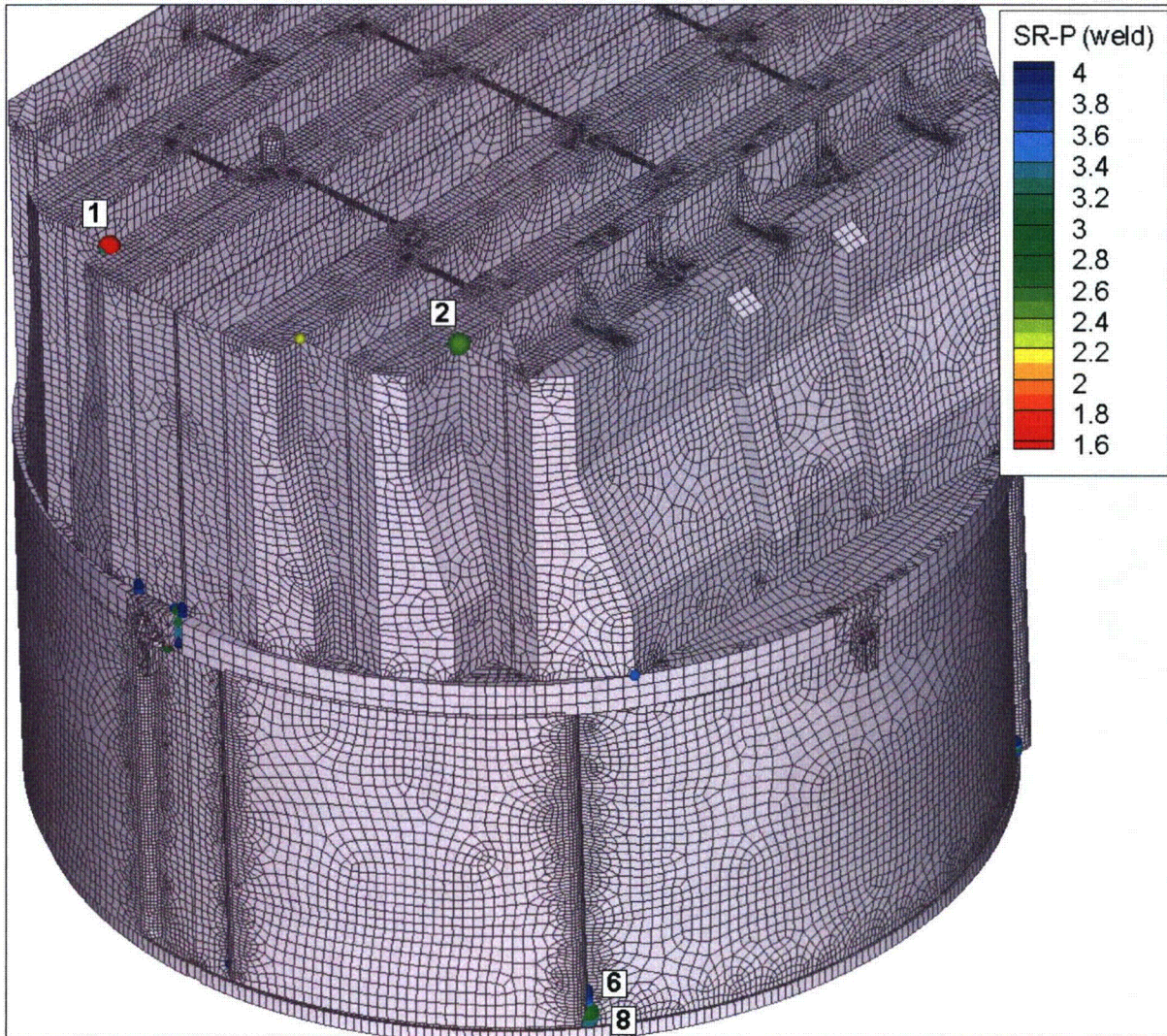


Figure 15c. Locations of minimum stress ratios, $SR-P \leq 4$, associated with maximum stress intensities at welds for CLTP operation with frequency shifts. The recorded stress ratio at a node is the minimum value taken over all frequency shifts. Numbers refer to the enumerated locations for SR-P values at welds in Table 8b. This view shows locations 1, 2, 6 and 8.

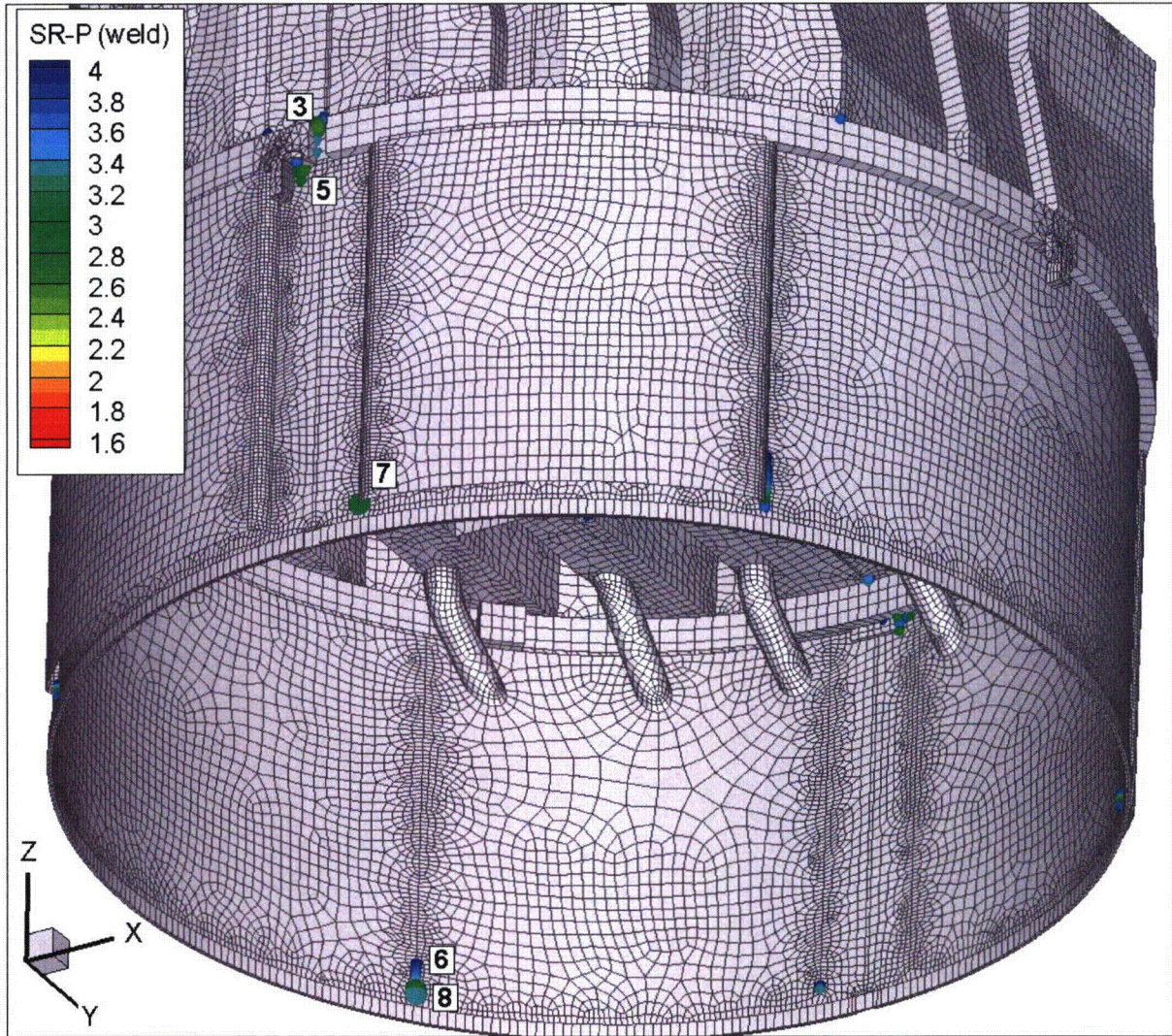


Figure 15d. Locations of minimum stress ratios, $SR-P \leq 4$, associated with maximum stress intensities at welds for CLTP operation with frequency shifts. The recorded stress ratio at a node is the minimum value taken over all frequency shifts. Numbers refer to the enumerated locations for SR-P values at welds in Table 8b. This view shows locations 3 and 5-8.

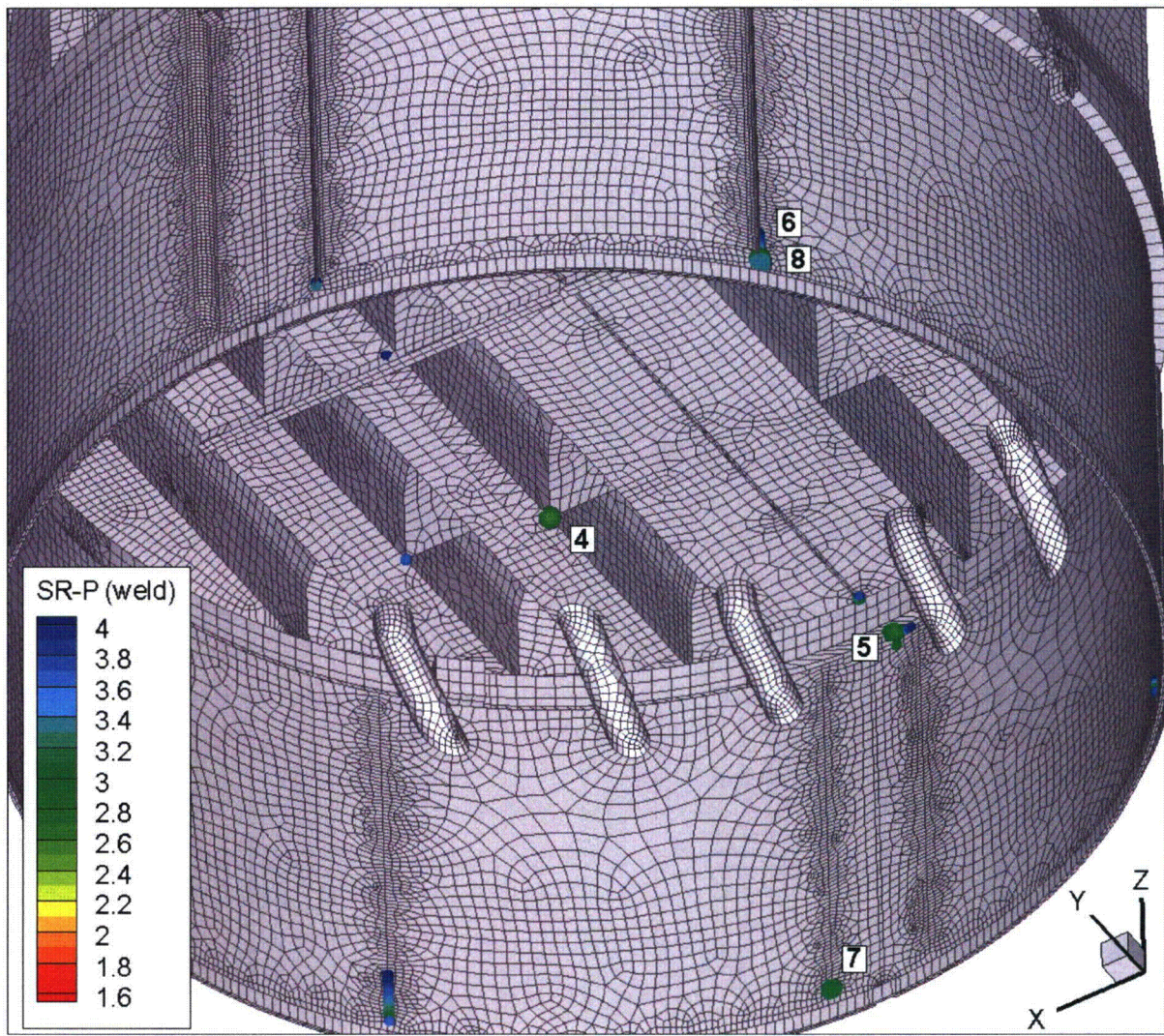


Figure 15e. Locations of minimum stress ratios, $SR-P \leq 4$, associated with maximum stress intensities at welds for CLTP operation with frequency shifts. The recorded stress ratio at a node is the minimum value taken over all frequency shifts. Numbers refer to the enumerated locations for SR-P values at welds in Table 8b. This view shows locations 4-8.

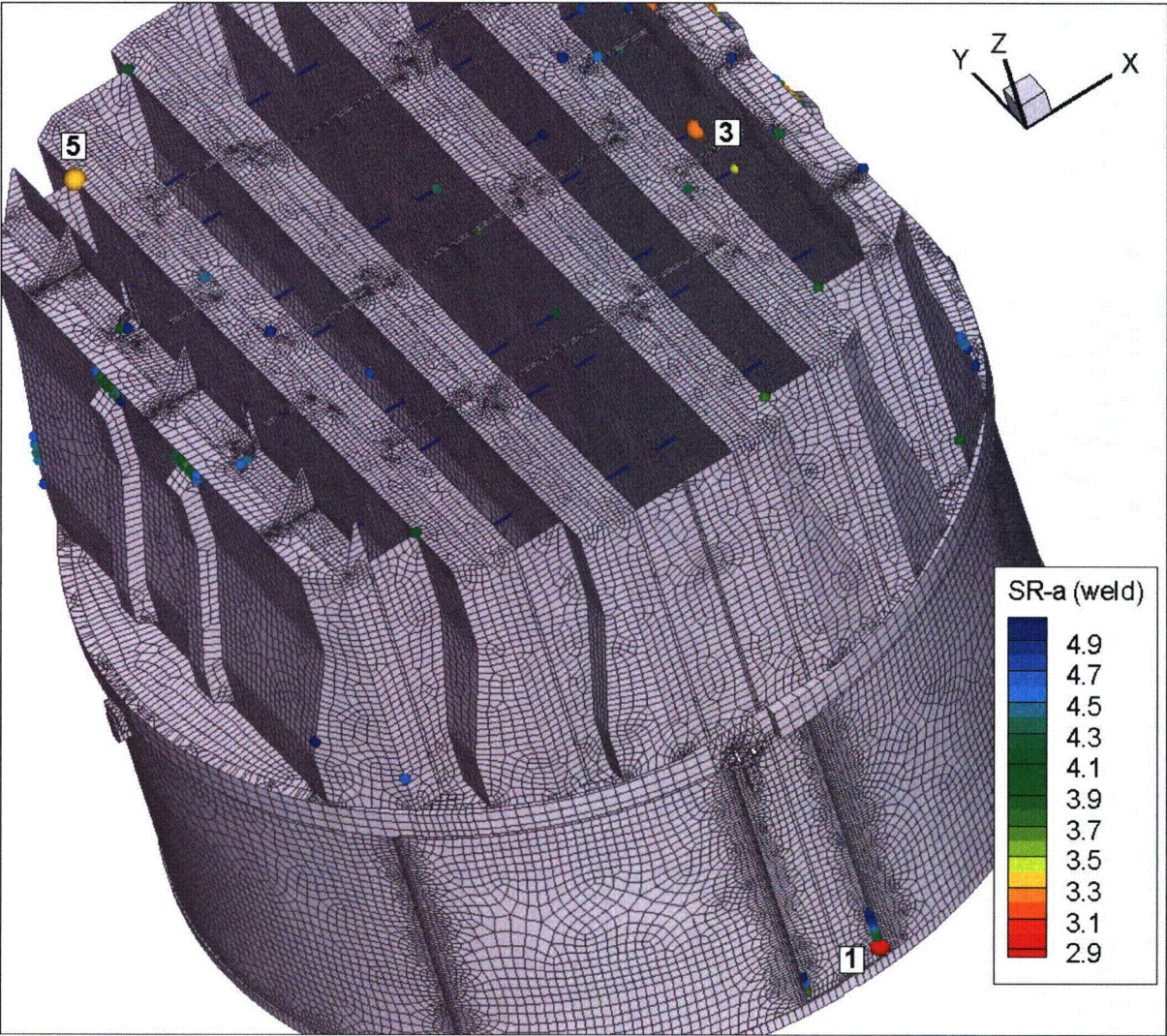


Figure 15f. Locations of minimum alternating stress ratios, $SR-a \leq 5$, at welds for CLTP operation with frequency shifts. The recorded stress ratio at a node is the minimum value taken over all frequency shifts. Numbers refer to the enumerated locations for SR-a values at welds in Table 8b. This view shows locations 1, 3 and 5.

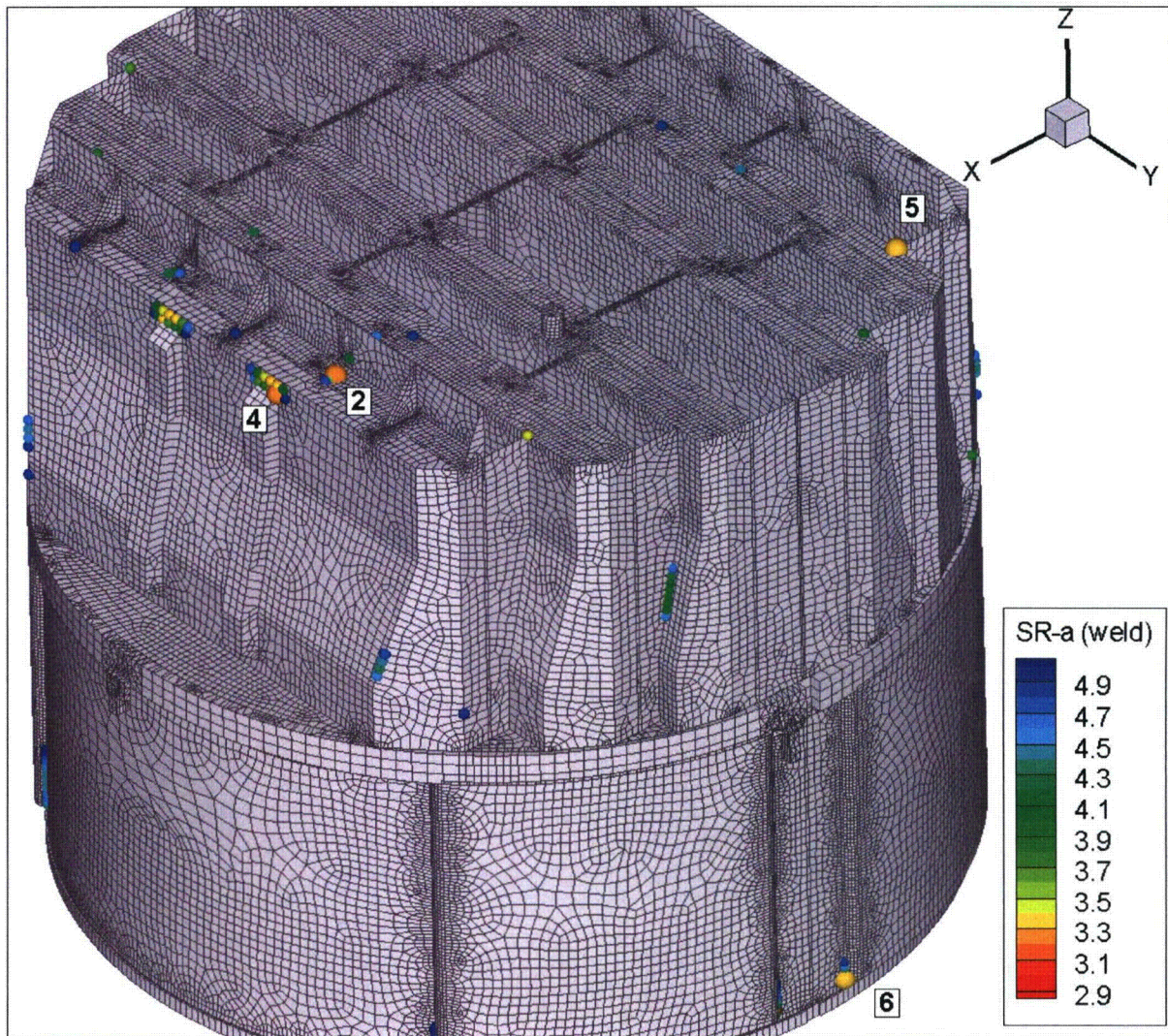


Figure 15g. Locations of minimum alternating stress ratios, $SR-a \leq 5$, at welds for CLTP operation with frequency shifts. The recorded stress ratio at a node is the minimum value taken over all frequency shifts. Numbers refer to the enumerated locations for SR-a values at welds in Table 8b. This view shows locations 2 and 4-6.

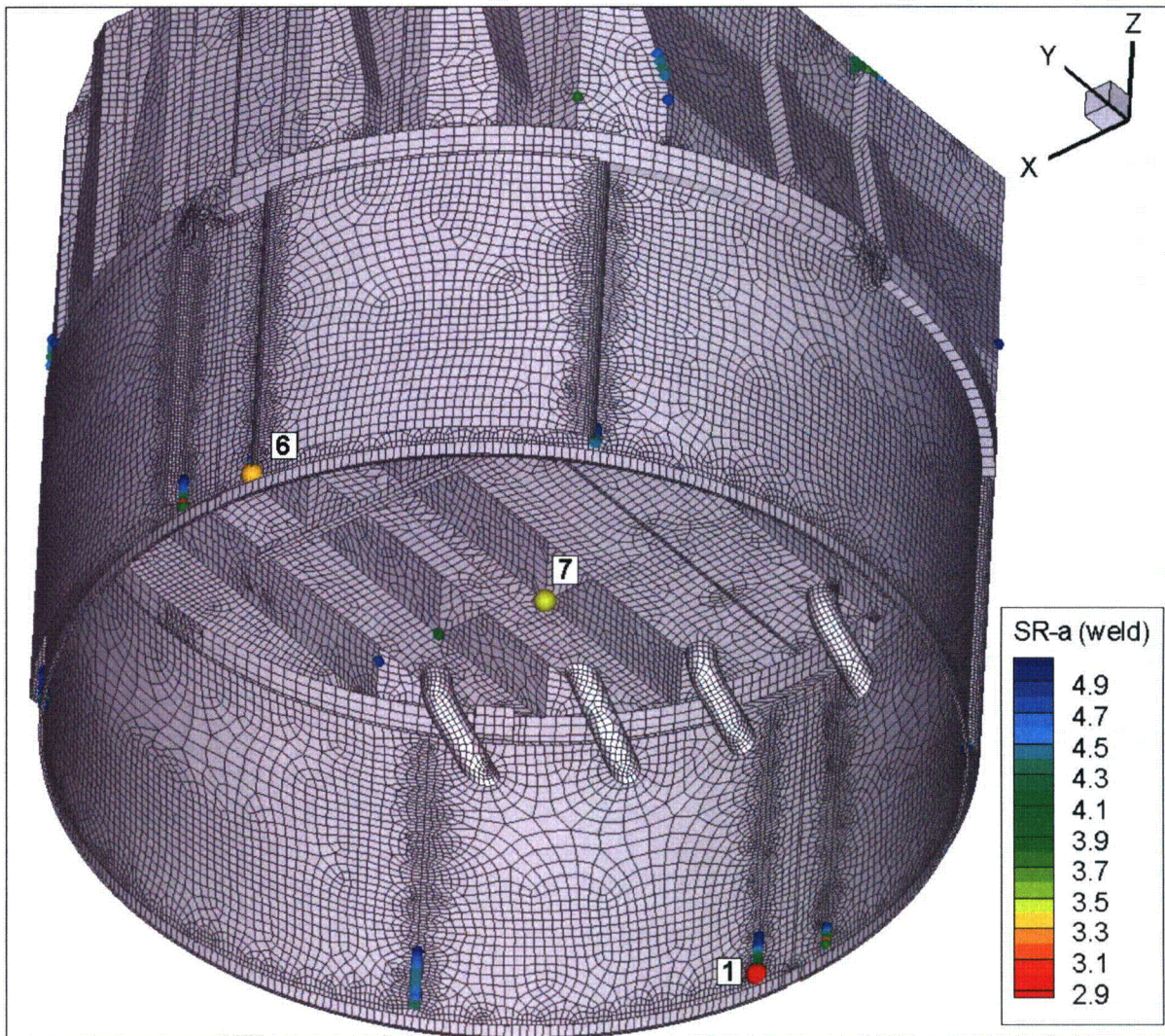


Figure 15h. Locations of minimum alternating stress ratios, $SR-a \leq 5$, at welds for CLTP operation with frequency shifts. The recorded stress ratio at a node is the minimum value taken over all frequency shifts. Numbers refer to the enumerated locations for SR-a values at welds in Table 8b. This view shows locations 1, 6 and 7.

5.3 Frequency Content

The frequency contribution to the stresses can be investigated by examining the power spectral density (PSD) curves and accumulative PSDs for selected nodes having low alternating stress ratios. The accumulative PSDs are computed directly from the Fourier coefficients as

$$\Sigma(\omega_n) = \sqrt{\sum_{k=1}^n |\tilde{\sigma}(\omega_k)|^2}$$

where $\tilde{\sigma}(\omega_k)$ is the complex stress harmonic at frequency, ω_k . Accumulative PSD plots are useful for determining the frequency components and frequency ranges that make the largest contributions to the fluctuating stress. Unlike PSD plots, no “binning” or smoothing of frequency components is needed to obtain smooth curves. Steep step-like rises in $\Sigma(\omega)$ indicate the presence of a strong component at a discrete frequency whereas gradual increases in the curve imply significant content over a broader frequency range. From Parseval’s theorem, equality between $\Sigma(\omega_N)$ (where N is the total number of frequency components) and the RMS of the stress signal in the time domain is established.

The selected nodes are the ones having the lowest alternating stress ratios (at a weld) in Table 8b. These are:

- Node 98,860 – this node has the lowest alternating stress ratio and is located on the weld connecting the drain channel to the skirt. The associated PSDs are shown in Figure 16a.
- Node 132,385 - located on the weld connecting the tie bar remnant (left in place to help support the steam dam) to the tie bar base on the outer hood top cover plate. The associated PSDs are shown in Figure 16b.
- Node 106,852 – connection of a mid-height tie bar to the vane banks. The associated PSDs are shown in Figure 16c.
- Node 111,407 –located at the top of one of the outer hood reinforcement channels. The associated PSDs are shown in Figure 16d.

In each case, since there are six stress components and up to three different section locations for shells (the top, mid and bottom surfaces), there is a total of 18 stress histories per component. Moreover, at junctions there are at least two components that meet at the junction. The particular stress component that is plotted is chosen as follows. First, the component and section location (top/mid/bottom) is taken as the one that has the highest alternating stress. This narrows the selection to six components. Of these, the component having the highest Root Mean Square (RMS) is selected.

For the first node, the peak in the PSD curve occurs at 49-50 Hz. This component is also present in the other nodes and, except for node 132,385, it is the dominant peak in the PSD distributions indicating that it is the main contributor to overall alternating stresses. This is corroborated by the accumulative PSD curves. Significant contributions to the stresses also occur at two other frequencies: 108 Hz (the dominant peak in node 132,385) and 59-62 Hz.

Peaks at these frequencies are also visible in all of the plotted PSDs. Finally, shifting the frequency of the applied load shifts does not seem to shift the 49-50 Hz peak significantly indicating that a structural mode is being excited by the shifted signal.

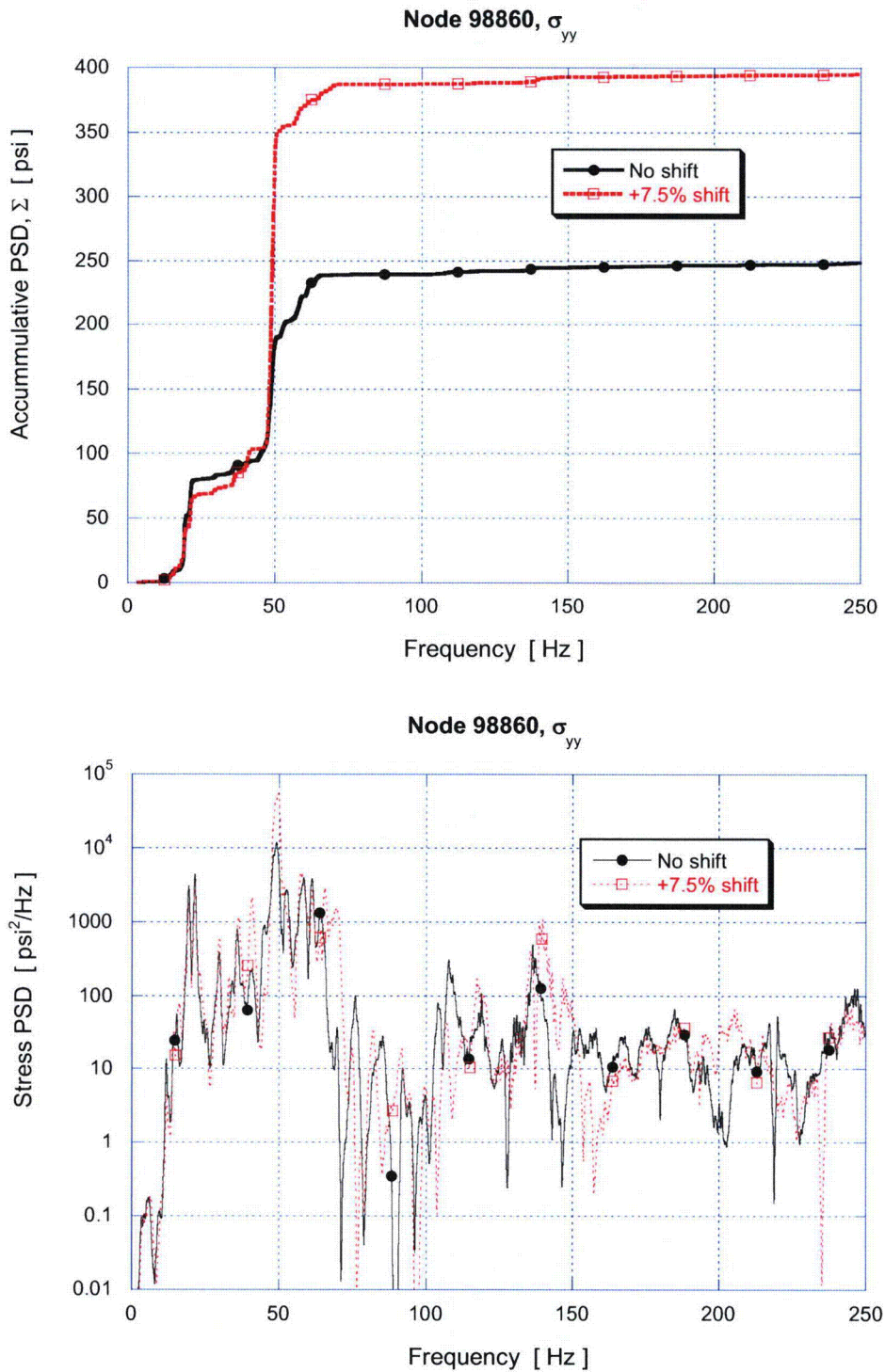


Figure 16a. Accumulative PSD and PSD curves of the σ_{yy} stress response at node 98,860.

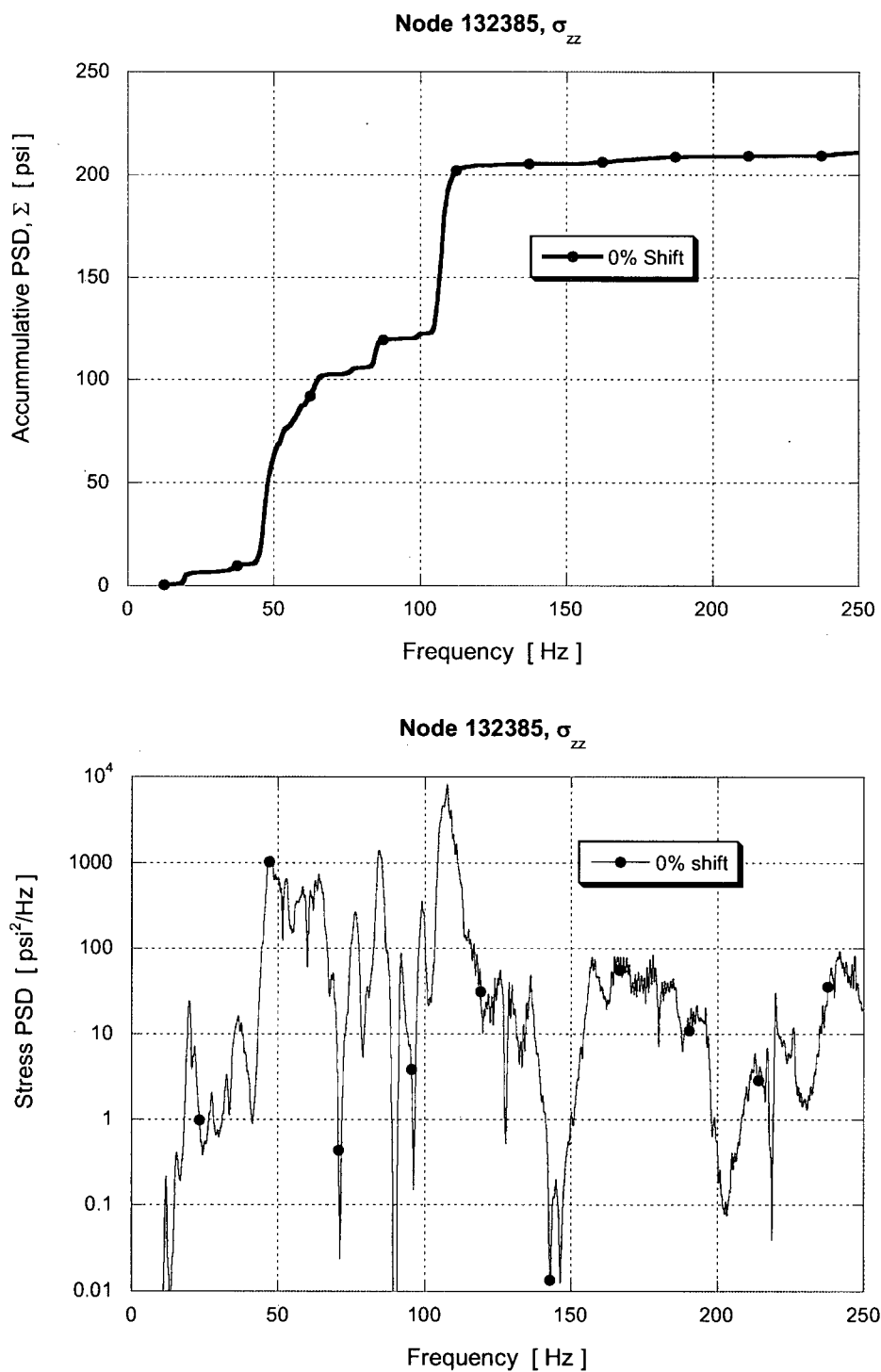
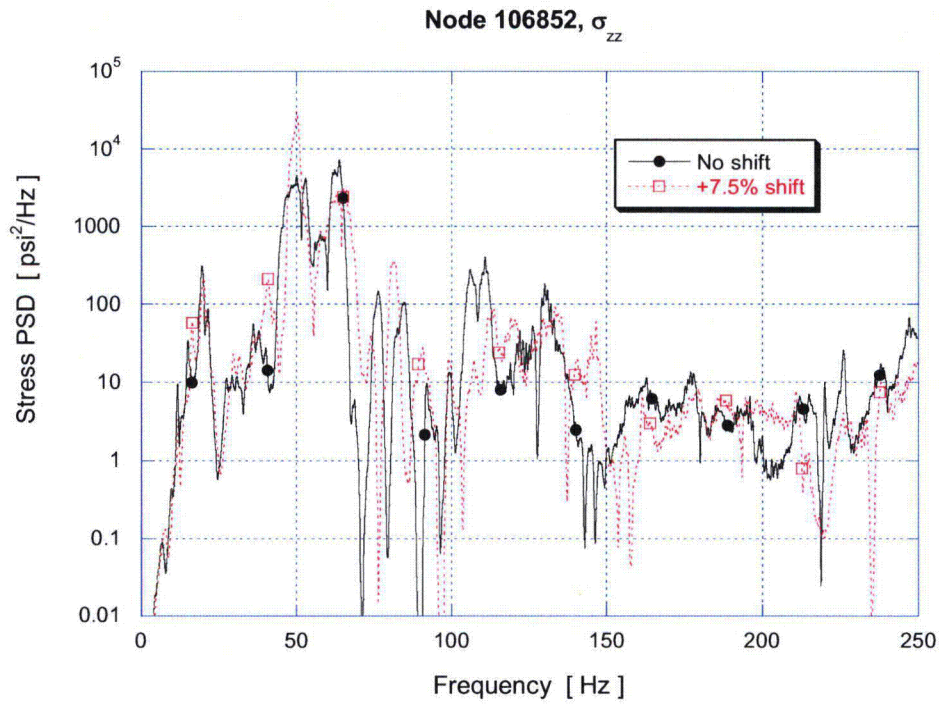
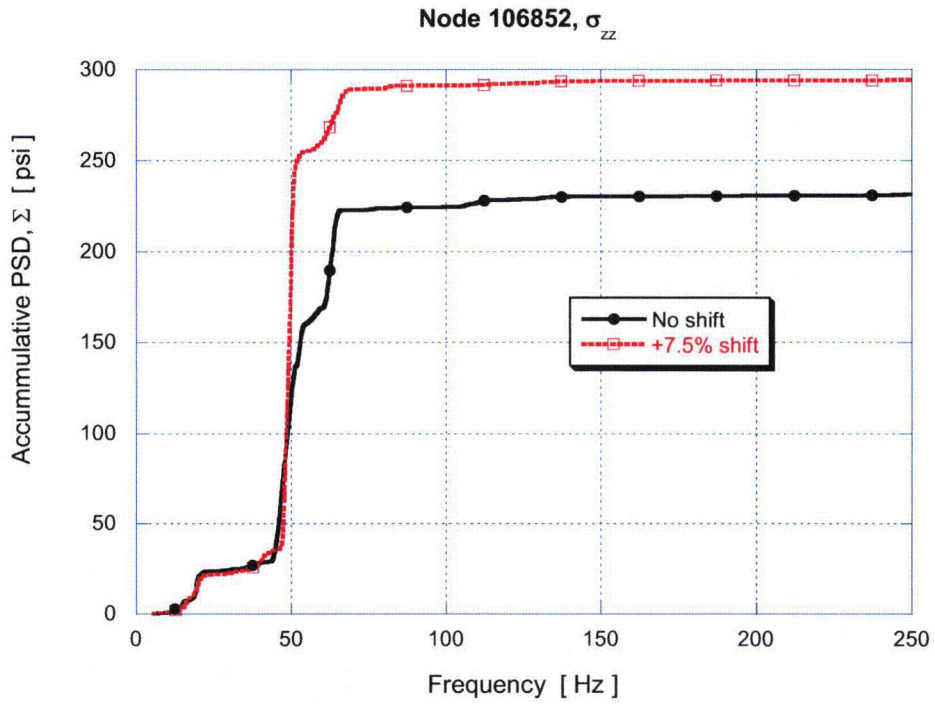


Figure 16b. Accumulative PSD and PSD of the σ_{zz} stress response at node 132,385.



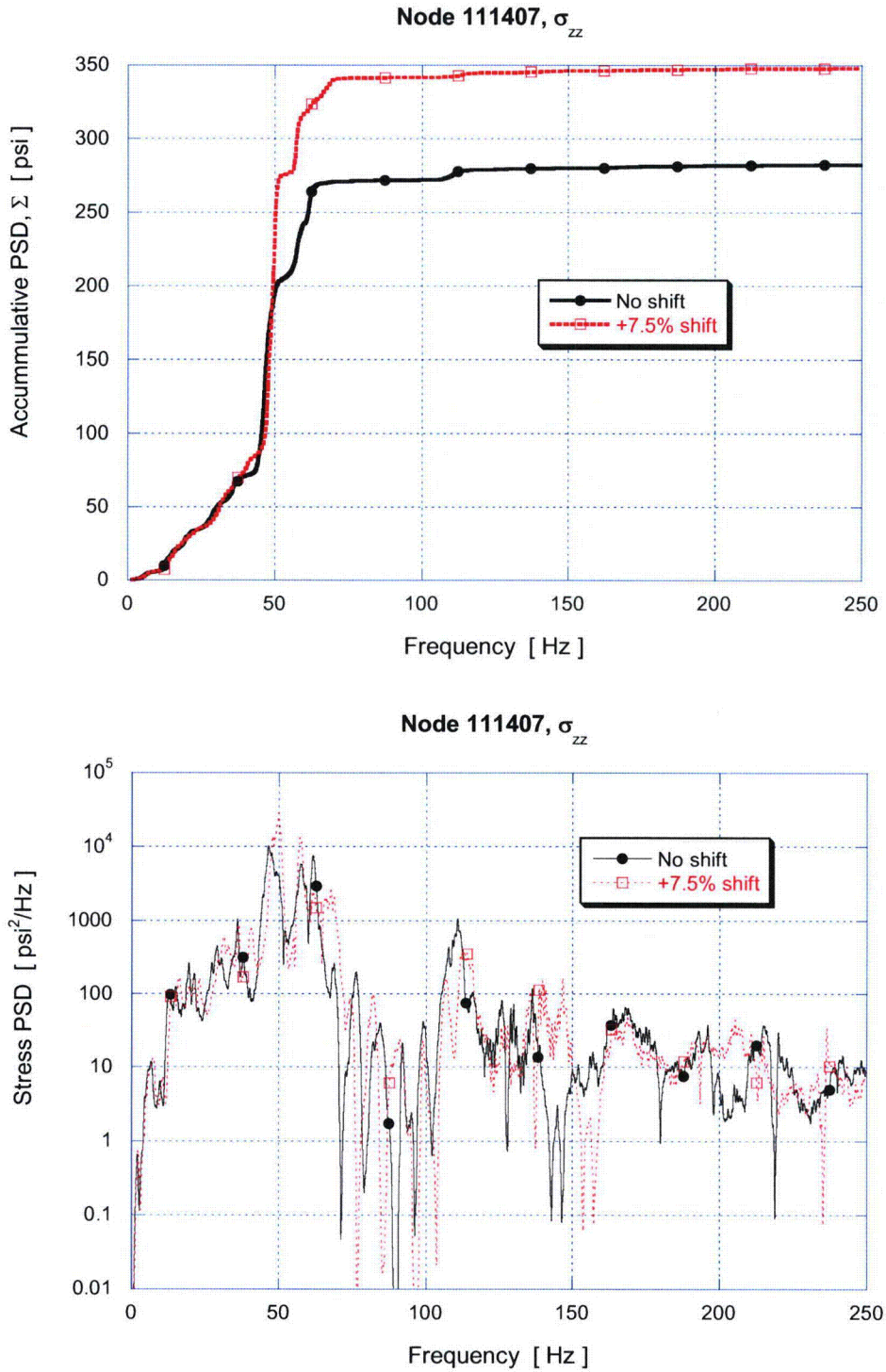


Figure 16d. Accumulative PSD and PSD of the σ_{zz} stress response at node 111,407.

6. Conclusions

A frequency-based steam dryer stress analysis has been used to calculate high stress locations and calculated / allowable stress ratios for the Browns Ferry Unit 1 steam dryer at CLTP load conditions using plant measurement data. A detailed description of the frequency-based methodology and the finite element model for the BFN1 steam dryer is presented. The CLTP loads obtained in a separate acoustic circuit model [2], including end-to-end bias and uncertainty for both the ACM [4] and FEA, were applied to a finite element model of the steam dryer consisting mainly of the ANSYS Shell 63 elements, brick continuum elements, and beam elements. The resulting stress histories were analyzed to obtain maximum and alternating stresses at all nodes for comparison against allowable levels.

The CLTP loads are applied with compensation for background noise based on 1000# data taken at 9% power. These results are tabulated in Table 8 of this report. The minimum alternating stress ratio at nominal operation is 3.23 and the minimum alternating stress ratio taken over all frequency shifts is 2.91. The stress ratios corresponding to maximum stresses are 1.75 at nominal operation and 1.67 when all frequency shifts are considered. The results show that the proposed tie-bars with widened and tapered ends successfully alleviate the highest stress regions associated with tie bar bases to alternating stress ratios, $SR-a > 4.5$.

On the basis of these CLTP plant loads, the dynamic analysis of the steam dryer shows that the combined acoustic, hydrodynamic, and gravity loads produce the following minimum stress ratios:

Frequency Shift	Minimum Stress Ratio at CLTP	
	Max. Stress, SR-P	Alternating Stress, SR-a
0% (nominal)	1.75	3.23
-10%	1.77	4.30
-7.5%	1.73	4.14
-5%	1.75	3.72
-2.5%	1.71	3.73
+2.5%	1.73	3.43
+5%	1.70	2.91
+7.5%	1.67	2.91
+10%	1.69	3.08
All shifts	1.67- 1.77	2.91 – 4.30

Assuming that alternating stresses scale approximately with the square of the steam flow speed, then at 115% CLTP the minimum alternating stress ratio is estimated as $SR-a=2.20$ which remains well above the EPU target of $SR-a=2.0$. The maximum stress ratio reduces to $SR-P=1.65$.

7. References

1. Continuum Dynamics, Inc. (2005). "Methodology to Determine Unsteady Pressure Loading on Components in Reactor Steam Domes (Rev. 6)." C.D.I. Report No. 04-09 (Proprietary).
2. Continuum Dynamics, Inc. (2008). "Acoustic and Low Frequency Hydrodynamic Loads at CLTP Power Level on Browns Ferry Nuclear Unit 1 Steam Dryer to 250 Hz, Rev. 1" C.D.I. Report No. 08-04P (Proprietary).
3. Continuum Dynamics, Inc. (2008). "Stress Assessment of Browns Ferry Nuclear Unit 1 Steam Dryer, Rev. 1," C.D.I. Report No. 08-06P (Proprietary).
4. Continuum Dynamics, Inc. (2007). "Methodology to Predict Full Scale Steam Dryer Loads from In-Plant Measurements, with the Inclusion of a Low Frequency Hydrodynamic Contribution," C.D.I. Report No. 07-09P (Proprietary).
5. Structural Integrity Associates, Inc. (2008). "Main Steam Line 100% CLTP Strain Data Transmission." Email from R. Horvath dated 06-03-2008 and data supplied from ibackup.com.
6. ANSYS Release 10.0. URL <http://www.ansys.com>. Documentation: ANSYS 10.0 Complete User's Manual Set.
7. Continuum Dynamics, Inc. (2007). "Response to NRC Request for Additional Information on the Hope Creek Generating Station, Extended Power Uprate, RAI No. 14.110
8. Press, W. H., S. A. Teukolsky, et al. (1992). *Numerical Recipes*, Cambridge University Press.
9. O'Donnell W.J. (1973). "Effective Elastic Constants For the Bending of Thin Perforated Plates With Triangular and Square Penetration Patterns," ASME Journal of Engineering for Industry, Vol. 95, pp. 121-128.
10. Idel'chik, I E. and Fried, E. (1989). *Flow Resistance, a Design Guide for Engineers*, Taylor & Francis, Washington D.C., p 260.
11. DeSanto, D.F. (1981). "Added Mass and Hydrodynamic Damping of Perforated Plates Vibrating in Water," Journal of Pressure Vessel Technology, Vol. 103, p. 176-182.
12. Continuum Dynamics, Inc. (2007). "Dynamics of BWR Steam Dryer Components," C.D.I. Report No. 07-11P
13. U.S. Nuclear Regulatory Commission, (2007). Regulatory Guide 1.20 "Comprehensive Vibration Assessment Program for Reactor Internals During Preoperational and Initial Startup Testing," March 2007.

14. WRC Bulletin 432 (1998). "Fatigue Strength Reduction and Stress Concentration Factors For Welds In Pressure Vessels and Piping," WRC, NY, p.32
15. Pilkey W.D. (1997). *Peterson's Stress Concentration Factors*, 2nd ed., John Wiley, NY, p.139.
16. Lawrence F.V., Ho N.-J., Mazumdar P.K. (1981). "Predicting the Fatigue Resistance of Welds," *Ann. Rev. Mater. Sci.*, vol. 11, pp. 401-425.
17. General Electric (GE) Nuclear Energy (2003). Supplement 1 to Service Information Letter (SIL) 644, "BWR/3 Steam Dryer Failure," September 5, 2003.
18. Tecplot 10 (2004). URL: <http://www.tecplot.com>. Documentation: *Tecplot User's Manual* Version 10 Tecplot, Inc. Bellevue, Washington October.
19. Structural Integrity Associates Calculation Package, 0006982.301, "Shell and Solid Sub-Model Finite Element Stress Comparison," June 04, 2008.
20. Continuum Dynamics, Inc., Response to NRC RAI EMCB 172, June 2008.